Electrochemistry of the instability at the liquid-liquid interface

Yuki Kitazumi

2010

Contents

General introduction

Background of this work

Unstable phenomena at the liquid-liquid interface, such as emulsification, irregularly increased currents, and oscillations of the meniscus, interfacial tension (γ), and phase-boundary potential ($\Delta_{\mathrm{O}}^{\mathrm{W}}\phi$), not driven by input of externally applying mechanical or thermal agitation have been studied for a long time. For example, the spontaneous emulsification was addressed by Gad as a scientifically interesting subject in 1878 [1]. The spontaneous emulsification is the formation of emulsions without the external energy. This phenomenon has been tackled by many researchers [1–25] because of its importance in surface chemistry and related applications, such as dispersion of chemicals in industrial and agricultural processes [6], drug delivery systems [22, 23], and the digestion of food in our body [5] as well as other animals. The fact that many hypotheses have been proposed for the mechanism of spontaneous emulsification, for example, the local surface tension gradient [2], the ultra-low γ [26], the diffusion and stranding [3, 6, 10], the differences in osmotic pressure [16], and the local super-saturation [17] attests that the mechanism is not fully explained yet. The oscillation phenomena have also been well-known as an expression of instability at the liquid-liquid interface [27–30] and studied mainly in two aspects: the generation of the spontaneous oscillation of $\Delta_{\mathrm{O}}^{\mathrm{W}}\phi$ and that of γ upon contact of two immiscible liquids directly [30–38] or their contact with a liquid membrane in-between [27–29, 36, 39–42]. The oscillation phenomena and the spontaneous emulsification often induce the interfacial turbulence [4, 18, 19, 30–33, 35, 37] caused by the Marangoni effect due to an irregular temporal change in γ. After the pioneering work by Sternling and Scriven [43], the

hydrodynamic instability of the liquid-liquid interface has been chiefly analyzed with a linear stability theory [36, 44–57]. Although the model has been refined over times, theoretical results do not fully agree with experimental results [36, 43, 49, 55, 56, 58, 59]. This disagreement suggests that the mass transfer and the energy transfer across the liquid-liquid interface treated within the framework of the linear stability theory are not the origin of the instability. The spontaneous emulsification and the oscillation phenomena not only invoke scientific curiosity but are of technological and physiological importance having a potential for wide applications. However, our understanding of these phenomena is still limited.

Ionic surfactants have been employed most commonly to study the spontaneous emulsification [1–5, 11, 16–18, 24] and the oscillation phenomena [30, 34, 37, 39–42]. The distribution of ions in the liquid-liquid two-phase system can be controlled through the applied voltage when the interface is electrochemically polarized [60, 61]. Therefore, the electrochemistry of liquid-liquid two-phase system has been used to study these unstable phenomena at the liquid-liquid interface. It should be noted that there exists a potential difference across the liquid-liquid interface even without the external application of a voltage across the interface. In this case, $\Delta_{\mathrm{O}}^{\mathrm{W}}\phi$ is a function of the composition of the adjacent solution phases. The significance of such $\Delta_{\mathrm{O}}^{\mathrm{W}}\phi$ in the absence of externally applied voltage has been demonstrated by Gavach et al. at the nitrobenzene|water interface [60]. However, this aspect has not been addressed in studies of the instability at the liquid-liquid interface described above.

Kučera found anomaly in electrocapillary curves at the mercury| solution interface [62], which led to the invention of polarography [63]. The regularly irregular augmentation of the current on polarograms beyond the level of diffusion-limited current, called polarographic maxima, was first studied by Shikata and Heyrovský in 1925 [64]. Typically, the maxima observed on the rising portion of a polarogram are suppressed by addition of surface-active agents such as gelatin. Antweiler described in detail the streaming of mercury at a dropping mercury electrode by a photographic technique [65]. Some researchers have proposed that the streaming was induced by heterogeneity of the current density on the electrode surface [66–73]. However, the

polarographic maxima occur even at a stationary mercury pool electrode. Moreover, this type of models based on the fluidics can not explain why the maxima appear in the certain potential region near the half-wave potential. The unstable phenomena at the mercury electrode have been revisited, recently using hanging drop electrodes [74–77] but its origin seems to remain unclear.

Many different aspects of the instability at the liquid-liquid interface have been described in papers so far published [14,20,21,37,38,76,78–88]. However, missing is the explanation of when and how a liquid-liquid system enters in the mode of instability and also gets out of it. The electrochemical instability [89] is a concept that explains the unstable phenomena at the liquid-liquid interface by clarifying the condition of the instability in terms of the thermodynamic stability of the liquid-liquid interface,

$$\left[\frac{\partial^2\gamma}{\partial\left(\Delta_{\mathrm{O}}^{\mathrm{W}}\phi\right)^2}\right]_{T,P,\mu_i} > 0,$$

where γ is the interfacial tension, T is the temperature, P is the pressure, and μ_i is the chemical potential of relevant chemical species, i. This is a special case of the condition of the thermodynamic instability, $(\partial^2 G/\partial X^2) > 0$ [90], where G is a thermodynamic function and X is an intensive variable. The emergence of the electrochemical instability has been observed in voltammetry of the transfer of various surface-active ions as an anomalous increase in the current [91–96], the turbulence at the liquid-liquid interface [91–95, 97], and the emulsification [91, 92, 95]. The characteristic features of the electrochemical instability include its appearance in the certain limited potential range on the voltammograms around the standard ion transfer potential of the surface active ion, the substantially high value of γ in the vicinity of stable-unstable transition, and the controllability of the stability-instability conditions based on $\Delta_{\mathrm{O}}^{\mathrm{W}}\phi$.

The previously proposed model for the electrochemical instability [89] assumed that the change in γ due to the potential-dependent adsorption of surface-active ions and that due to the presence of the diffuse double layers were additive. However, this assumption oversimplifies the picture in that the structure of the electrical double layer is independent of the specifically adsorbed surface-active ions. The linear dependence of the adsorption Gibbs energy on

$\Delta_{\mathrm{O}}^{\mathrm{W}}\phi$ [98] is also assumed in this model. However, we have little information about specific parameters of the potential-dependent adsorption of various surface-active ions. Moreover, the electrochemical instability may be able to explain why the interface is unstable, but does not tell how the interface falls into the unstable conditions. Although several photographic observations of the instability at the liquid-liquid interface have been reported [25,38,65,82,83,99,100], microscopic details of the instability have not been investigated.

Outline of this work

In chapter 1, the author proposed a revised model of the electrochemical instability at the liquid-liquid interface, allowing for the effect of the specifically adsorbed ions on the structure of the diffuse part of the double layers, which was ignored in the previous model [89]. Then, the new model was used for the analysis of the electrocapillarity of the liquid-liquid interface in the presence of common ions distributed in both phases.

The precise knowledge of the potential-dependent adsorption of surface-active ions is crucial in quantitatively understanding the electrochemical instability. In chapter 2, the author developed a method for the simultaneous recording of an electrocapillary curve and an ion transfer voltammogram and determined the potential-dependent adsorption of the surface-active ions. The author showed that decylammonium and decylsulfate strongly adsorb at the interface in the potential range where the ions were predominantly distributed in the aqueous phase and that they adsorb only weakly, if any, at the potential region where the ions were predominantly distributed in the 1,2-dichloroethane (DCE) [97].

The emergence of the electrochemical instability has been mainly observed as the irregularly increased current in voltammetry [91–96]. However, such a macroscopic method provides no information about a way how the interface falls into the state of the electrochemical instability. In chapter 3, for the sensitive detection of the emergence of the electrochemical instability at the microscopic level and for the clarification of the structure of the interface under the electrochemical instability, the author developed a method of directly imaging the liquid-liquid

interface under the potential control using confocal fluorescence microscopy. The commencement of the hydrodynamic movement of the solutions due to the electrochemical instability has been detected as the appearance of heterogeneous domains at the edge of the interface, that is, along the three-phase contact line of the DCE-W-glass wall confining the interface. The dark domains where fluorophores were much less populated than the interface before the electrochemical instability gradually grew with time while applying the potential for the onset of the instability and with the scanning of the potential. When the entire interface became unstable, the domains moved vertiginously due to the Marangoni convection of the adjacent solution phases [101].

The microscopic observation in chapter 3 demonstrated the electrochemical instability appeared at the three-phase contact line. In chapter 4, the author estimated the effect of the area of the interface on the emergence of the electrochemical instability by forming the interface supported at the tip of the glass micropipette. The concentration of the surface-active ion required to induce the irregular current on the voltammogram due to the electrochemical instability at the micro liquid-liquid interface was significantly higher than that at the interface of conventional size, i.e., the decrease in the diameter of the pipette suppressed the irregular current [96].

The observations of the electrochemical instability have been carried out under the transfer of surface-active ions by external control of the potential in chapters 2, 3, and 4. However, the electrochemical instability is a general concept that is valid no matter how $\Delta_{\mathrm{O}}^{\mathrm{W}}\phi$ is controlled or determined. The spontaneous emulsification and the oscillation phenomena at the liquid-liquid interface are considered to be due to the electrochemical instability, which is conditioned by the inner potential difference determined not only by the externally applied voltage but by the partition of ionic species between the two phases. In chapter 5, liquid-liquid two-phase systems that expressed the spontaneous emulsification were interpreted in terms of the electrochemical instability.

The potential-dependencies of the adsorption of the conventional surface-active ions having

a charged hydrophilic part and an uncharged hydrophobic part possibly reflect the position of the charge in the adsorbed ions [97]. In chapter 6, for the control of the potential-dependent adsorption on the basis of the molecular structure, the author synthesized novel surface-active ions having a charged hydrophobic part and an uncharged hydrophilic part. The synthesized surface-active ions showed the adsorption behaviour that is fundamentally different from that of conventional surface-active ions. For example, the adsorption of the newly synthesized ions at the air|water interface was far weaker than that at the oil|water interface and the adsorption of these aerophobic ions at the liquid-liquid interface at the potentials where the ions were distributed in the oil phase was stronger than the adsorption at the potential where the ions were distributed in the aqueous phase.

Chapter 7 concludes my study on the electrochemical instability at the liquid-liquid interface and summarized the remained problems and scope for future studies.

References

[1] Gad, J. *Arch. Anat. Physiol., Lpz.,* **1878**, 181–205.

[2] Quincke, G. *Ann. Phys., Lpz.,* **1904**, *15*, 1–54.

[3] McBain, J. W.; Woo, T.-M. *Proc. Roy. Soc. A* **1937**, *163*, 182–188.

[4] Kaminski, A.; McBain, J. W. *Proc. Roy. Soc. A* **1949**, *198*, 447–454.

[5] Frazer, A. C.; Schulman, J. H.; Stewart, H. C. *J. Physiol.-London* **1944**, *103*, 306–316.

[6] Groves, M. J. *Chem. Ind.* **1978**, *17*, 417–423.

[7] Ruschak, K. J.; Miller, C. A. *Ind. Eng. Chem. Fundam.* **1972**, *11*, 534–540.

[8] Kunieda, H.; Shinoda, K. *J. Colloid Interface Sci.* **1979**, *70*, 577–583.

[9] Shioi, A.; Harada, M.; Matsumoto, K. *J. Phys. Chem.* **1991**, *95*, 7495–7502.

[10] Miller, C. A. *Colloid Surf.* **1988**, *29*, 89–102.

[11] Murthy, A. K.; Kaler, E. W.; Zasadzinski, J. A. N. *J. Colloid Interface Sci.* **1991**, *145*, 598–600.

[12] Eastoe, J.; Towey, T. F.; Robinson, B. H.; Williams, J.; Heenan, R. K. *J. Phys. Chem.* **1993**, *97*, 1459–1463.

[13] Eastoe, J.; Chatfield, S. *Langmuir* **1994**, *10*, 1650–1653.

[14] Shahidzadeh, N.; Bonn, D.; Meunier, J. *Europhys. Lett.* **1997**, *40*, 459–464.

[15] Nave, S.; Eastoe, J.; Penfold, J. *Langmuir* **2000**, *16*, 8733–8740.

[16] Greiner, R. W.; Evans, D. F. *Langmuir* **1990**, *6*, 1793–1796.

[17] Rang, M. J.; Miller, C. A. *Prog. Colloid Polym. Sci.* **1998**, *109*, 101–117.

[18] Nishimi, T.; Miller, C. A. *Langmuir* **2000**, *16*, 9233–9241.

[19] López-Montilla, J. C.; Herrera-Morales, P. E.; Pandey, S.; Shah, D. O. *J. Disp. Sci. Tech.* **2002**, *23*, 219–268.

[20] Schott, R.; Pfennig, A. *Mol. Phys.* **2004**, *102*, 331–339.

[21] Tauer, K.; Kozempel, S.; Rother, G. *J. Colloid Interface Sci.* **2007**, *312*, 432–438.

[22] Constantinides, P. P. *Pharm. Res.* **1995**, *12*, 1561–1572.

[23] Pouton, C. W. *Adv. Drug Deliv. Rev.* **1997**, *25*, 47–58.

[24] Srivastava, V. K.; Kini, G.; Rout, D. *J. Colloid Interface Sci.* **2006**, *304*, 214–221.

[25] Aoki, K.; Li, M.; Chen, J.; Nishiumi, T. *Electrochem. Commun.* **2009**, *11*, 239–241.

[26] Miller, C. A.; Hwan, R.; Benton, W. J.; Fort, T. *J. Colloid Interface Sci.* **1977**, *61*, 554–568.

[27] Teorell, T. *J. Gen. Physiol* **1959**, *42*, 831–845.

[28] Mueller, P.; Rudin, D. O. *J. Theoret. Biol.* **1968**, *18*, 222–258.

[29] Pant, H. C.; Rosenberg, B. *Biochim. Biophys. Acta* **1971**, *225*, 379–381.

[30] Dupeyrat, M.; Nakache, E. *Bioelectrochem. Bioenerg.* **1978**, *5*, 134–141.

[31] Shioi, A.; Sugiura, Y.; Nagaoka, R. *Langmuir* **2000**, *16*, 8383–8389.

[32] Shioi, A. K.; Kumagai, H.; Sugiura, Y.; Kitayama, Y. *Langmuir* **2002**, *18*, 5516–5522.

[33] Shioi, A.; Katano, K.; Onodera, Y. *J. Colloid Interface Sci.* **2003**, *266*, 415–421.

[34] Yui, H.; Ikezoe, Y.; Takahashi, T.; Sawada, T. *J. Phys. Chem. B* **2003**, *107*, 8433–8438.

[35] Kovalchuk, N. A.; Vollhardt, D. *J. Phys. Chem. B* **2005**, *109*, 15037–15047.

[36] Kovalchuk, N. M.; Vollhardt, D. *Adv. Colloid Interface Sci.* **2006**, *120*, 1–31.

[37] Pradines, V.; Tadmouri, R.; Lavabre, D.; Micheau, J. C.; Pimienta, V. *Langmuir* **2007**, *23*, 11664–11672.

[38] Wojciechowski, K.; Kucharek, M. *J. Phys. Chem. B* **2009**, *113*, 13457–13461.

[39] Yoshikawa, K.; Matsubara, Y. *J. Am. Chem. Soc.* **1984**, *106*, 4423–4427.

[40] Kihara, S.; Maeda, K. *Prog. Surf. Sci.* **1994**, *47*, 1–54.

[41] Sutou, S.; Yoshihisa, H.; Miyamura, K.; Gohshi, Y. *J. Colloid Interface Sci.* **1997**, *187*, 544–546.

[42] Pimienta, V.; Etchenique, R.; Buhse, T. *J. Phys. Chem. A* **2001**, *105*, 10037–10044.

[43] Sternling, C. V.; Scriven, L. E. *AIChE J.* **1959**, *5*, 514–523.

[44] Gross, B.; Hixson, A. N. *Ind. Eng. Chem. Fundam.* **1969**, *8*, 289–296.

[45] Brian, P. L. T.; Vivian, J. E.; Mayr, S. T. *Ind. Eng. Chem. Fundam.* **1971**, *10*, 75–83.

[46] Hennenberg, M.; Bisch, P. M.; Vignesadler, M.; Sanfeld, A. *J. Colloid Interface Sci.* **1979**, *69*, 128–137.

[47] Reichenbach, J.; Linde, H. *J. Colloid Interface Sci.* **1981**, *84*, 433–443.

[48] Vedove, W. D.; Sanfeld, A. *J. Colloid Interface Sci.* **1981**, *84*, 318–327.

[49] Bekki, S.; Vignes-Adler, M.; Nakache, E.; Adler, P. M. *J. Colloid Interface Sci.* **1990**, *140*, 492–506.

[50] Bragard, J.; Slavtchev, S. G.; ; Lebon, G. *J. Colloid Interface Sci.* **1994**, *168*, 402–413.

[51] Rabinovich, L. M.; Vyazmin, A. V.; Buyevich, Y. A. *J. Colloid Interface Sci.* **1995**, *173*, 1–7.

[52] Mendes-Tatsis, M. A.; de Ortiz, E. S. P. *Chem. Eng. Sci.* **1996**, *51*, 3755–3761.

[53] Slavtchev, S.; Hennenberg, M.; Legros, J. C.; Lebon, G. *J. Colloid Interface Sci.* **1998**, *203*, 354–368.

[54] Kang, K. H.; Choi, C. K.; Hwang, I. G. *AICHE J.* **2000**, *46*, 15–23.

[55] Slavtchev, S.; Mendes, M. A. *Int. J. Heat Mass Transfer* **2004**, *47*, 3269–3278.

[56] Slavtchev, S.; Kalitzova-Kurteva, P.; Mendes, M. A. *Colloid Surf. A-Physicochem. Eng. Asp.* **2006**, *282*, 37–49.

[57] Zimmerman, W. B.; Rees, J. M.; Hewakandamby, B. N. *Adv. Colloid Interface Sci.* **2007**, *134-35*, 346–359.

[58] Chu, X.-L.; Velarde, M. G. *J. Colloid Interface Sci.* **1989**, *131*, 471–484.

[59] Agble, D.; Mendes-Tatsis, M. M. A. *Int. J. Heat. Mass. Transfer* **2001**, *44*, 1439–1449.

[60] Gavach, C.; Seta, P.; Henry, F. *Bioelectrochem. Bioenerg.* **1974**, *1*, 329–342.

[61] Koryta, J.; Vanýsek, P.; Bŕezina, M. *J. Electroanal. Chem.* **1976**, *67*, 263–266.

[62] Kučra, G. *Ann. Physik* **1903**, *11*, 698–725.

[63] Heyrovský, J.; Shikata, M. *Rec. Trav. Chim.* **1925**, *44*, 496–498.

[64] Shikata, M. *Trans. Faraday Soc.* **1925**, *21*, 42–61.

[65] Antweiler, H. J. *Z. Elektrochem.* **1938**, *44*, 719–724.

[66] Stackelberg, M.; Antweiler, H. J.; Kieselbach, L. *Z. Elektrochem. Angew. Phys. Chem.* **1938**, *44*, 663–674.

[67] Stackelberg, M. *Z. Elektrochem.* **1939**, *45*, 466–491.

[68] Frumkin, A. *J. Colloid Sci.* **1946**, *1*, 277–291.

[69] Frumkin, A.; Levich, V. *Acta Physicochim. USSR* **1946**, *21*, 193–212.

[70] Heyrovský, J.; Kůta, J. *Principles of Polarography*; Academic Press, Inc., 1966.

[71] Bauer, H. H. *Streaming Maxima in Polarography*; Vol. 8 of *Electroanalytical Chemistry*; Marcel Dekker, Inc., 1975.

[72] Becker, J. Y.; Ginzburg, G.; Willner, I. *J. Electroanal. Chem.* **1980**, *108*, 355–368.

[73] Ginzburg, G.; Becker, J. Y.; Lederman, E. *Electrochim. Acta* **1981**, *26*, 851–856.

[74] Saha, M. S.; Che, Y.; Okajima, T.; Kiguchi, T.; Nakamura, Y.; Tokuda, K.; Ohsaka, T. *J. Electroanal. Chem.* **2001**, *496*, 61–68.

[75] Ortiz, M. E.; Nunez-Vergara, L. J.; Squella, J. A. *J. Electroanal. Chem.* **2002**, *519*, 46–52.

[76] Islam, M. M.; Okajima, T.; Ohsaka, T. *J. Phys. Chem. B* **2004**, *108*, 19425–19431.

[77] Islam, M. M.; Saha, M. S.; Okajima, T.; Ohsaka, T. *J. Electroanal. Chem.* **2005**, *577*, 145–154.

[78] Sherwood, T. K.; Wei, J. C. *Ind. Eng. Chem.* **1957**, *49*, 1030–1034.

[79] Pearson, J. R. A. *J. Fruid Mech.* **1958**, *4*, 489–500.

[80] Nawab, M. A.; Mason, S. G. *J. Colloid Sci.* **1958**, *13*, 179–187.

[81] Nakaike, Y.; Tadenuma, Y.; Sato, T.; Fujinawa, K. *Int. J. Heat Mass Transfer* **1971**, *14*, 1951–1961.

[82] Magome, N.; Yoshikawa, K. *J. Phys. Chem.* **1996**, *100*, 19102–19105.

[83] Kitahata, H.; Yoshikawa, K. *Physica D* **2005**, *205*, 283–291.

[84] Takhistov, P.; Paul, S. *Food Biophys.* **2006**, *1*, 57–73.

[85] Shinshi, M.; Sugihara, T.; Osakai, T.; Goto, M. *Langmuir* **2006**, *22*, 5937–5944.

[86] Daikhin, L. I.; Urbakh, M. *J. Chem. Phys.* **2008**, *128*, 014706.

[87] Sczech, R.; Eckert, K.; Acker, M. *J. Phys. Chem. A* **2008**, *112*, 7357–7364.

[88] Liu, X. H.; Zhang, K.; Dong, C. W.; Zhang, S. H.; He, Y. H.; Wang, X. Y.; Lu, X. Q. *J. Phys. Chem. C* **2009**, *113*, 16015–16020.

[89] Kakiuchi, T. *J. Electroanal. Chem.* **2002**, *536*, 63–69.

[90] Callen, H. B. *Thermodynamics*; John Wiley & Sons, Inc.: New York, 1960.

[91] Kakiuchi, T.; Chiba, M.; Sezaki, N.; Nakagawa, M. *Electrochem. Commun.* **2002**, *4*, 701–704.

[92] Kakiuchi, T.; Nishi, N.; Kasahara, T.; Chiba, M. *ChemPhysChem* **2003**, *4*, 179–185.

[93] Kasahara, T.; Nishi, N.; Yamamoto, M.; Kakiuchi, T. *Langmuir* **2004**, *20*, 875–881.

[94] Kakiuchi, T. *J. Electroanal. Chem.* **2004**, *569*, 287–291.

[95] Sakka, T.; Tanaka, K.; Shibata, Y.; Ogata, Y. H. *J. Electroanal. Chem.* **2006**, *591*, 168–174.

[96] Kitazumi, Y.; Kakiuchi, T. *J. Phys.: Condens. Matter* **2007**, *19*, 375104.

[97] Kitazumi, Y.; Kakiuchi, T. *Langmuir* **2009**, *25*, 8062–8068.

[98] Kakiuchi, T. *J. Electroanal. Chem.* **2001**, *496*, 137–142.

[99] Islam, M. M.; Okajima, T.; Ohsaka, T. *Electrochem. Commun.* **2004**, *6*, 556–561.

[100] Islam, M. M.; Okajima, T.; Ohsaka, T. *J. Phys. Chem. B* **2006**, *110*, 8619–8625.

[101] Kitazumi, Y.; Kakiuchi, T. *Langmuir* **2009**, *25*, 10829–10833.

Chapter 1

A model of the electrochemical instability at the liquid-liquid interface based on the potential-dependent adsorption and Gouy's double layer theory

A new model has been formulated for the electrochemical instability at the liquid|liquid interface, for which only a rudimentary model (T. Kakiuchi *J. Electroanal. Chem. 536* (2002) 63-69) had been available. The new model considers the diffuse double layers in the presence of the specifically adsorbed surface-active ions, whose adsorption Gibbs energy linearly varies with the phase-boundary potential. The electrocapillary equation in the presence of the common ions partitioning in both phases is employed under the assumption that the partition of the surface-active ions is described by the Nernst equation. The excess surface charge due to the specific adsorption of surface active ions is allowed for in calculating the structure of the diffuse part of the electrical double layers on both sides of the interface. The calculated electrocapillary curves agree with the experimental results. Electrocapillary curves may have positive curvature

in a certain potential region, which signifies the presence of an instability window.

1.1 Introduction

The electrochemical instability (EI) is a thermodynamic instability of the liquid-liquid interface caused by the potential-dependent adsorption of surface-active ions [1]. The EI has been observed in various liquid-liquid two-phase systems containing surface-active ions [2–12], which fact suggests the general significance of the potential-dependent adsorption of surface-active ions in a variety of surface phenomena [13]. The EI is a pivotal concept to explain abnormal interfacial phenomena, such as spontaneous emulsification [14–17] and oscillation of the interfacial tension or phase-boundary potential [18–21]. The previous model of the EI assumed that structure of the electrical double layer (EDL) is independent of the specific adsorption of surface-active ions, i.e., the variation in the interfacial tension (γ) due to the specific adsorption of the ions and that due to the presence of the diffuse double layer are additive [1]. Although this simplistic model can explain the salient features of EI [1], it is obviously an oversimplification to neglect the effect of specifically adsorbed ions on the structure of the diffuse part of the EDL. A more realistic model of the EI should be formulated by taking into account the effect of the specific adsorption of surface-active ions on the structure of the diffuse double layer. In this work, we have developed an improved model of the EI, allowing for the effect of specifically adsorbed surface-active ions on the structure of the diffuse double layer, for which we used the Gouy's theory [22]. When a charge transfer across an electrochemical interface, either a liquid-liquid or liquid-metal, takes place under the external control of the phase-boundary potential, the interface is nonpolarized with respect to the relevant chemical species, because the phase-boundary potential is uniquely related to their compositions in both phases. Even in such a situation, we can still control the phase-boundary potential through a potentiostat or other appropriate means, although the interface is not rigorously a completely polarized interface. To deal with such partially nonpolarized interface relevant to the EI, the electrocapillary equation for the liquid|liquid interface in the presence of ionic components distributed between the two phases is formulated.

1.2 Theoretical

1.2.1 Electrocapillary equation.

To consider the structure of the interface between two immiscible electrolyte solutions in the presence of surface-active ions that not only adsorb at the interface but distribute between the two phases, we start with an electrocapillary equation for a nonpolarized interface where the distribution of constituent ionic species may take place [23].

An electrochemical cell containing a liquid-liquid interface may be represented as:

$$\mathrm{M|R1|O|W|R2|M'}, \tag{1.1}$$

where M and M' are the same metal, R1 is a reference electrode reversible to a cation in the oil phase (O), and R2 is a reference electrode reversible to an anion in the water phase (W). The phase O contains i cations, j anions, and k neutral components, while the phase W contains p cations, q anions, and h neutral components. Among these ions, α cations and β anions, and l neutral components exist in both phases. The potential of M' with respect to the M in the cell (1) is denoted as $E^{\mathrm{W}-}_{\mathrm{O}+}$. The salts $i'j'$ and $q'p'$ are the indicator salts composed of the ions reversible to R1 and R2, and l' and l'' are the reference components for surface excesses quantities. When the interface between O and W is planar, the electrocapillary equation of the

cell (1) is expressed as follows [23]

$$
\begin{aligned}
-\mathrm{d}\gamma = &\left(\eta - J\overline{s}^{\mathrm{O}} - K\overline{s}^{\mathrm{W}} + \frac{Q^{\mathrm{O}}}{F}\left(\frac{s_{R1}}{z_{i'}} + \frac{s_{R2}}{|z_{q'}|}\right)\right)\mathrm{d}T \\
&- \left(\tau - J\overline{v}^{\mathrm{O}} - K\overline{v}^{\mathrm{W}} + \frac{Q^{\mathrm{O}}}{F}\left(\frac{v_{R1}}{z_{i'}} + \frac{v_{R2}}{|z_{q'}|}\right)\right)\mathrm{d}P \\
&+ \sum_{k\neq l}\left(\Gamma_k - Jx_k^{\mathrm{O}}\right)\mathrm{d}\mu_k + \sum_{h\neq l}\left(\Gamma_h - Kx_h^{\mathrm{W}}\right)\mathrm{d}\mu_h + \sum_{l\neq l',l''}\left(\Gamma_l - Jx_l^{\mathrm{O}} - Kx_l^{\mathrm{W}}\right)\mathrm{d}\mu_l \\
&+ \sum_{i\neq i',\alpha}\left(\frac{\Gamma_i}{\nu_{ij'}^{+}} - Jx_{ij'}^{\mathrm{O}}\right)\mathrm{d}\mu_{ij'} + \sum_{j\neq j',\beta}\left(\frac{\Gamma_j}{\nu_{i'j}^{-}} - Jx_{i'j}^{\mathrm{O}}\right)\mathrm{d}\mu_{i'j} \\
&+ \sum_{p\neq p',\alpha}\left(\frac{\Gamma_p}{\nu_{pq'}^{+}} - Kx_{pq'}^{\mathrm{W}}\right)\mathrm{d}\mu_{pq'} + \sum_{q\neq q',\beta}\left(\frac{\Gamma_q}{\nu_{p'q}^{-}} - Kx_{p'q}^{\mathrm{W}}\right)\mathrm{d}\mu_{p'q} \\
&+ \sum_{\alpha}\left(\frac{\Gamma_\alpha}{\nu_{\alpha q'}^{+}} - Jx_{\alpha j'}^{\mathrm{O}}\frac{\nu_{\alpha j'}^{+}}{\nu_{\alpha q'}^{+}} - Kx_{\alpha q'}^{\mathrm{W}}\right)\mathrm{d}\mu_{\alpha q'} + \sum_{\beta}\left(\frac{\Gamma_\beta}{\nu_{p'\beta}^{-}} - Jx_{i'\beta}^{\mathrm{O}}\frac{\nu_{i'\beta}^{-}}{\nu_{p'\beta}^{-}} - Kx_{p'\beta}^{\mathrm{W}}\right)\mathrm{d}\mu_{p'\beta} \\
&+ \frac{1}{\nu_{i'j'}^{-}}\left(\Gamma_{i'} - \sum_{i\neq i',\alpha}\frac{z_i}{|z_{j'}|}\Gamma_i - J\sum_{\alpha}\nu_{\alpha j'}^{-}x_{\alpha j'}^{\mathrm{O}} - J\nu_{p'j'}^{-}x_{p'j'}^{\mathrm{O}} - K\nu_{p'j'}^{-}x_{p'j'}^{\mathrm{W}} - J\nu_{i'j'}^{-}x_{i'j'}^{\mathrm{O}}\right)\mathrm{d}\mu_{i'j'} \\
&+ \frac{1}{\nu_{p'q'}^{+}}\left(\Gamma_{p'} - \sum_{q\neq q'}\frac{|z_q|}{z_{p'}}\Gamma_q + J\sum_{\beta}\frac{|z_\beta|}{z_{p'}}\nu_{i'\beta}^{-}x_{i'\beta}^{\mathrm{O}} - J\nu_{p'j'}^{+}x_{p'j'}^{\mathrm{O}} - K\nu_{p'j'}^{+}x_{p'j'}^{\mathrm{W}} - K\nu_{p'q'}^{+}x_{p'q'}^{\mathrm{W}}\right)\mathrm{d}\mu_{p'q'} \\
&- Q^{\mathrm{O}}\mathrm{d}E_{\mathrm{O}+}^{\mathrm{W}-}, \quad (1.2)
\end{aligned}
$$

where Q^{O}, J, and K are given by

$$
\begin{aligned}
-\frac{Q^{\mathrm{O}}}{F} = &\sum_{p} z_p\Gamma_p - \sum_{q}|z_q|\Gamma_q - J\sum_{\alpha}|z_{j'}|\nu_{\alpha j'}^{-}x_{\alpha j'}^{\mathrm{O}} \\
&+ J\sum_{\beta} z_{i'}\nu_{i'\beta}^{+}x_{i'\beta}^{\mathrm{O}} + J\left(z_{i'}\nu_{i'q'}^{+}x_{i'q'}^{\mathrm{O}} - |z_{j'}|\nu_{p'j'}^{-}x_{p'j'}^{\mathrm{O}}\right) \\
&+ K\left(z_{i'}\nu_{i'q'}^{+}x_{i'q'}^{\mathrm{W}} - |z_{j'}|\nu_{p'j'}^{-}x_{p'j'}^{\mathrm{W}}\right), \quad (1.3)
\end{aligned}
$$

$$
J = \frac{\Gamma_{l''}x_{l'}^{\mathrm{W}} - \Gamma_{l'}x_{l''}^{\mathrm{W}}}{x_{l'}^{\mathrm{W}}x_{l''}^{\mathrm{O}} - x_{l'}^{\mathrm{O}}x_{l''}^{\mathrm{W}}}, \quad (1.4)
$$

and

$$
K = \frac{\Gamma_{l'}x_{l''}^{\mathrm{O}} - \Gamma_{l''}x_{l'}^{\mathrm{O}}}{x_{l'}^{\mathrm{W}}x_{l''}^{\mathrm{O}} - x_{l'}^{\mathrm{O}}x_{l''}^{\mathrm{W}}}. \quad (1.5)
$$

The symbols, Γ, x, z, ν, T, P, and F denote the surface excess, the mole fraction, the charge of an ion, the stoichiometric number of an ion in a salt, the absolute temperature, the pressure, and the Faraday constant, respectively. The superscripts W and O denote the phase W and

O, respectively. The subscripts i, j, k, ... designate the chemical species. The symbols $\overline{s}$, $\overline{v}$, η, and τ denote the mean molar entropy of bulk phase, the mean molar volume of bulk phase, the entropy of the surface phase, and the thickness of the surface phase, respectively. The quantities $\mu^{\cdot}$, $s^{\cdot}$, and $v^{\cdot}$ are linear combinations of the chemical potentials, the molar entropies, and the molar volumes of the neutral substances involved in the electrochemical reactions at the reference electrodes, respectively.

Assuming that the activity coefficients are unity, the Nernst equation for the partition of α and β is written in the form

$$E_{\mathrm{O}+}^{\mathrm{W}-} = E_{\alpha}^{\ominus} - \frac{RT}{z_{\alpha}F} \ln \frac{x_{\alpha q'}^{\mathrm{W}}}{x_{\alpha j'}^{\mathrm{O}}} = E_{\beta}^{\ominus} + \frac{RT}{|z_{\beta}|F} \ln \frac{x_{p'\beta}^{\mathrm{W}}}{x_{i'\beta}^{\mathrm{O}}}, \tag{1.6}$$

where $E^{\ominus}$ is $E_{\mathrm{O}+}^{\mathrm{W}-}$ when the activity of an ion in O is equal to that in W.

The total amounts of α (X_{α}) and β (X_{β}) in the system are defined as

$$m^{\mathrm{W}} x_{\alpha q'}^{\mathrm{W}} + m^{\mathrm{O}} x_{\alpha j'}^{\mathrm{O}} = X_{\alpha} \tag{1.7}$$

and

$$m^{\mathrm{W}} x_{p'\beta}^{\mathrm{W}} + m^{\mathrm{O}} x_{i'\beta}^{\mathrm{O}} = X_{\beta}, \tag{1.8}$$

where m^{W} and m^{O} are the total amounts of chemical species in W and O, respectively. According to equations 1.6 $\sim$ 1.8, the mole fractions of salts contained α and β are written as

$$x_{\alpha j'}^{\mathrm{O}} = \frac{X_{\alpha}}{m^{\mathrm{W}}\xi_{\alpha} + m^{\mathrm{O}}}, \tag{1.9}$$

$$x_{\alpha q'}^{\mathrm{W}} = \frac{X_{\alpha}\xi_{\alpha}}{m^{\mathrm{W}}\xi_{\alpha} + m^{\mathrm{O}}}, \tag{1.10}$$

$$x_{i'\beta}^{\mathrm{O}} = \frac{X_{\beta}}{m^{\mathrm{W}}\xi_{\beta} + m^{\mathrm{O}}}, \tag{1.11}$$

and

$$x_{p'\beta}^{\mathrm{W}} = \frac{X_{\beta}\xi_{\beta}}{m^{\mathrm{W}}\xi_{\beta} + m^{\mathrm{O}}}, \tag{1.12}$$

where, ξ_{α} and ξ_{β} are given by

$$\xi_{\alpha} = \exp\left[-\frac{z_{\alpha}F}{RT}\left(E_{\mathrm{O}+}^{\mathrm{W}-} - E_{\alpha}^{\ominus}\right)\right] \tag{1.13}$$

and

$$\xi_\beta = \exp\left[\frac{|z_\beta|F}{RT}\left(E^{\mathrm{W}-}_{\mathrm{O}+} - E^{\ominus}_{\beta}\right)\right]. \tag{1.14}$$

The derivatives of the logarithms of mole fractions are expressed as

$$\mathrm{d}\ln x^{\mathrm{W}}_{\alpha q'} = \mathrm{d}\ln X_\alpha - \frac{z_\alpha F}{RT}\mathrm{d}E^{\mathrm{W}-}_{\mathrm{O}+} + \frac{z_\alpha F}{RT}\frac{m^{\mathrm{W}}\xi_\alpha}{m^{\mathrm{O}} + m^{\mathrm{W}}\xi_\alpha}\mathrm{d}E^{\mathrm{W}-}_{\mathrm{O}+} \tag{1.15}$$

and

$$\mathrm{d}\ln x^{\mathrm{W}}_{p'\beta} = \mathrm{d}\ln X_\beta + \frac{|z_\beta|F}{RT}\mathrm{d}E^{\mathrm{W}-}_{\mathrm{O}+} - \frac{|z_\beta|F}{RT}\frac{m^{\mathrm{W}}\xi_\beta}{m^{\mathrm{O}} + m^{\mathrm{W}}\xi_\beta}\mathrm{d}E^{\mathrm{W}-}_{\mathrm{O}+}. \tag{1.16}$$

Substitution of equations 1.9 $\sim$ 1.16 into equation 1.2 to eliminate the chemical potential

terms of the salts contained α and β, we obtain

$$
\begin{aligned}
-\mathrm{d}\gamma = & \left[\eta - J\overline{s}^{\mathrm{O}} - K\overline{s}^{\mathrm{W}} + \frac{Q^{\mathrm{O}}}{F}\left(\frac{s_{R1}}{z_{i'}} + \frac{s_{R2}}{|z_{q'}|}\right)\right]\mathrm{d}T \\
& - \left[\tau - J\overline{v}^{\mathrm{O}} - K\overline{v}^{\mathrm{W}} + \frac{Q^{\mathrm{O}}}{F}\left(\frac{v_{R1}}{z_{i'}} + \frac{v_{R2}}{|z_{q'}|}\right)\right]\mathrm{d}P \\
& + \sum_{k\neq l}\left(\Gamma_k - Jx_k^{\mathrm{O}}\right)\mathrm{d}\mu_k + \sum_{h\neq l}\left(\Gamma_h - Kx_h^{\mathrm{W}}\right)\mathrm{d}\mu_h + \sum_{l\neq l',l''}\left(\Gamma_l - Jx_l^{\mathrm{O}} - Kx_l^{\mathrm{W}}\right)\mathrm{d}\mu_l \\
& + \sum_{i\neq i',\alpha}\left(\frac{\Gamma_i}{\nu_{ij'}^{+}} - Jx_{ij'}^{\mathrm{O}}\right)\mathrm{d}\mu_{ij'} + \sum_{j\neq j',\beta}\left(\frac{\Gamma_j}{\nu_{i'j}^{-}} - Jx_{i'j}^{\mathrm{O}}\right)\mathrm{d}\mu_{i'j} \\
& + \sum_{p\neq p',\alpha}\left(\frac{\Gamma_p}{\nu_{pq'}^{+}} - Kx_{pq'}^{\mathrm{W}}\right)\mathrm{d}\mu_{pq'} + \sum_{q\neq q',\beta}\left(\frac{\Gamma_q}{\nu_{p'q}^{-}} - Kx_{p'q}^{\mathrm{W}}\right)\mathrm{d}\mu_{p'q} \\
& + \frac{1}{\nu_{i'j'}^{-}}\left[\Gamma_{i'} - \sum_{i\neq i',\alpha}\frac{z_i\Gamma_i}{|z_{j'}|} - J\sum_{\alpha}\left(\frac{\nu_{\alpha j'}^{-}X_\alpha}{m^{\mathrm{W}}\xi_\alpha + m^{\mathrm{O}}}\right)\right. \\
& \qquad \left. - \nu_{p'j'}^{-}\left(Jx_{p'j'}^{\mathrm{O}} + Kx_{p'j'}^{\mathrm{W}}\right) - J\nu_{i'j'}^{-}x_{i'j'}^{\mathrm{O}}\right]\mathrm{d}\mu_{i'j'} \\
& + \frac{1}{\nu_{p'q'}^{+}}\left[\Gamma_{p'} - \sum_{q\neq q'}\frac{|z_q|\Gamma_q}{z_{p'}} + \frac{J}{z_{p'}}\sum_{\beta}\left(\frac{|z_\beta|\nu_{i'\beta}^{-}X_\beta}{m^{\mathrm{W}}\xi_\beta + m^{\mathrm{O}}}\right)\right. \\
& \qquad \left. - \nu_{p'j'}^{+}\left(Jx_{p'j'}^{\mathrm{O}} + Kx_{p'j'}^{\mathrm{W}}\right) - K\nu_{p'q'}^{+}x_{p'q'}^{\mathrm{W}}\right]\mathrm{d}\mu_{p'q'} \\
& + RT\sum_{\alpha}\left[\frac{\Gamma_\alpha}{\nu_{\alpha q'}^{+}} - \frac{X_\alpha}{m^{\mathrm{W}}\xi_\alpha + m^{\mathrm{O}}}\left(J\frac{\nu_{\alpha j'}^{+}}{\nu_{\alpha q'}^{+}} + K\xi_\alpha\right)\right]\mathrm{d}\ln X_\alpha \\
& + RT\sum_{\beta}\left[\frac{\Gamma_\beta}{\nu_{p'\beta}^{-}} - \frac{X_\beta}{m^{\mathrm{W}}\xi_\beta + m^{\mathrm{O}}}\left(J\frac{\nu_{i'\beta}^{-}}{\nu_{p'\beta}^{-}} + K\xi_\beta\right)\right]\mathrm{d}\ln X_\beta \\
& - F\left\{-\sum_{p\neq\alpha}z_p\Gamma_p + \sum_{q\neq\beta}|z_q|\Gamma_q\right. \\
& \quad + \sum_{\alpha}\frac{z_\alpha}{\nu_{\alpha q'}^{+}}\left[\left(1-\nu_{\alpha q'}^{+}\right)\Gamma_\alpha - \frac{\left(\nu_{\alpha q'}^{+}KX_\alpha + \Gamma_\alpha m^{\mathrm{W}}\right)\xi_\alpha - JX_\alpha\nu_{\alpha j'}^{+}\left(\nu_{\alpha q'}^{+}-1\right)}{m^{\mathrm{W}}\xi_\alpha + m^{\mathrm{O}}}\right. \\
& \qquad \left. + \frac{\left(J\nu_{\alpha j'}^{+} + \nu_{\alpha q'}^{+}K\xi_\alpha\right)X_\alpha m^{\mathrm{W}}\xi_\alpha}{\left(m^{\mathrm{W}}\xi_\alpha + m^{\mathrm{O}}\right)^2}\right] \\
& \quad - \sum_{\beta}\frac{|z_\beta|}{\nu_{p'\beta}^{-}}\left[\left(1-\nu_{p'\beta}^{-}\right)\Gamma_\beta - \frac{JX_\beta\nu_{i'\beta}^{-}\left(\nu_{p'\beta}^{-}-1\right) - \left(\nu_{p'\beta}^{-}KX_\beta + \Gamma_\beta m^{\mathrm{W}}\right)\xi_\beta}{m^{\mathrm{W}}\xi_\beta + m^{\mathrm{O}}}\right. \\
& \qquad \left. - \frac{\left(J\nu_{i'\beta}^{-} + \nu_{p'\beta}^{-}K\xi_\beta\right)X_\beta m^{\mathrm{W}}\xi_\beta}{\left(m^{\mathrm{W}}\xi_\beta + m^{\mathrm{O}}\right)^2}\right] \\
& \quad \left. - J\left(z_{i'}\nu_{i'q'}^{+}x_{i'q'}^{\mathrm{O}} - |z_{j'}|\nu_{p'j'}^{-}x_{p'j'}^{\mathrm{O}}\right) - K\left(z_{i'}\nu_{i'q'}^{+}x_{i'q'}^{\mathrm{W}} - |z_{j'}|\nu_{p'j'}^{-}x_{p'j'}^{\mathrm{W}}\right)\right\}\mathrm{d}E_{\mathrm{O}+}^{\mathrm{W}-}.
\end{aligned}
\tag{1.17}
$$

The differentiation of γ with respect to $E^{\mathrm{W}-}_{\mathrm{O}+}$ at constant T, P, and μ, except the salts including α and β, gives

$$\left(\frac{\partial\gamma}{\partial E^{\mathrm{W}-}_{\mathrm{O}+}}\right)_{T,P,\mu_{ij,pq},k,h,l} = F\left\{-\sum_{p\neq\alpha} z_p\Gamma_p + \sum_{q\neq\beta}|z_q|\Gamma_q \right.$$
$$+\sum_{\alpha}\frac{z_\alpha}{\nu^+_{\alpha q'}}\left[\left(1-\nu^+_{\alpha q'}\right)\Gamma_\alpha + \frac{JX_\alpha\nu^+_{\alpha j'}\left(\nu^+_{\alpha q'}-1\right)-\left(\nu^+_{\alpha q'}KX_\alpha+\Gamma_\alpha m^{\mathrm{W}}\right)\xi_\alpha}{m^{\mathrm{W}}\xi_\alpha+m^{\mathrm{O}}}\right.$$
$$\left.-\frac{\left(-J\nu^+_{\alpha j'}-\nu^+_{\alpha q'}K\xi_\alpha\right)X_\alpha m^{\mathrm{W}}\xi_\alpha}{\left(m^{\mathrm{O}}+m^{\mathrm{W}}\xi_\alpha\right)^2}\right]$$
$$-\sum_{\beta}\frac{|z_\beta|}{\nu^-_{p'\beta}}\left[\left(1-\nu^-_{p'\beta}\right)\Gamma_\beta - \frac{JX_\beta\nu^-_{i'\beta}\left(\nu^-_{p'\beta}-1\right)-\left(\nu^-_{p'\beta}KX_\beta+\Gamma_\beta m^{\mathrm{W}}\right)\xi_\beta}{m^{\mathrm{W}}\xi_\beta+m^{\mathrm{O}}}\right.$$
$$\left.-\frac{\left(J\nu^-_{i'\beta}+\nu^-_{p'\beta}K\xi_\beta\right)X_\beta m^{\mathrm{W}}\xi_\beta}{\left(m^{\mathrm{O}}+m^{\mathrm{W}}\xi_\beta\right)^2}\right]$$
$$\left.-J\left(z_{i'}\nu^+_{i'q'}x^{\mathrm{O}}_{i'q'}-|z_{j'}|\nu^-_{p'j'}x^{\mathrm{O}}_{p'j'}\right)-K\left(z_{i'}\nu^+_{i'q'}x^{\mathrm{W}}_{i'q'}-|z_{j'}|\nu^-_{p'j'}x^{\mathrm{W}}_{p'j'}\right)\right\}. \quad (1.18)$$

The value

$$q = -\left(\frac{\partial\gamma}{\partial E^{\mathrm{W}-}_{\mathrm{O}+}}\right)_{T,P,\mu_{ij,pq},k,h,l} \quad (1.19)$$

is formally identified with the excess charge per unit area in W. We note that q is not the same as the excess surface charge density at a polarized interface, in that the commonly distributed ions obscure the unequivocal meaning of the excess surface charge density that belongs to either O or W. The value of q may be regarded as the surface charge density of a capacitor with the potential-dependent leakage with regards to α and β, which reduces to the double layer capacitance of a polarized liquid-liquid interface only when α and β are absent. Differentiating q with respect to $E^{\mathrm{W}-}_{\mathrm{O}+}$, we obtain the formal capacitance, C', of the interface

$$C' = \left(\frac{\partial q}{\partial E^{\mathrm{W}-}_{\mathrm{O}+}}\right)_{T,P,\mu_{ij,pq},k,h,l} = -\left(\frac{\partial^2\gamma}{\partial\left(E^{\mathrm{W}-}_{\mathrm{O}+}\right)^2}\right)_{T,P,\mu_{ij,pq},k,h,l}. \quad (1.20)$$

The electrochemically unstable condition of the interface [1], i.e., $\left(\partial^2\gamma/\partial\Delta^{\mathrm{W}}_{\mathrm{O}}\phi^2\right) > 0$, translates to the negative value of the formal capacitance $C' < 0$.

When an oil-water two-phase system contains a surface-active cation α distributed in the both phases, while monovalent ions p' and q' (i' and j') are present only in W (O), and X_α is

negligibly small. Then, equation 1.18 is simplified to

$$\left(\frac{\partial\gamma}{\partial E_{\mathrm{O}+}^{\mathrm{W}-}}\right)_{T,P,\mu_{i'j'},\mu_{p'q'}} = F\left(-\Gamma_{p'} + \Gamma_{q'} - \frac{z_\alpha \Gamma_\alpha m^{\mathrm{W}} \xi_\alpha}{m^{\mathrm{W}}\xi_\alpha + m^{\mathrm{O}}}\right). \tag{1.21}$$

Similarly, when a surface-active anion β distributes in the both phases and X_β is negligibly small, eq 1.18 reduces to

$$\left(\frac{\partial\gamma}{\partial E_{\mathrm{O}+}^{\mathrm{W}-}}\right)_{T,P,\mu_{i'j'},\mu_{p'q'}} = F\left(-\Gamma_{p'} + \Gamma_{q'} + \frac{|z_\beta| \Gamma_\beta m^{\mathrm{W}} \xi_\beta}{m^{\mathrm{W}}\xi_\beta + m^{\mathrm{O}}}\right). \tag{1.22}$$

On the other hand, the differentiation of γ with respect to the logarithms of X_α and X_β at constant T, P, $E_{\mathrm{O}+}^{\mathrm{W}-}$, and μ, expect the salts including α and β under the former conditions, gives

$$\left(\frac{\partial\gamma}{\partial \ln X_\alpha}\right)_{T,P,\mu_{ij,pq,k,h,l},E_{\mathrm{O}+}^{\mathrm{W}-}} = -RT\Gamma_\alpha \tag{1.23}$$

and

$$\left(\frac{\partial\gamma}{\partial \ln X_\beta}\right)_{T,P,\mu_{ij,pq,k,h,l},E_{\mathrm{O}+}^{\mathrm{W}-}} = -RT\Gamma_\beta. \tag{1.24}$$

Equations 1.23 and 1.24 mean that γ does not vary with the variations of X_α and X_β at the potential where the adsorbed amounts of α and β are virtually zero.

1.2.2 Model of the interface without the inner layer.

To understand the EI, we first consider a simple model for the partially nonpolarized interface in the presence of the potential-dependent adsorption of surface-active ions adsorbed at the interface of two back-to-back diffuse parts of the double layers (Figure 1.1A). The relative permittivities of O and W and the permittivity of the vacuum are denoted as ε^{O}, ε^{W}, and ε_0, respectively. The concentrations of a hydrophobic 1:1 electrolyte in O and a hydrophilic 1:1 electrolyte in W are denoted as c^{O} and c^{W}, respectively. According to the Gouy theory [22], the charge per unit area of the diffuse double layer in O (q^{O}) is written in terms of the potential at the interface (ϕ^{i}) as

$$q^{\mathrm{O}} = -\sqrt{8\varepsilon_0\varepsilon^{\mathrm{O}}RTc^{\mathrm{O}}}\sinh\frac{F\left(\phi^{\mathrm{i}} - \phi^{\mathrm{O}}\right)}{2RT}, \tag{1.25}$$

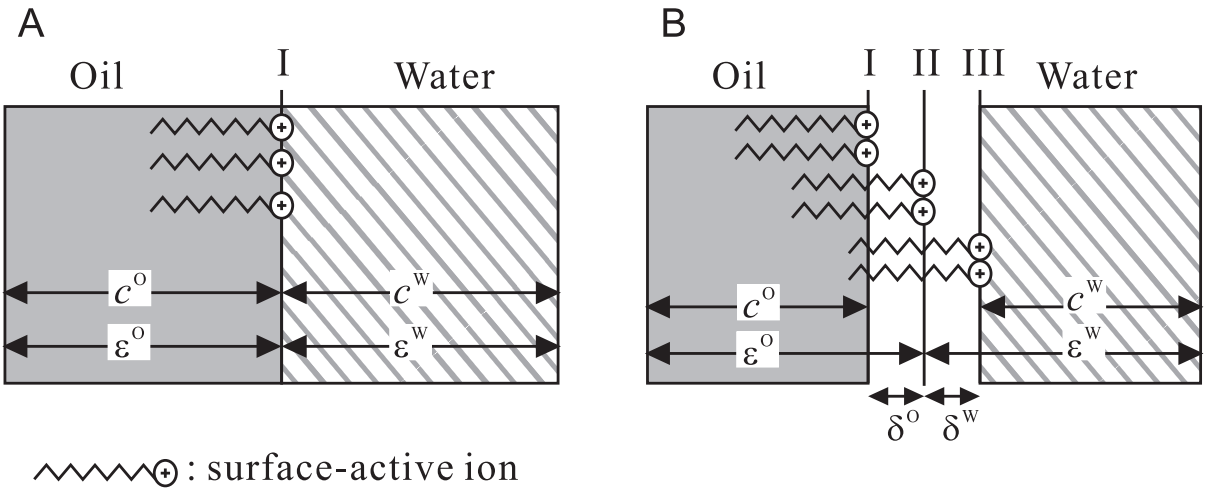

Figure 1.1: The models of the liquid-liquid interface without (A) and with (B) the inner layer. The symbols I, II, and III in B show the available positions of the adsorbed surface-active ions.

where ϕ^{O} is the bulk potential in O. The charge per unit area of diffuse double layer in W (q^{W}) is written by using the bulk potential in W (ϕ^{O}) as

$$q^{W} = -\sqrt{8\varepsilon_0 \varepsilon^{W} RT c^{W}} \sinh \frac{F\left(\phi^{i} - \phi^{W}\right)}{2RT}. \tag{1.26}$$

In this model, the charged moiety of specifically adsorbed surface-active ions (S) is located at the interface. The charge density caused by the specific adsorption of S is written as

$$q^{i} = z_S F \Gamma_{\max,S} \theta_S \tag{1.27}$$

where, θ_S is the surface coverage of S, $\Gamma_{\max,S}$ is the maximum adsorption of S, and z_S is the charge of S. We assume that the adsorption of S is described by the Frumkin isotherm [24]

$$\exp\left(-\frac{\Delta G^{W,\ominus}_{ads,S}}{RT}\right) c^{W}_{S} = \frac{\theta_S}{1-\theta_S} \exp(-2g\theta_S), \tag{1.28}$$

where $\Delta G^{W,\ominus}_{ads,S}$ is the standard adsorption Gibbs energy for the adsorption of S from W, g is the interaction parameter, and c^{W}_{S} is the bulk concentration of S in W. We further assume that the $\Delta G^{W,\ominus}_{ads,S}$ linearly varies with $\Delta^{W}_{O}\phi$ and is written in the form: [13]

$$\Delta G^{W,\ominus}_{ads,S} = \Delta G^{\ominus}_{ads,S} - z_S F (1-\beta)\left(\Delta^{W}_{O}\phi - \Delta^{W}_{O}\phi^{\ominus}_{S}\right), \tag{1.29}$$

where $\Delta_{\mathrm{O}}^{\mathrm{W}}\phi_{\mathrm{S}}^{\mathrm{e}}$ is the standard transfer potential of S, z_{S} is the charge of S and $\Delta G_{\mathrm{ads,S}}^{\mathrm{e}}$ is the standard adsorption energy of S at $\Delta_{\mathrm{O}}^{\mathrm{W}}\phi_{\mathrm{S}}^{\mathrm{e}}$. The bulk concentrations of S in O and W, $c_{\mathrm{S}}^{\mathrm{O}}$ and $c_{\mathrm{S}}^{\mathrm{W}}$, are related through the Nernst equation. We assumed that the activity coefficients of S in W and O are unity. Assuming that the volume of O is equal to the volume of W, V, the mass balance is written as follows.

$$c_{\mathrm{S}}^{\mathrm{W}}V + c_{\mathrm{S}}^{\mathrm{O}}V = m_{\mathrm{S}}, \tag{1.30}$$

where m_{S} is the total amount of S in the system.

The electroneutrality condition of the interface is written as

$$q^{\mathrm{W}} + q^{\mathrm{O}} + q^{\mathrm{i}} = 0. \tag{1.31}$$

From the equations 1.25 $\sim$ 1.31, the values of q^{W}, q^{O},and q^{i} at a certain $\Delta_{\mathrm{O}}^{\mathrm{W}}\phi$ are determined. The value of q can then be as

$$q = q^{\mathrm{W}} + \frac{q^{\mathrm{i}} \exp\left[-\frac{z_{\mathrm{S}}F}{RT}\left(\Delta_{\mathrm{O}}^{\mathrm{W}}\phi - \Delta_{\mathrm{O}}^{\mathrm{W}}\phi_{\mathrm{S}}^{\mathrm{e}}\right)\right]}{1 + \exp\left[-\frac{z_{\mathrm{S}}F}{RT}\left(\Delta_{\mathrm{O}}^{\mathrm{W}}\phi - \Delta_{\mathrm{O}}^{\mathrm{W}}\phi_{\mathrm{S}}^{\mathrm{e}}\right)\right]}. \tag{1.32}$$

The values of

$$C = \frac{\mathrm{d}q}{\mathrm{d}\Delta_{\mathrm{O}}^{\mathrm{W}}\phi} \tag{1.33}$$

and

$$\gamma = -\int q \mathrm{d}\Delta_{\mathrm{O}}^{\mathrm{W}}\phi + \mathrm{const}, \tag{1.34}$$

are calculated, where const means the integration constant.

1.2.3 Model of the interface with the inner layer.

It is more realistic to suppose that the diffuse double layers are separated by an inner layer which contains no ion except specifically adsorbed S [25–27] (Figure 1.1B). The thicknesses of W side and O side of the inner layers are denoted as δ^{W} and δ^{O}, respectively. We assume that the permittivities in the inner layers are the same as the values in the respective bulk phases. In this model, the position of the charged parts of specifically adsorbed ions must be defined.

Three possible locations I, II, and III are shown in Figure 1.1B. The expressions for potential drop in the inner layers when S is adsorbed at the positions I, II, and III are written as

$$\phi_{\delta^{\mathrm{W}}}^{\mathrm{W}} - \phi_{\delta^{\mathrm{O}}}^{\mathrm{O}} = -\left(q^{\mathrm{i}} + q^{\mathrm{O}}\right)\left(\frac{\delta^{\mathrm{O}}}{\varepsilon_0\varepsilon^{\mathrm{O}}} + \frac{\delta^{\mathrm{W}}}{\varepsilon_0\varepsilon^{\mathrm{W}}}\right), \tag{1.35}$$

$$\phi_{\delta^{\mathrm{W}}}^{\mathrm{W}} - \phi_{\delta^{\mathrm{O}}}^{\mathrm{O}} = -q^{\mathrm{O}}\left(\frac{\delta^{\mathrm{O}}}{\varepsilon_0\varepsilon^{\mathrm{O}}} + \frac{\delta^{\mathrm{W}}}{\varepsilon_0\varepsilon^{\mathrm{W}}}\right) - q^{\mathrm{i}}\frac{\delta^{\mathrm{W}}}{\varepsilon_0\varepsilon^{\mathrm{W}}}, \tag{1.36}$$

and

$$\phi_{\delta^{\mathrm{W}}}^{\mathrm{W}} - \phi_{\delta^{\mathrm{O}}}^{\mathrm{O}} = -q^{\mathrm{O}}\left(\frac{\delta^{\mathrm{O}}}{\varepsilon_0\varepsilon^{\mathrm{O}}} + \frac{\delta^{\mathrm{W}}}{\varepsilon_0\varepsilon^{\mathrm{W}}}\right), \tag{1.37}$$

respectively, where $\phi_{\delta^{\mathrm{O}}}^{\mathrm{O}}$ is the potential at the position I in Figure 1.1B and $\phi_{\delta^{\mathrm{W}}}^{\mathrm{W}}$ is the potential at the position III in Figure 1.1B.

In this model, the charges in the diffuse double layers are written as

$$q^{\mathrm{O}} = -\sqrt{8\varepsilon_0\varepsilon^{\mathrm{O}}RTc^{\mathrm{O}}}\sinh\frac{F\left(\phi_{\delta^{\mathrm{O}}}^{\mathrm{O}} - \phi^{\mathrm{O}}\right)}{2RT} \tag{1.38}$$

and

$$q^{\mathrm{W}} = -\sqrt{8\varepsilon_0\varepsilon^{\mathrm{W}}RTc^{\mathrm{W}}}\sinh\frac{F\left(\phi_{\delta^{\mathrm{W}}}^{\mathrm{W}} - \phi^{\mathrm{W}}\right)}{2RT}. \tag{1.39}$$

The electroneutrality (equation 1.31) also holds in this model. The values of q, C, and γ at a given value of $\Delta_{\mathrm{O}}^{\mathrm{W}}\phi$ may be calculated from to equations 1.32, 1.33, and 1.34, respectively.

1.3 Results and Discussion

1.3.1 Potential-dependence of q and C based on the model without the inner layer.

The simple model without the inner layer will obviously show the effect of the adsorbed ions on the diffuse double layers. The following parameters are used in following the calculation: $c^{\mathrm{O}} = c^{\mathrm{W}} = 100$ mol m^{-3}, $\varepsilon^{\mathrm{O}} = 10$, $\varepsilon^{\mathrm{W}} = 78$, $\Gamma_{\mathrm{max,S}} = 8.5 \times 10^{-6}$ mol m^{-2}, $\Delta_{\mathrm{O}}^{\mathrm{W}}\phi_{\mathrm{S}}^{\ominus} = 0$ V, $\Delta G_{\mathrm{ads,S}}^{\ominus} = 0$ J mol^{-1}, $g = 1$, $z_{\mathrm{S}} = 1$, and $\beta = 0.9$. These parameters are selected to compare with the experimental results [11].

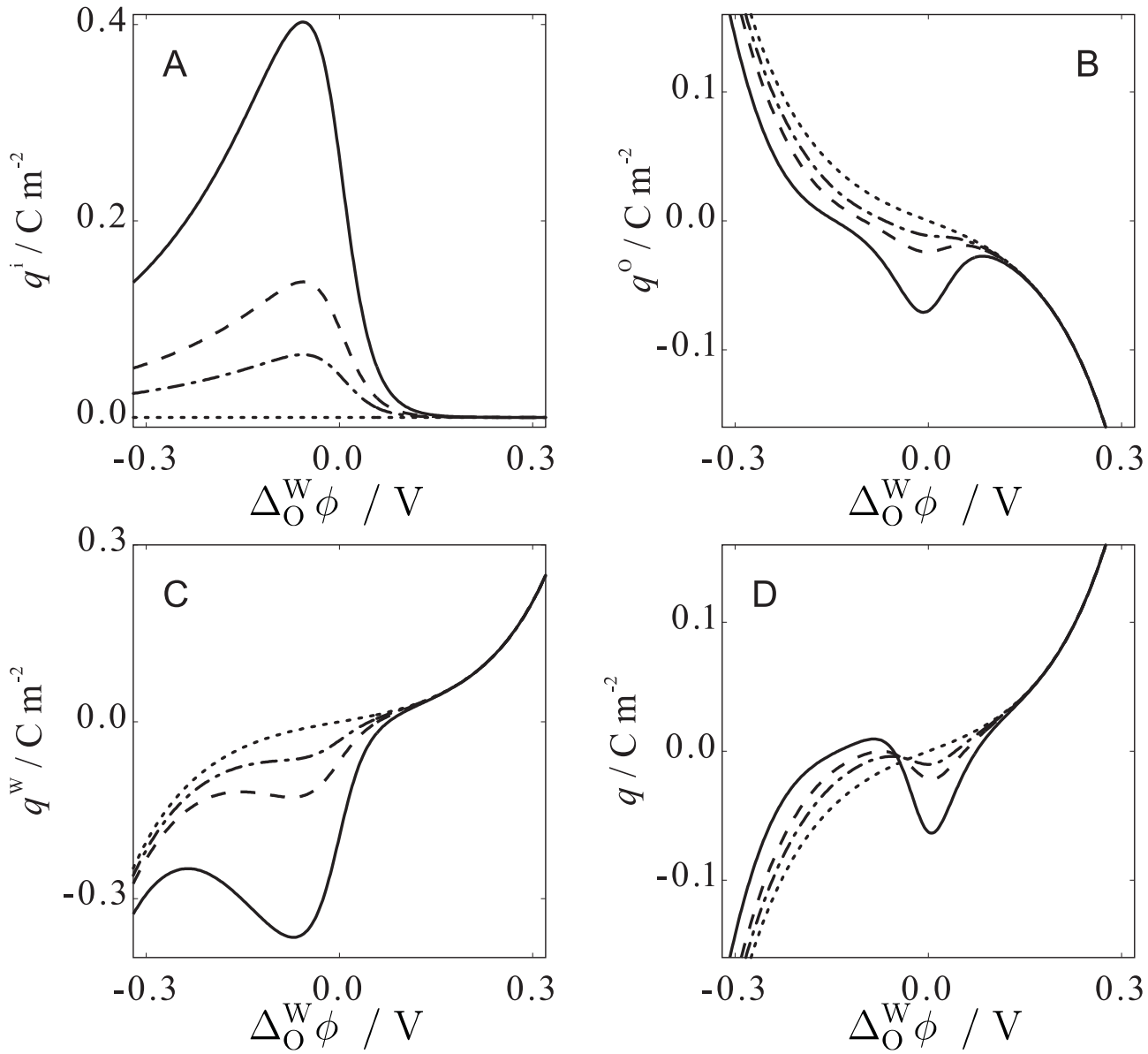

Figure 1.2: Potential-dependences of q^{i} (A), q^{O} (B), q^{W} (C) and q (D). The values of c_{S} are 0 (dotted lines), 0.1 (dash-dotted lines), 0.2 (broken lines), and 0.5 mol m^{-3} (solid lines).

Potential-dependencies of q^{i}, q^{O}, and q^{W} in the model in Figure 1.1A are shown in Figures 1.2A, 1.2B, and 1.2C at different value of c_{S}, respectively. The dotted lines in Figure 1.2 show the charges in the absence of S. The solid, broken, and dash-dotted lines show the charges when $c_{\mathrm{S}} = 0.5$, 0.2, and 0.1 mol m^{-1}, respectively. When $c_{\mathrm{S}} > 0.1$ mol m^{-3}, the regions with a positive slope in Figure 1.2B and a negative slope in Figure 1.2C are observed. The calculated q based on equation 1.32 is shown in Figure 1.2D. The negative slope of q appears in Figure 1.2D, for example, between -0.084 and -0.006 V on the solid line. In this potential-regions, the excess charge in W decreases with the increase of $\Delta_{\mathrm{O}}^{\mathrm{W}}\phi$. This potential-dependence of q means that the interface is under the EI.

To determine the potential range where the interface is under the EI (instability window, IW), C is calculated from the potential-dependence of q. Figure 1.3A shows the calculated C when $c_{\mathrm{S}} = 0$ (dotted line), 0.1 (dash-dotted line), 0.2 (broken line), and 0.5 mol m^{-3} (solid line). The curves in the presence of S in Figure 1.3A show the minimum at $\Delta_{\mathrm{O}}^{\mathrm{W}}\phi = -0.01$ V. The observed negative value of C means $\left(\partial^2\gamma/\partial\Delta_{\mathrm{O}}^{\mathrm{W}}\phi^2\right) > 0$, i.e., the interface is under the EI [1]. When c_{S} increases, the IW widens with its center remaining unchanged.

The calculated electrocapillary curves are shown in Figure 1.3B. The calculation was carried out assuming that θ_{S} at $\Delta_{\mathrm{O}}^{\mathrm{W}}\phi = 0.4$ V is zero. Such a merge of electrocapillary curves in the presence of surface-active ions to that in the absence of surfactant is typically observed in the positive branch experimentally for the adsorption of cationic surfactants [12].

The electrocapillary curves in the negative branch ($\Delta_{\mathrm{O}}^{\mathrm{W}}\phi < 0$) in Figure 1.3B depend on c_{S}. In the more negative potential region, γ increases with c_{S}, which shows the negative adsorption of S. According to equation 1.23, the negative adsorption of S is unrealistic. Therefore the model shown in Figure 1.1A are inadequate to describe the potential-dependent adsorption of ionic surfactant, although the model does exhibit an EI depending on the concentration of the surfactant.

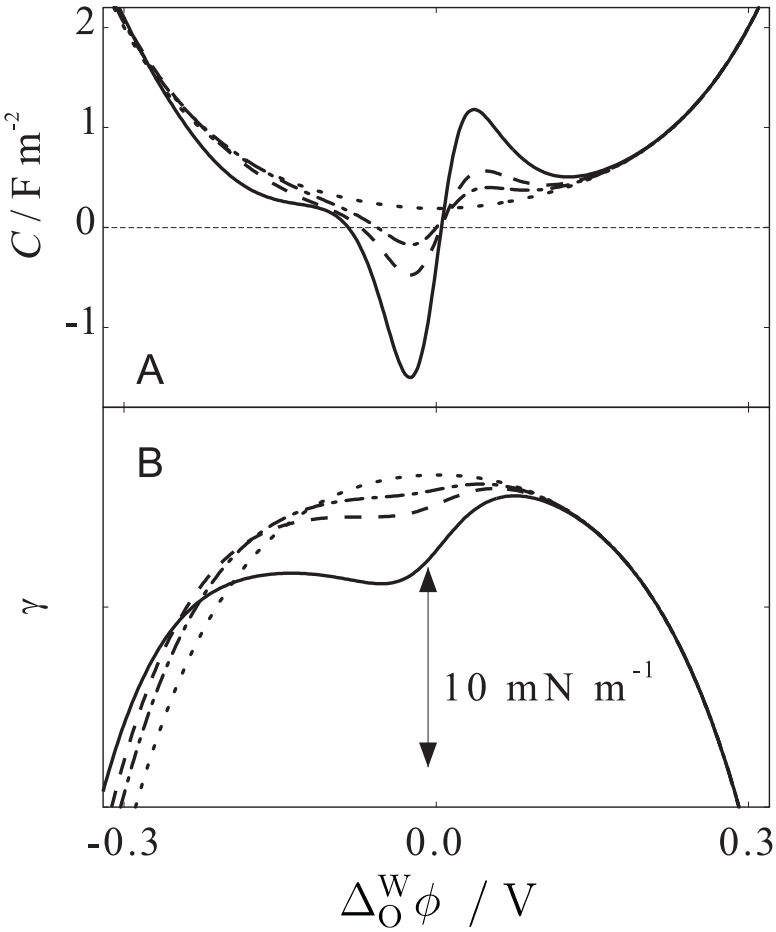

Figure 1.3: Potential-dependence of C (A) and γ (B), when $c_{\mathrm{S}} = 0$ (dotted lines), 0.1 (dash-dotted lines), 0.2 (broken lines), and 0.5 mol m^{-3} (solid lines).

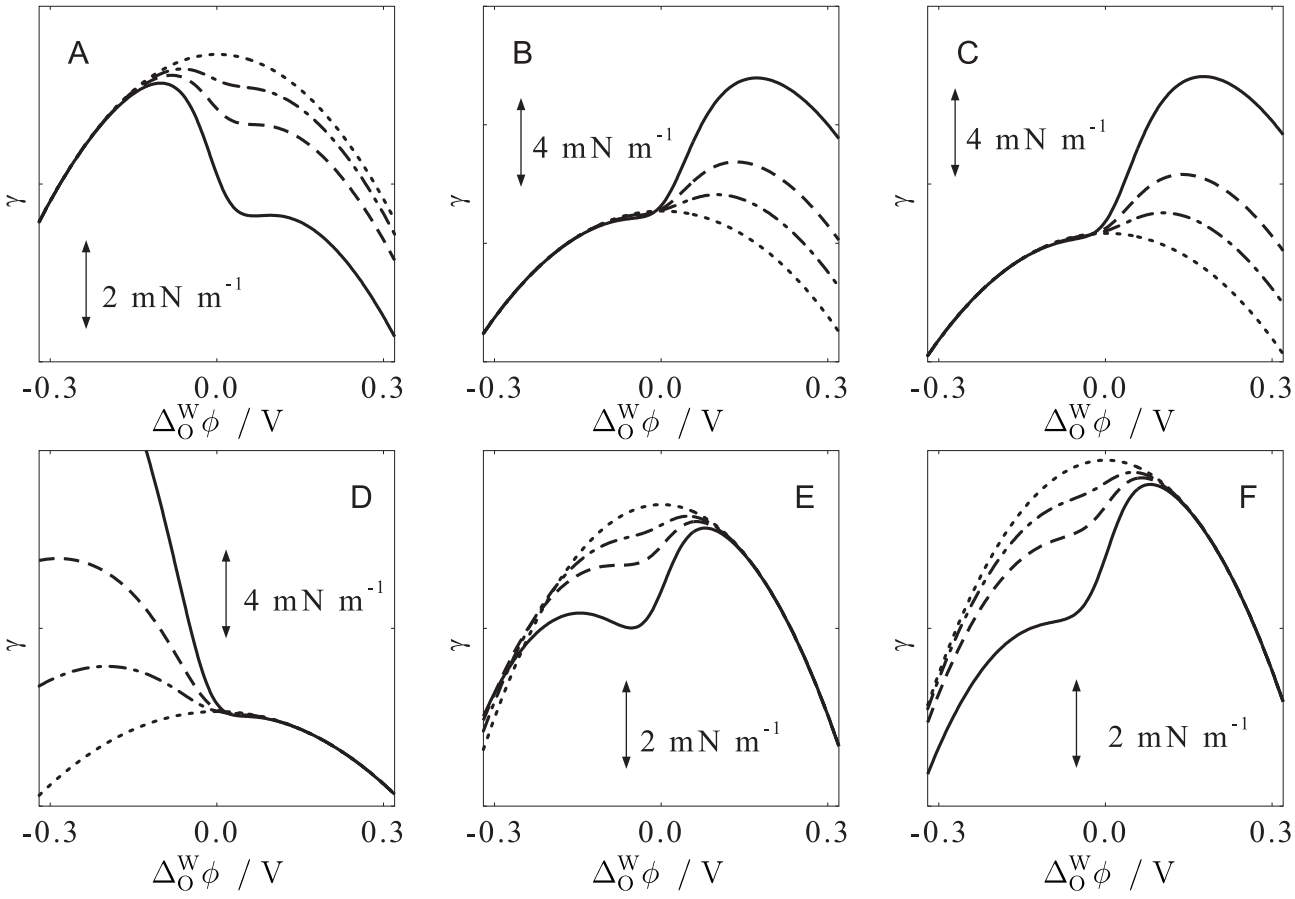

Figure 1.4: Effect of the position of the adsorbed surface-active ions and β parameters on the electrocapillary curves, when the adsorbed S exists at position I (A and D), II (B and E), and III (C and F) in Figure 1.1B. β is 0.3 (A, B, and C) and 0.9 (D, E, and F) and c_S is 0 (dotted lines), 50 (dash-dotted lines), 100 (broken lines), and 200 mol m^{-3} (solid lines).

1.3.2 Electrocapillarity based on the model with the inner layer.

In addition to the parameters used above, we introduced an inner layer of $\delta^{\mathrm{W}} = \delta^{\mathrm{O}} = 4 \times 10^{-10}$ m (Figure 1.1B) for calculating γ, q, and C. The effects of the positions of the adsorbed S (Figure 1.4B) and the value of β on the electrocapillary curves are shown in Figure 1.4. Figures 1.4A, 1.4B, and 1.4C show the electrocapillary curves calculated for $\beta = 0.3$ and Figures 1.4D, 1.4E, and 1.4F show the electrocapillary curves calculated for $\beta = 0.9$ when S is adsorbed at three different positions in Figure 1.1B, that is, the positions I (1.4A and 1.4D), II (1.4B and 1.4E), and III (1.4C and 1.4F). The dotted, dash-dotted, broken, and solid lines show the results when $c_{\mathrm{S}} = 0$, 0.05, 0.1, and 0.2 mol m^{-3}, respectively. The calculation of γ was carried out under the assumption that the adsorbed amount of α is virtually zero at $\Delta_{\mathrm{O}}^{\mathrm{W}}\phi = -0.4$ when $\beta = 0.3$ (Figures 1.4A, 1.4B, and 1.4C) and that at $\Delta_{\mathrm{O}}^{\mathrm{W}}\phi = 0.4$ when $\beta = 0.9$ (Figures 1.4D, 1.4E, and 1.4F).

When $\beta = 0.3$, the adsorption of S occurs mainly in the region, $\Delta_{\mathrm{O}}^{\mathrm{W}}\phi > \Delta_{\mathrm{O}}^{\mathrm{W}}\phi^{\mathrm{e}}$. However, the increase in γ with an increase in c_{S} is seen in Figures 1.4B and 1.4C. When $\beta = 0.9$, although the adsorbed amount of S in $\Delta_{\mathrm{O}}^{\mathrm{W}}\phi < \Delta_{\mathrm{O}}^{\mathrm{W}}\phi^{\mathrm{e}}$ is positive, the increase in γ with an increase in c_{S} is seen in Figure 1.4D. Also in Figure 1.4E, the negative adsorption of S appears when $\Delta_{\mathrm{O}}^{\mathrm{W}}\phi < -200$ mV. The negative adsorption shown in Figures 1.4B, 1.4C, 1.4D, and 1.4E indicates that those conditions are inadequate for reproducing experimental results [12].

The electrocapillary curves in Figures 1.4A and 1.4F when β is 0.3 and 0.9 are physically acceptable in the sense that the adsorption of surfactant does not raise γ. The electrocapillary curves in Figure 1.4F well reproduce experimental results for the adsorption of decylammonium with an experimental value of $\beta = 0.9$, showing strong adsorption when $\Delta_{\mathrm{O}}^{\mathrm{W}}\phi < 0$ mV and no adsorption when $\Delta_{\mathrm{O}}^{\mathrm{W}}\phi > 0$ mV [11]. In contrast, when $\beta = 0.3$ (Figure 1.4A), the potential-dependency of the adsorption is opposite. The calculated electrocapillary curves in Figure 1.4 suggest that the magnitude of β is related to the position of the adsorption. When the S has a high β value, the adsorption of S from W is little depend on $\Delta_{\mathrm{O}}^{\mathrm{W}}\phi$, that is, the potential at the bulk of the W phase is nearly equal to the potential at the location of the adsorbed ions.

Then, the charged part of the specifically adsorbed S would exist at the aqueous side of the interfacial region (position III in Figure 1.1B). When S has a low β value, the charged part of S would exist at the oil side of the interfacial region (position I in Figure 1.1B). The magnitude of β may thus be taken to be a parameter to infer the position of specifically adsorbed ions.

Capacitance of the liquid-liquid interface.

Since the liquid-liquid interface shown as the model in Figure 1.1B is seen as the series-connected capacitors, the value of C is written as follows.

$$\frac{1}{C} = \frac{1}{C^{\mathrm{O}}} + \frac{1}{C^{\mathrm{W}}} + \frac{1}{C^{\mathrm{i}}}, \tag{1.40}$$

where C^{O}, C^{W}, and C^{i} are the capacitance of the diffuse layer in W, the capacitance of the diffuse layer in O, and the capacitance of the inner layer. Figure 1.5A shows the potential-dependence of C when $\beta = 0.9$ and S adsorbs at the position III in Figure 1.1B. The dotted lines, dash-dotted lines, broken lines, and solid lines in Figure 1.5 shows the curves calculated at $c_{\mathrm{S}} = 0$, 0.05, 0.1, and 0.2 mol m^{-3}, respectively. The introduction of the inner layer weakens the potential-dependence of C at $c_{\mathrm{S}} = 0$ and widens the width of the IW at $c_{\mathrm{S}} = 0.1$ mol m^{-3} from 56 mV in Figure 1.3A to 90 mV in Figure 1.5A.

Figure 1.5B and C show the potential-dependence of calculated C^{O} and C^{W} from the Gouy's theory using $\phi^{\mathrm{O}}_{\delta\mathrm{O}}$ and $\phi^{\mathrm{W}}_{\delta\mathrm{W}}$, respectively. Since the values of $\phi^{\mathrm{O}}_{\delta\mathrm{O}}$ and $\phi^{\mathrm{W}}_{\delta\mathrm{W}}$ change with the adsorption of S, the values of C^{O} and C^{W} depend on c_{S} in the potential region where S adsorbs at the interface. The adsorption of S increases C^{W} and decreases C^{O} except the potential region around $\Delta^{\mathrm{W}}_{\mathrm{O}}\phi^{\ominus}_{\mathrm{S}}$. Around $\Delta^{\mathrm{W}}_{\mathrm{O}}\phi^{\ominus}_{\mathrm{S}}$, C^{O} increases with the increase of c_{S}. The effect of the adsorbed S on C^{W} is greater than that on C^{O}. The difference between the potential-dependence of C^{O} and the potential-dependence of C^{W} reflects the permittivities of the phases and the position of the adsorbed S.

The potential-dependence of C^{i} is shown in Figure 1.5D. When $c_{\mathrm{S}} = 0$, C^{i} is independent of $\Delta^{\mathrm{W}}_{\mathrm{O}}\phi$ and the value is 0.196 F m^{-2} in this condition. In the potential region where $\Delta^{\mathrm{W}}_{\mathrm{O}}\phi < -0.2$ V and $\Delta^{\mathrm{W}}_{\mathrm{O}}\phi > 0.15$ V, C^{i} hardly depends on c_{S}. In the IW, C^{i} contributes to the main part of

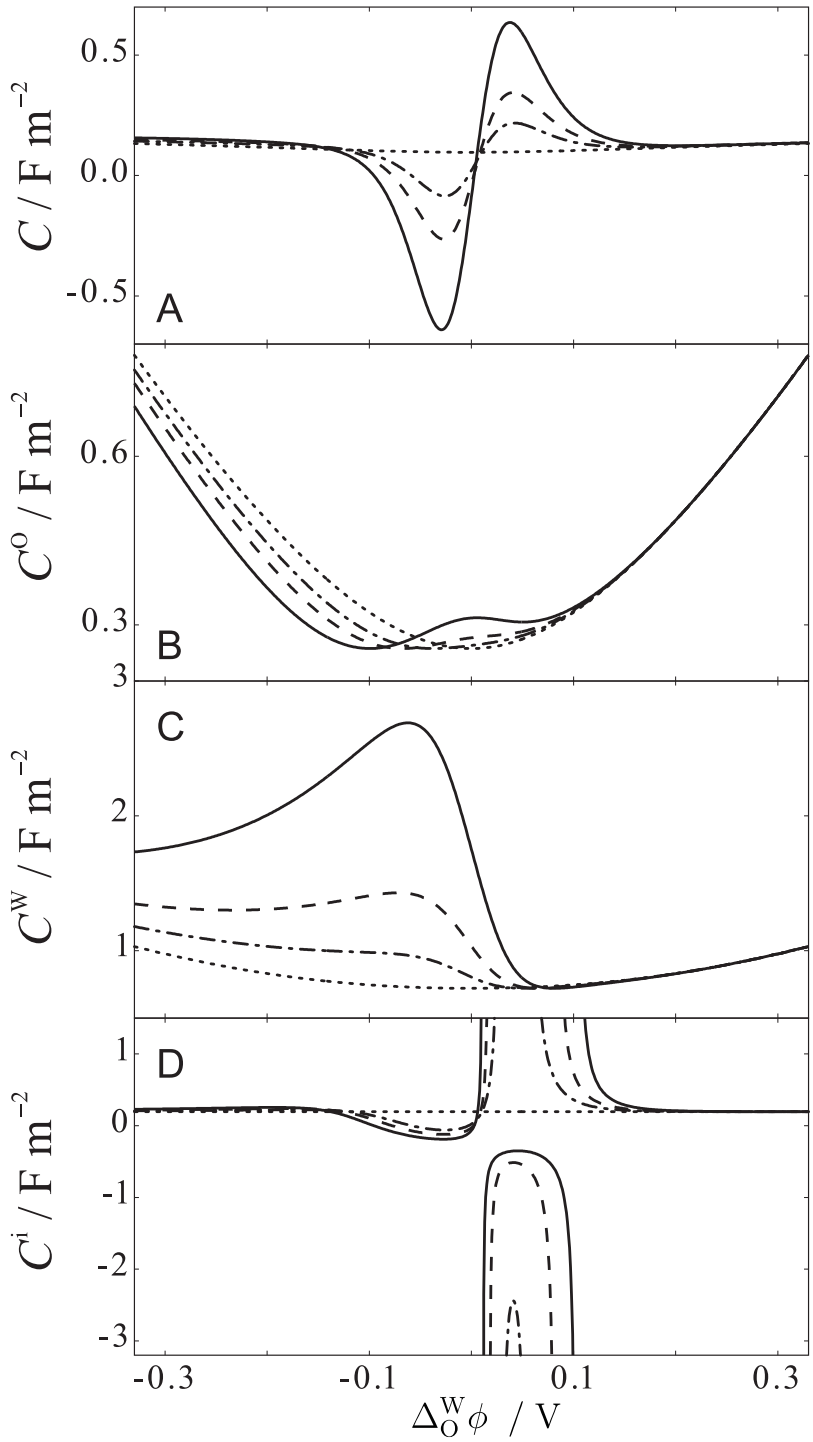

Figure 1.5: Potential-dependence of C (A), C^{O} (B), C^{W} (C), and C (D) when $c_{\mathrm{S}} = 0$ (dotted lines), 50 (dash-dotted lines), 100 (broken lines), and 200 mol m^{-3} (solid lines), $\beta = 0.9$ and S adsorbs at the position III.

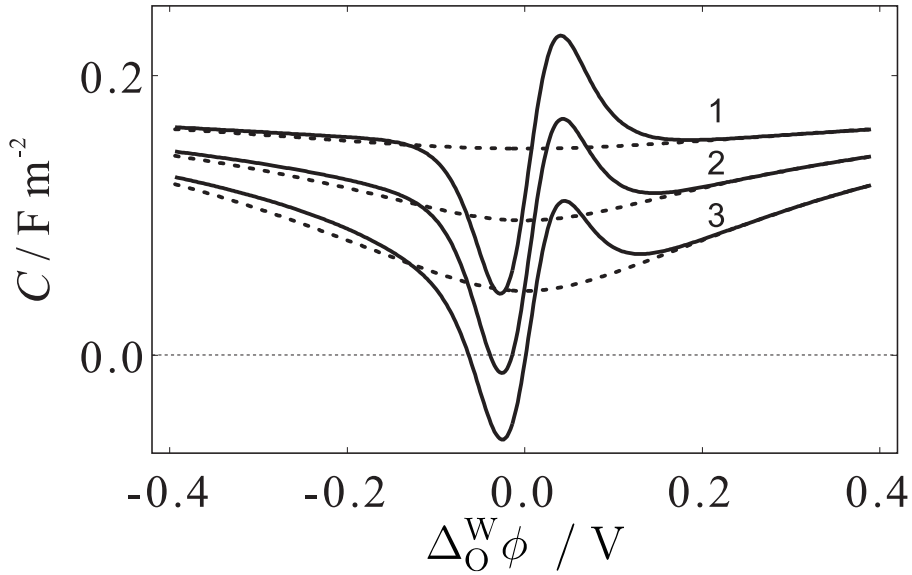

Figure 1.6: Effect of the concentration of the supporting electrolyte on C at $c_{\mathrm{S}} = 0.03$ (solid lines) and 0 mol m^{-3} (dotted lines), when $c^{\mathrm{W}} = c^{\mathrm{O}} = 1000$ (1), 100 (2), and 10 mol m^{-3} (3), $\beta = 0.9$, and S adsorbs at the position III.

C because of its slightly negative value. In the potential region where $0 < \Delta_{\mathrm{O}}^{\mathrm{W}}\phi < 0.15$ V, C^{i} has highly negative or highly positive values, therefore, the contribution of C^{i} on C is smaller than that of C^{O}.

1.3.3 Effect of the conditions on EI.

The effect of the parameters on the calculated EI are examined. The concentration of the supporting electrolyte affects the EI, through the charge density in the diffuse double layer, which is determined by the concentration of the supporting electrolyte. Calculated C values under three concentrations of the supporting electrolytes are shown in Figure 1.6 for $c^{\mathrm{W}} = c^{\mathrm{O}} =$ 1000 (1), 100 (2), and 10 mol m^{-3} (3) at $\beta = 0.9$ when adsorbed S is located at position III. The solid and dotted lines in Figure 1.6 show $c_{\mathrm{S}} = 0.3$ and 0 mol m^{-3}, respectively. The dotted lines are always positive at any $\Delta_{\mathrm{O}}^{\mathrm{W}}\phi$. In the cases of the solid lines 2 and 3, IW appears around -0.03 V. The IW narrows with increasing the concentration of the supporting electrolytes. When c_{S} is low enough and the concentration of the supporting electrolytes is high enough, the

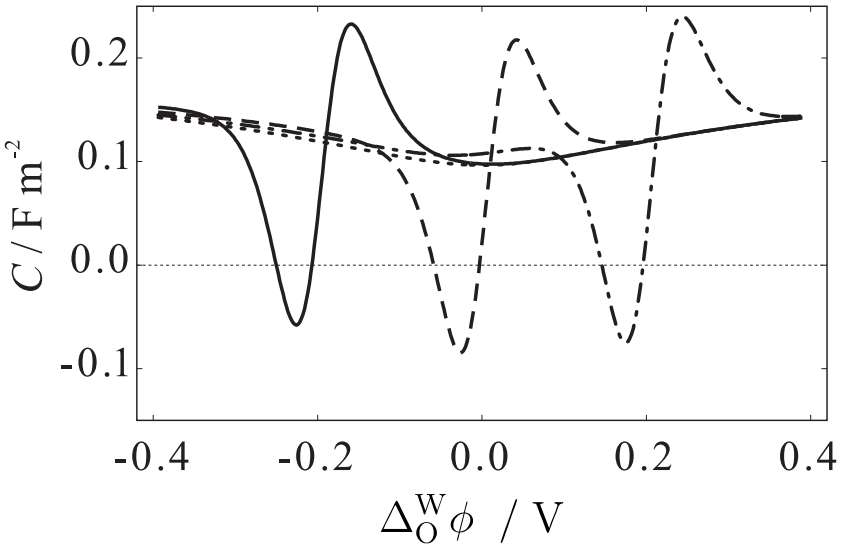

Figure 1.7: Effect of $\Delta_{\mathrm{O}}^{\mathrm{W}}\phi_{\mathrm{S}}^{\circ}$ on C at $c_{\mathrm{S}} = 0.05$ mol m^{-3}, when $\Delta_{\mathrm{O}}^{\mathrm{W}}\phi_{\mathrm{S}}^{\circ} = -0.2$ (solid line), 0 (broken line), 0.2 (dash-dotted line), $\beta = 0.9$, and S adsorbs at the position III. The dotted line is calculated at $c_{\mathrm{S}} = 0$ mol m^{-3}.

IW disappears. This tendency has been predicted by the previous model [1].

To compare surface-activity of ions on the EI, the effect of the location of $\Delta_{\mathrm{O}}^{\mathrm{W}}\phi_{\mathrm{S}}^{\circ}$ on the IW was examined. Figure 1.7 shows the potential-dependences of C at $c_{\mathrm{S}} = 0.05$ mol m^{-3} when $\Delta_{\mathrm{O}}^{\mathrm{W}}\phi_{\mathrm{S}}^{\circ} = -0.2$ (solid line), 0 (broken line), and 0.2 V (dash-dotted line). The dotted line in Figure 1.7 shows C in the absence of S. The effect of $\Delta_{\mathrm{O}}^{\mathrm{W}}\phi_{\mathrm{S}}^{\circ}$ on the width of IW is negligibly small, which is different from a prediction of the previous model [1]. In the latter, the system becomes stable when $\Delta_{\mathrm{O}}^{\mathrm{W}}\phi_{\mathrm{S}}^{\circ}$ is away from the potential of zero charge, which is determined by the type and concentration of the supporting electrolyte.

1.3.4 Comparison between the present and previous models.

To show the difference between the previous model of the EI [1] and the present model of the EI, the electrocapillary curves and potential-dependence of C were calculated under the same condition. The value of γ based on the previous model using the Frumkin isotherm is written

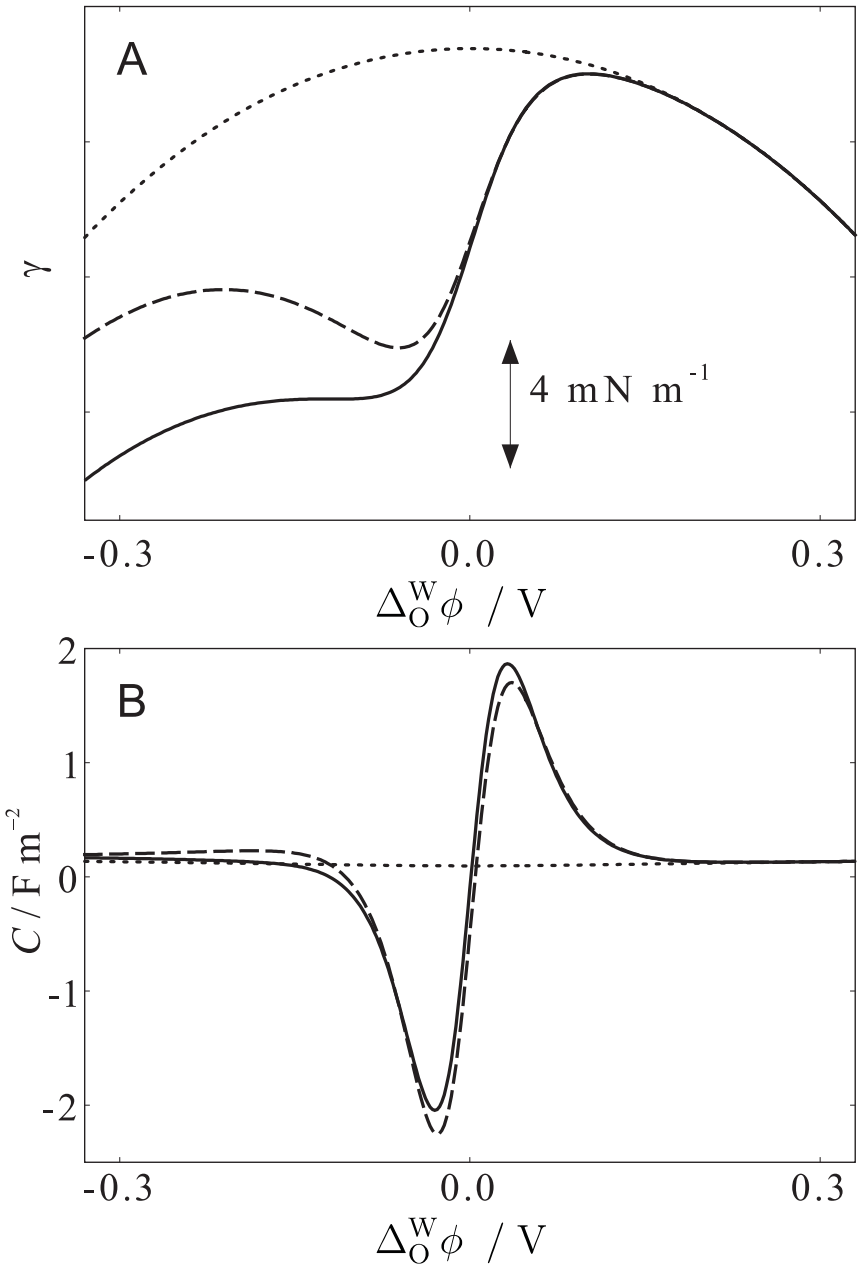

Figure 1.8: The comparison between the present model (solid lines) and the previous model (broken line) of the EI based on γ (A) and C (B), when $c_{\mathrm{S}} = 0.5$ and $\beta = 0.9$. In the present model, S adsorbs at the position III. The dotted lines are calculated at $c_{\mathrm{S}} = 0$ mol m^{-3}.

as follows.

$$\gamma = \gamma_0 - RT\Gamma_{\max}\left[\ln(1-\theta) + g\theta^2\right], \tag{1.41}$$

where γ_0 is γ determined by the supporting electrolyte at $c_S = 0$. The solid lines in Figures 1.8A and B show the electrocapillary curve and the potential-dependence of C based on the present model at $c_S = 0.5$ mol m^{-3} and the broken lines in Figures 1.8A and B show those based on the previous model. The dotted lines were calculated in the absence of S. In the potential region $\Delta_O^W\phi < 0$ V, γ of the previous model is greater than γ of the present model. The broken line in Figure 1.8A has an apparent dent, while the solid line in Figure 1.8A have no dent. The condition which provides a dent on the electrocapillary curve based on the improved model is limited compared with that based on the previous model.

The difference between C based on the previous model and C based on the present model is observed in the potential region $\Delta_O^W\phi < 0.05$ V in Figure 1.8B. In the potential region where $-0.05 < \Delta_O^W\phi < 0.05$ V, C from the present model is greater than C from the previous model. When $\Delta_O^W\phi < -0.05$ V, C from the present model is smaller than C from the previous model. Under this condition, the IW based on the present model (between -120 mV and 0 mV) is wider and more negative than the IW based on the previous model (between -106 mV and 4 mV).

According to equation 1.23, Γ_S should be determined from c_S regardless of the model. Therefore, the previous and present models based on the same isotherm should give the same electrocapillarities. The disagreement of the electrocapillary curves is caused by the oversimplification of the models shown in Figure 1.1B.

1.3.5 Comparison of the location of IW with experiments.

In the present model, EI appears on the negative sides of $\Delta_O^W\phi_S^\ominus$ in all three cases in Figure 1.7. However, the experimental observations of the EI induced by the transfer of surface-active ions [5–7, 9–11] show that the EI appears around the midpoint potential and extends to the limiting current region on voltammograms of ion-transfers. There are possible reasons for this

discrepancy. First is the difference between the mid-point potential determined experimentally and $\Delta_{\mathrm{O}}^{\mathrm{W}}\phi_{\mathrm{S}}^{\circ}$ of the surface-active ion. In experimental condition employed, the activity coefficient of ions is significantly less than unity and the ion-pair formation may not be negligible in O. Second, the structure of the interface can be much more complicated than that illustrated in Figure 1.1B. At this moment, we have little information about the thickness of the inner layer, the position of adsorbed ions, and the permittivity in the inner layer, granted that such a compact layer does exist. Third, the potential-dependence of the adsorption Gibbs energy may not be well described by the linear variation of the adsorption Gibbs energy with $\Delta_{\mathrm{O}}^{\mathrm{W}}\phi$ [13]. These are the points to be addressed in future detailed modelling of the EI.

1.4 Conclusion

The electrocapillary equation of the oil|water interface in the presence of the common ion in both phases was formulated under the condition that the Nernst equation describes the partition of the common ion. On the basis of this equation, an improved model for the EI has been presented. The model consists of the structure of the diffuse double layer under the influence of the specific adsorption of surface-active ions. The present model predicts the potential-dependence of the capacitances of the interface, the excess charge in the aqueous phase, and the electrocapillary curve in the presence of the common ion in both phase. In addition to the diffuse double layer, the introduction of the inner layer and the consideration of the position of the adsorbed ion provides a more reasonable picture of electrocapillarity in the presence of the EI. The calculated electrocapillary curves suggest that the potential-dependence of the adsorption Gibbs energy reflects the position of the charged part of adsorbed ions. In the strictly model of the EI, the electrocapillary curve based on q should agree with that based on Γ_{S}.

References

[1] Kakiuchi, T. *J. Electroanal. Chem.* **2002**, *536*, 63–69.

[2] Vanýsek, P. *J. Electroanal. Chem.* **1981**, *121*, 149–152.

[3] Kihara, S.; Suzuki, M.; Sugiyama, M.; Matui, M. *J. Electroanal. Chem.* **1988**, *249*, 109–122.

[4] Suzuki, M.; Kihara, S.; Maeda, K.; Ogura, K.; Matsui, M. *J. Electroanal. Chem.* **1990**, *292*, 231–244.

[5] Kakiuchi, T.; Chiba, M.; Sezaki, N.; Nakagawa, M. *Electrochem. Commun.* **2002**, *4*, 701–704.

[6] Kakiuchi, T.; Nishi, N.; Kasahara, T.; Chiba, M. *ChemPhysChem* **2003**, *4*, 179–185.

[7] Kasahara, T.; Nishi, N.; Yamamoto, M.; Kakiuchi, T. *Langmuir* **2004**, *20*, 875–881.

[8] Goto, T.; Maeda, K.; Yoshida, Y. *Langmuir* **2005**, *21*, 11788–11794.

[9] Sakka, T.; Tanaka, K.; Shibata, Y.; Ogata, Y. H. *J. Electroanal. Chem.* **2006**, *591*, 168–174.

[10] Kitazumi, Y.; Kakiuchi, T. *J. Phys.: Condens. Matter* **2007**, *19*, 375104.

[11] Kitazumi, Y.; Kakiuchi, T. *Langmuir* **2009**, *25*, 8062–8068.

[12] Kitazumi, Y.; Kakiuchi, T. *Langmuir* **2009**, *25*, 10829–10833.

[13] Kakiuchi, T. *J. Electroanal. Chem.* **2001**, *496*, 137–142.

[14] Gad, J. *Arch. Anat. Physiol., Lpz.,* **1878**, 181–205.

[15] McBain, J. W.; Woo, T.-M. *Proc. Roy. Soc. A* **1937**, *163*, 182–188.

[16] Groves, M. J. *Chem. Ind.* **1978**, *17*, 417–423.

[17] Nishimi, T.; Miller, C. A. *Langmuir* **2000**, *16*, 9233–9241.

[18] Dupeyrat, M.; Nakache, E. *Bioelectrochem. Bioenerg.* **1978**, *5*, 134–141.

[19] Yoshikawa, K.; Matsubara, Y. *J. Am. Chem. Soc.* **1984**, *106*, 4423–4427.

[20] Kihara, S.; Maeda, K. *Prog. Surf. Sci.* **1994**, *47*, 1–54.

[21] Kovalchuk, N. M.; Vollhardt, D. *Adv. Colloid Interface Sci.* **2006**, *120*, 1–31.

[22] Gouy, G. *Ann. Phys.* **1917**, *(9) 7*, 129.

[23] Kakiuchi, T.; Senda, M. *Bull. Chem. Soc. Jpn.* **1983**, *56*, 2912–2918.

[24] Frumkin, A. N. *Z. Phys. Chem.* **1925**, *116*, 466–484.

[25] Gavach, C.; Seta, P.; d'Epenoux, B. *J. Electroanal. Chem.* **1977**, *83*, 225–235.

[26] Kakiuchi, T.; Senda, M. *Bull. Chem. Soc. Jpn.* **1983**, *56*, 1753–1760.

[27] Samec, Z.; Mareček, V.; Holub, K.; Račinský, S.; Hájková, P. *J. Electroanal. Chem.* **1987**, *225*, 65–78.

Chapter 2

Potential-dependent adsorption of decylsulfate and decylammonium prior to the onset of electrochemical instability at the 1,2-dichloroethane|water interface

The adsorption of decylsulfate ($DeSO_4^-$) and decylammonium ($DeNH_3^+$) at the 1,2-dichloroethane (DCE)|water (W) interface has been examined as a function of the phase-boundary potential by simultaneous recording of electrocapillary curves and voltammograms. The standard Gibbs energies for the adsorption of $DeSO_4^-$ and $DeNH_3^+$ at the DCE|W interface from the W phase depend linearly on the phase-boundary potential, having the slopes of 9.1 and -9.8 kJ mol^{-1} V^{-1}, respectively. These values suggest that the charged head-groups of adsorbed surface-active ions are located almost outside of the diffuse-part of the electrical double layer in W. It has also been demonstrated that the interface enters into the mode of the electrochemical instability in the potential region where the current is slightly augmented in comparison with that of the diffusion-limited current, that is, prior to the appearance of irregularly increased

currents on the voltammogram.

2.1 Introduction

The electrochemical instability of a liquid-liquid interface [1] emerges when the interface is under the thermodynamically unstable condition due to the potential-dependent adsorption of surface-active ions, that is, when

$(\partial^2\gamma/\partial E^2)_{T,P} > 0$ where, γ is the interfacial tension, E is the applied voltage, T is the temperature, and P is the pressure. This instability explains unstable phenomena at the interface induced by the transfer of surface-active ions [2–6] and facilitated ion transfer by surface-active ligands [7] across the liquid-liquid interface. Irregularly increased currents in ion-transfer voltammetry in a certain limited potential window caused by the convective motion of the solution adjacent to the liquid-liquid interface provide evidence that the interface is under the condition of the electrochemical instability.

To explain the electrochemical instability, a model has been proposed based on the interplay of potential-dependent adsorption of surface-active ions and the energy of the electrical double layer at the interface [1]. This simple model assumes a linear dependence of the standard Gibbs energies of adsorption of the surface-active ions at the oil (O)-water (W) interface from W ($\Delta G_{\mathrm{ads}}^{\mathrm{W},\ominus}$) and from O ($\Delta G_{\mathrm{ads}}^{\mathrm{O},\ominus}$) on the phase-boundary potential ($\Delta_{\mathrm{O}}^{\mathrm{W}}\phi$) in the forms [8],

$$\Delta G_{\mathrm{ads}}^{\mathrm{W},\ominus} = \Delta G_{\mathrm{ads}}^{\ominus} - zF(1-\beta)\left(\Delta_{\mathrm{O}}^{\mathrm{W}}\phi - \Delta_{\mathrm{O}}^{\mathrm{W}}\phi^{\ominus}\right) \tag{2.1}$$

and

$$\Delta G_{\mathrm{ads}}^{\mathrm{O},\ominus} = \Delta G_{\mathrm{ads}}^{\ominus} + zF\beta\left(\Delta_{\mathrm{O}}^{\mathrm{W}}\phi - \Delta_{\mathrm{O}}^{\mathrm{W}}\phi^{\ominus}\right) \tag{2.2}$$

where z, β, $\Delta_{\mathrm{O}}^{\mathrm{W}}\phi^{\ominus}$ and $\Delta G_{\mathrm{ads}}^{\ominus}$ are the charge of the ion, the coefficient which is independent of $\Delta_{\mathrm{O}}^{\mathrm{W}}\phi$ ($0 \leq \beta \leq 1$), the standard ion-transfer potential of the surface-active ion, and the standard adsorption Gibbs energy at $\Delta_{\mathrm{O}}^{\mathrm{W}}\phi^{\ominus}$, respectively. The experimental determination of β is crucial to quantitatively describe the electrochemical instability. The potential-dependent adsorption of ions at the liquid-liquid interface has been reported for the adsorption of hexadecyltrimethylammonium [9,10] and ion-pairs of sodium and cesium ions with organic anions [11,12] at the nitrobenzene (NB)|W interface, bis-quaternary ammoniums at NB and 1,2-dichloro-

ethane (DCE)|W interfaces [13], and 2-(*N*-octadecylamino)naphthalene-6-sulfonate [14], ionic dyes [15–17], tetraalkylammoniums [18, 19], complexes of metal ions with Triton X [20], and porphyrin derivatives [21–23] at the DCE|W interface. The potential-dependent adsorption of ions under the ion-transfer across the liquid-liquid interface has also been detected in a second harmonic generation study of the Methyl Orange adsorption [15] and in ac-modulated voltfluorometry of Erythrosine B, Eosin Y, and Rose Bengal [16, 17]. However, the determination of β has never been reported for the ionic surfactant under the current flow, i.e., in the presence of the ion-transfer across the interface. Electrocapillary measurements are useful to determine β from the surface excess of ionic surfactants, while voltammetry can visualize the stable-unstable transition of the interface. In the present work, voltammograms and electrocapillary curves at the DCE|W interface were recorded simultaneously in the presence of either decylsulfate ($DeSO_4^-$) or decylammonium ($DeNH_3^+$). From the dependence of the relative surface excesses of $DeSO_4^-$ and $DeNH_3^+$ on $\Delta_O^W\phi$, the values of $\Delta G_{ads}^{W,\circ}$ for the adsorption of $DeSO_4^-$ and $DeNH_3^+$ were determined as a function of the applied potential before the onset of the electrochemical instability.

2.2 Experimental section

2.2.1 Measurement of the interfacial tension.

A pendant drop method was employed to measure γ [24,25]. Although the basic principle is the same as that we used previously [25], we thoroughly renewed both hardware and software for the determination of γ. The optical cell (width, height, and optical length are 24, 40, and 50 mm, respectively) filled with an aqueous solution (W) was set in a jacketed holder at 25.0 ± 0.1 $^\circ$C. A typical size of a pendant drop (O) was about 3 mm equatorial diameter. A pendant drop of O in W was illuminated with paralleled light from a light-emitting diode (MCVP-CG3430, Moritex, Japan). A monochrome camera with a trigger input (DMK41BF02, The Imaging Source, Germany) equipped with a telecentric zoom lens (ML-Z07545, Moritex) was employed

to acquire an image of the drop. The maximum frame rate of the camera is 15 frames per second. High-accuracy silicon nitride balls for bearings of two different diameters (5.5562 and 3.9689 mm) were used for the calibration of camera images. The optical axis of the apparatus was aligned with a laser beam from a He-Ne laser (05-LHP-151, Melles Griot).

Homemade programs were used to extract the contour of a drop. The Bashforth-Adams equation [26] was fitted to the contour using a software for the nonlinear least squares fitting, SALS [27]. Three fitting parameters R_0, ΔY, and σ are the radius of curvature at the origin of the contour of the drop, an error of origin of y axis, and $\sigma = \Delta\rho g R_0^2/\gamma$, where $\Delta\rho$, and g are the difference of the densities, and the acceleration of gravity. The introduction of ΔY is to take into account the error due to the quantization of the contour of the drop [28]. The length of $R_0\Delta Y$ is smaller than the length per pixel. The value of γ at the DCE|W interface determined by the present method was 27.92 ± 0.02 (95% confidence interval) mN m^{-1} at 25.0 °C. This value well agrees with the literature value 27.93 ± 0.09 (95% confidence interval) mN m^{-1} [25].

2.2.2 Chemicals.

DCE was washed with concentrated sulfuric acid, water, an aqueous solution of Na_2CO_3, and water, successively. After being dried with $CaCl_2$, the DCE was distilled and washed with water three times before use. Water was purified with a Milli-Q system (Milli-Q Gradient, Millipore). Tetrapentylammonium tetraphenylborate (TPnATPB) and tetrapentylammonium tetrakis[3,5-bis(trifluoromethyl)phenyl]borate (TPnATFPB) were synthesized as described elsewhere [16, 29]. Tetrapentylammonium chloride (TPnACl), hydrochloric acid, $MgCl_2$, sorbitan monooleate (SMO), sodium decylsulfate ($NaDeSO_4$), and decylamine ($DeNH_2$) were all reagent grade and were used without further purification. Aqueous solutions of $DeNH_3^+$ were prepared by dissolving $DeNH_2$ in aqueous hydrochloric acid solutions.

2.2.3 Simultaneous recording of an electrocapillary curve and a voltammogram.

Two electrochemical cells employed in the present study are

$$\mathrm{Ag}\left|\mathrm{AgCl}\right|\begin{matrix}\text{5 mM TPnACl}\\\text{10 mM }\mathrm{MgCl_2}\end{matrix}\Big|\begin{matrix}\text{50 mM}\\\text{TPnATPB}\end{matrix}\Big|\begin{matrix}\text{100 mM }\mathrm{MgCl_2}\\\text{0 }\sim\text{ 500 }\mu\text{M NaDeSO}_4\end{matrix}\Big|\mathrm{AgCl}\left|\mathrm{Ag}\right.\quad\text{(I)}$$

$$\qquad\qquad\mathrm{W_{ref}}\qquad\quad\mathrm{DCE}\qquad\quad\mathrm{W}$$

and

$$\mathrm{Ag}\left|\mathrm{AgCl}\right|\begin{matrix}\text{5 mM TPnACl}\\\text{10 mM }\mathrm{MgCl_2}\end{matrix}\Big|\begin{matrix}\text{50 mM}\\\text{TPnATFPB}\end{matrix}\Big|\begin{matrix}\text{100 mM HCl}\\\text{0 }\sim\text{ 400 }\mu\text{M DeNH}_2\end{matrix}\Big|\mathrm{AgCl}\left|\mathrm{Ag}\right.\quad\text{(II)}$$

$$\qquad\qquad\mathrm{W_{ref}}\qquad\quad\mathrm{DCE}\qquad\quad\mathrm{W}$$

where M stands for mol dm^{-3} and $\mathrm{W_{ref}}$ designates the aqueous phase for the reference of the potential in the DCE phase. The bulk concentrations of $\mathrm{DeSO_4^-}$ and $\mathrm{DeNH_3^+}$ in W phase are represented by $c^{\mathrm{b,W}}_{\mathrm{DeSO_4^-}}$ and $c^{\mathrm{b,W}}_{\mathrm{DeNH_3^+}}$, respectively. The potential of the right-hand-side terminal with respect to the left is hereafter denoted as E. The current (I) due to the flow of the positive charge from W to DCE was taken to be positive. A four-electrode potentiostat equipped with a positive-feedback circuit (HA10100mM1A, Hokutodenko, Japan) was used to apply the potential.

A homemade program was used for synchronized recording of video images, at intervals of 5 mV and I at intervals of 1 mV at the scan rate (v) of 10 mV s^{-1}. The accuracy of timing between the image recording and the control of E depends on the exposure time of the camera in this apparatus. A typical exposure time was 5 ms, which corresponds to a change in the applied voltage by 0.05 mV at $v = 10$ mV s^{-1}.

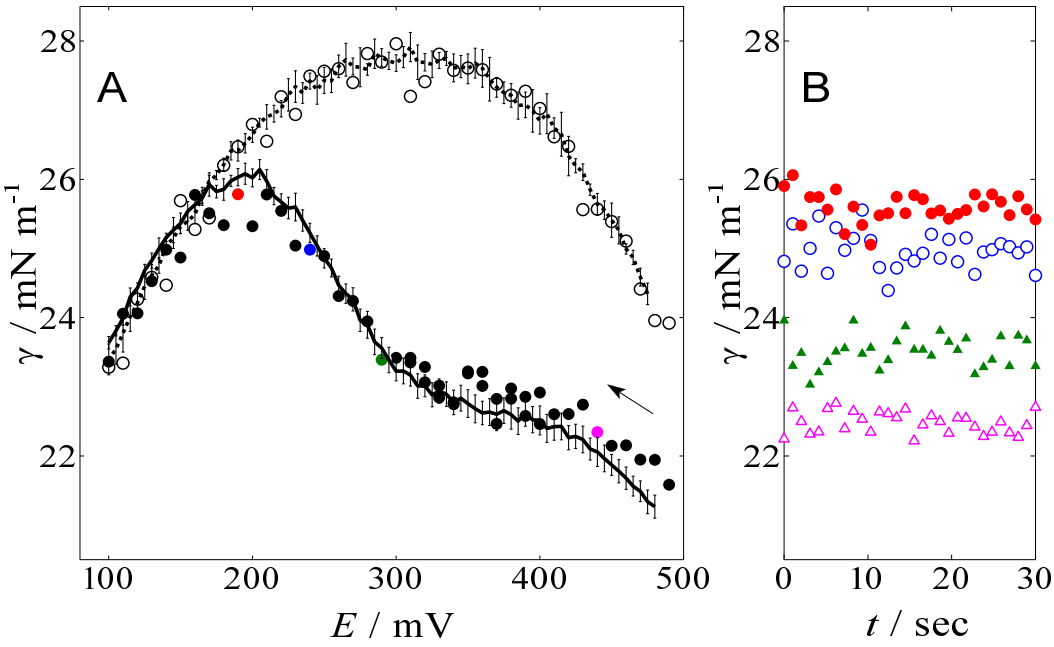

Figure 2.1: A: Electrocapillary curves recorded in the presence of 100 μmol dm^{-3} $DeSO_4^-$ in the W phase (filled circles and solid line) and in the absence of $DeSO_4^-$ (open circles and dotted line). The circles were recorded by potential-step with holding time of 25 seconds (open circles) and the lines were recorded by potential sweep at v = 10 mV s^{-1}. B: Time dependence of γ when the potential was stepped from 450 to 440 (open triangles), 300 to 290 (filled triangles), 250 to 240 (open circles), and 200 to 190 mV (filled circles) in the presence of the 100 μmol dm^{-3} $DeSO_4^-$ in the W phase.

2.3 Results and discussion

2.3.1 A comparison of interfacial tensions under the potential sweep and potential step.

First, we compare the electrocapillary curves recorded by the potential sweep with those recorded by the potential-step method. If the response of γ to the change in E is fast enough, γ recorded under the potential sweep should give the same values as those recorded with the potential-step method. The dotted line in Figure 2.1A shows an electrocapillary curve recorded by potential sweep from 480 mV to 100 mV at $v = 10$ mV s^{-1} at $c^{\mathrm{b,W}}_{\mathrm{DeSO_4^-}} = 0$. Open circles in Figure 2.1A show γ recorded by the potential-step method after E was kept at the stepped potential for 25 s. The electrocapillary curve represented by the open circles agrees well with the electrocapillary curve of the dotted line over the entire potential region studied. These electrocapillary curves have parabolic shapes, as previously reported for similar systems [4,5,24,30–32]. The point of zero charge (pzc) of this interface is located at $E = 300$ mV. This pzc agrees with a reported value [4] when E is corrected for the change in the supporting electrolyte in W from LiCl to $MgCl_2$.

When E is set to a certain value, the liquid-liquid interface in the absence of the transferring ions across the interface reaches an electrochemical equilibrium through charging the double layer. When the uncompensated resistance is 500 Ω and the capacitance of the DCE|W interface is 0.15 μF m^{-2} [33], the time constant of charging the liquid-liquid interface with the interfacial area of 28 mm^2 is 2 ms. Hence, γ after a potential-step should be settled to a constant value at least within a few ms. This fast response of γ at the O|W interface to the change in E assures that γ recorded by the potential sweep at a moderate scan rate is regarded as that in the thermodynamic equilibrium [34] at DCE|W interface. In other words, γ is determined by the surface concentration and is not affected by the concentration gradient.

An electrocapillary curve for $c^{\mathrm{b,W}}_{\mathrm{DeSO_4^-}} = 100$ μmol dm^{-3} recorded from 490 mV to 100 mV by potential-step at the interval of 10 mV is shown as filled circles in Figure 2.1A. The potential

was kept for 25 s after each potential-step. The electrocapillary curve recorded by the potential sweep from 480 to 100 mV at $v = 10$ mV s^{-1} is shown as the solid line in Figure 2.1A. The solid line and filled circles in Figure 2.1A generally well agree with each other, although γ values from the potential-step method are slightly greater (smaller) than those from the potential sweep method in the E values between 400 and 500 (180 and 230) mV.

Figure 2.1B shows the time-dependences of γ after E was stepped from 450 to 440 (open triangles), 300 to 290 (filled triangles), 250 to 240 (open circles), and 200 to 190 mV (filled circles). No significant time dependence of γ was observed. The agreement of the electrocapillary curve recorded by the potential sweep with that by the potential-step in Figure 2.1A and also the time-invariant γ values at a given value of E in Figure 2.1B assure that the electrocapillary curves recorded under the ion transfer can be a subject for thermodynamic analysis.

2.3.2 Simultaneous recording of a voltammogram and an electrocapillary curve.

Electrocapillary curves in Figure 2.2A and voltammograms in Figure 2.2B were recorded simultaneously with sweep E from 480 to 100 mV at $v = 10$ mV s^{-1}. The solid lines and dotted lines in Figure 2.2 represent the forward and reverse scans, respectively. Curves 1 and 1′ were recorded when $c^{\mathrm{b,W}}_{\mathrm{DeSO_4^-}} = 0$. Curves 2 and 2′ were recorded at $c^{\mathrm{b,W}}_{\mathrm{DeSO_4^-}} = 200$ μmol dm^{-3}. Curves 3 and 3′ in Figure 2.2 were recorded at $c^{\mathrm{b,W}}_{\mathrm{DeSO_4^-}} = 200$ μmol dm^{-3} in the presence of 3 mmol dm^{-3} SMO in the DCE phase, which was used to suppress irregularly increased currents induced by the electrochemical instability [2–6]. From curve 3′, the mid-point potential (E_{mid}) of the transfer of $\mathrm{DeSO_4^-}$ was estimated to be 288 ± 3 mV in this system (cell I). The electrocapillary curves recorded in the forward scan agree with those recorded in the reverse scan. The value of γ in curve 3 was lower than curve 2 throughout the range of E by nearly a constant amount, 12 mN m^{-1}. This indicates that SMO adsorbs in the entire range of E studied [35].

Comparing the electrocapillary curves with the voltammograms in Figures 2.2A and 2.2B, we may distinguish four regions in E in curves 2 and 2′. In the potential region between 480 and

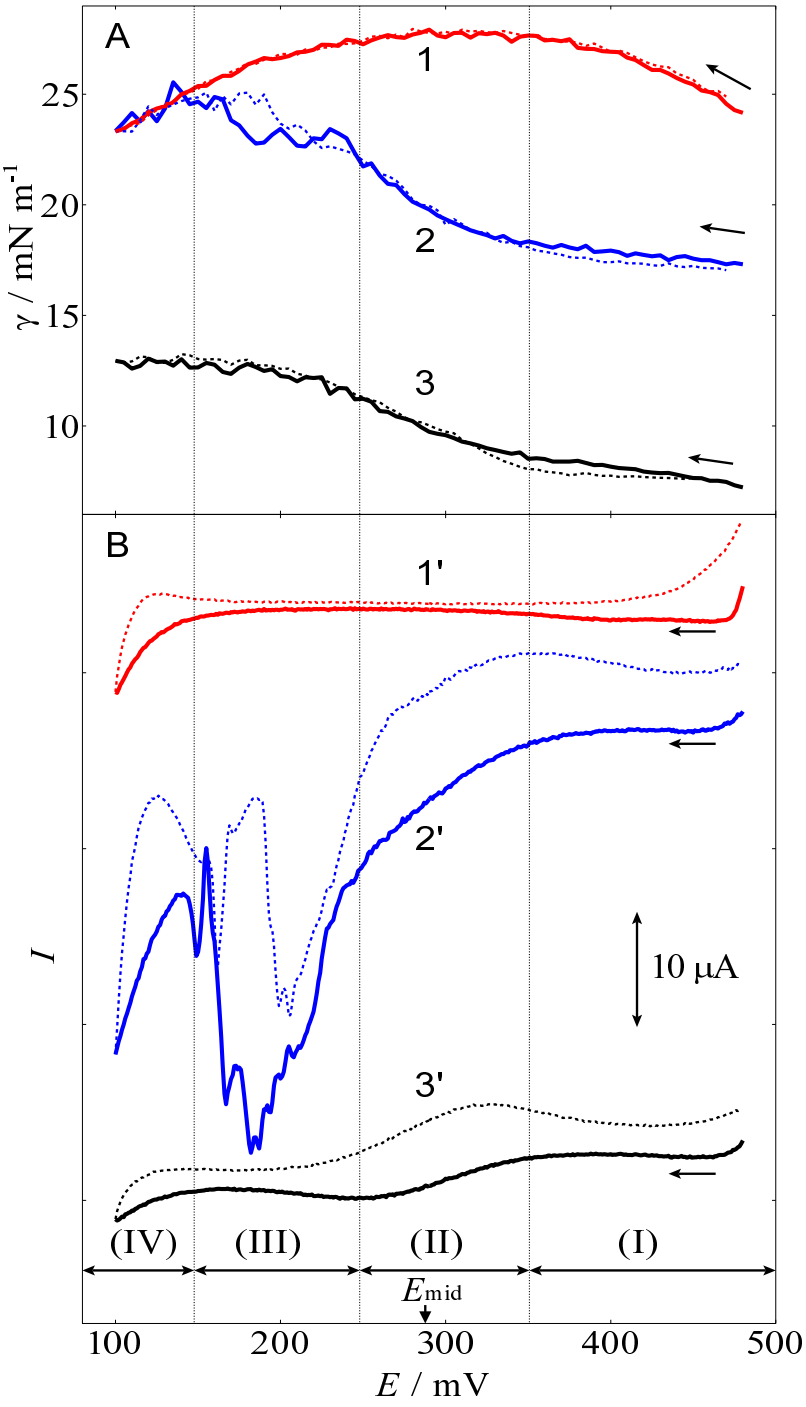

Figure 2.2: Simultaneously recorded electrocapillary curves (A) and voltammograms (B) in the absence of $DeSO_4^-$ (1 and 1′) and presence of 200 μmol dm^{-3} $DeSO_4^-$ (2 and 2′) in W at $v = 10$ mV s^{-1}. The curves 3 and 3′ are recorded in the presence of 200 μmol dm^{-3} $DeSO_4^-$ in the W phase and 3 mmol dm^{-3} SMO in the DCE phase. Solid and dotted lines are recorded in the forward and reverse scan, respectively. E_{mid} indicates the mid-point potential of transfer of $DeSO_4^-$. Vertical lines roughly distinguish characteristic regions of E, reflecting the manner of adsorption of $DeSO_4^-$.

350 mV (region I), ion transfer currents were not observed. In the region I, γ increased with potential sweep. In the potential more negative than 350 mV, the ion-transfer current due to the transfer of $DeSO_4^-$ from W to DCE appeared on curve $2'$. In the potential region between 250 and 350 mV (region II), curve 2 has a positive curvature, which is thermodynamically forbidden. The current increased conspicuously in curve $2'$, but with no irregularities. The negative current in curve $2'$ grew rapidly from 250 mV and showed irregular changes in the potential region between 250 and 150 mV (region III). In the region III, curve 2 also showed a similar irregularity. In the region more negative than 150 mV (region IV), the pendant drops were still and curve 2 agreed with curve 1. In the reverse scans, basically similar distinctions are seen in curves 2 and $2'$.

In the region I, the system is in an equilibrium state because no significant ion-transfer takes place across the DCE|W interface. The decrease in γ in curve 2 in this region reflects the adsorption of $DeSO_4^-$ ions at the DCE|W interface. In the region II, a pendant drop of DCE in W looked still in the video images, though the current in curve $2'$ began to deviate from the reversible ion transfer [3]. In the region II, the DCE|W interface is probably under the electrochemical instability condition, because the electrocapillary curve has a positive curvature.

The sudden and irregular increase in the negative current on curve $2'$ in the region III is ascribed to the convective motion of the bulk liquid phases. In this region, the pendant-drop showed irregular movements, which made the meanings of γ obtained from the drop shape from video imaging obscure. In the following section, the electrocapillary curve in this region in the presence of $DeSO_4^-$ adsorption was not analyzed. The irregularly increased currents are caused by the Marangoni effect [2, 36, 37]. The lowering of γ by addition of SMO probably reduces the gradient of γ between the desorbed domains and adsorbed domains at the interface. The driving force of the movement of the interface should then become weaker.

In the region IV, the similarity between curves 1 and 2 indicates that the adsorption of $DeSO_4^-$ at the DCE|W interface is negligibly small, if present. In this region, the convection of the interface was not observed, although the current was greater than that expected

for a diffusion-limited case in the presence of SMO. This indicates that the aftereffect of the convection remains in the region IV.

2.3.3 Potential-dependent adsorption of $DeSO_4^-$.

Figure 2.3 shows voltammograms for the transfer of $DeSO_4^-$ at eight different $c^{b,W}_{DeSO_4^-}$ between 0, 20, 50, 80, 100, 200, 300, and 500 μmol dm^{-3} (curves 1 to 8, in this order). On curves 2, 3, and 4, the negative current peaks due to the transfer of $DeSO_4^-$ from the W phase to the DCE phase appeared around 250 mV in the forward scans and positive peaks appeared around 320 mV in the reverse scans. E_{mid} of the transfer of $DeSO_4^-$, 284 $\pm$ 2 mV, agrees with the value recorded in the presence of SMO as described above. On the curves 4 and 5, the irregular currents in the reverse scans appeared in $150 < E < 200$ mV. On the curves 6, 7, and 8, the irregular currents appeared when $E < 260$ mV in both forward and reverse scans. In the present study, the irregularly increased currents were thus appreciable at lower concentrations than the concentration used in our previous studies of the electrochemical instability for alkylsulfates, alkylsulfonate, and alkylammoniums at the DCE|W interface [3, 4, 6]. The spherical shape of the interface in recording voltammograms in the present study may be responsible to the lower threshold concentration for the electrochemical instability.

Electrocapillary curves recorded simultaneously with voltammograms in the forward scans are shown in Figure 2.4. Each electrocapillary curve is the average of ten measurements and vertical bars on the electrocapillary curves indicate the 90% confidence interval. The dotted parts in the capillary curves in Figure 2.4 are γ values obtained in the regions where the irregularly increased currents appeared clearly on the voltammograms. The concentration dependence of the electrocapillary curves (Figure 2.4) shows that the adsorption of $DeSO_4^-$ when $E > E_{mid}$ is stronger than that when $E < E_{mid}$.

When $c^{b,W}_{DeSO_4^-} \geq 50$ μmol dm^{-3}, the electrocapillary curves have a positive curvature in the region around E_{mid}. The width of this potential region became wider with the increase in $c^{b,W}_{DeSO_4^-}$. This widening with the concentration of surface-active ions agrees with the prediction

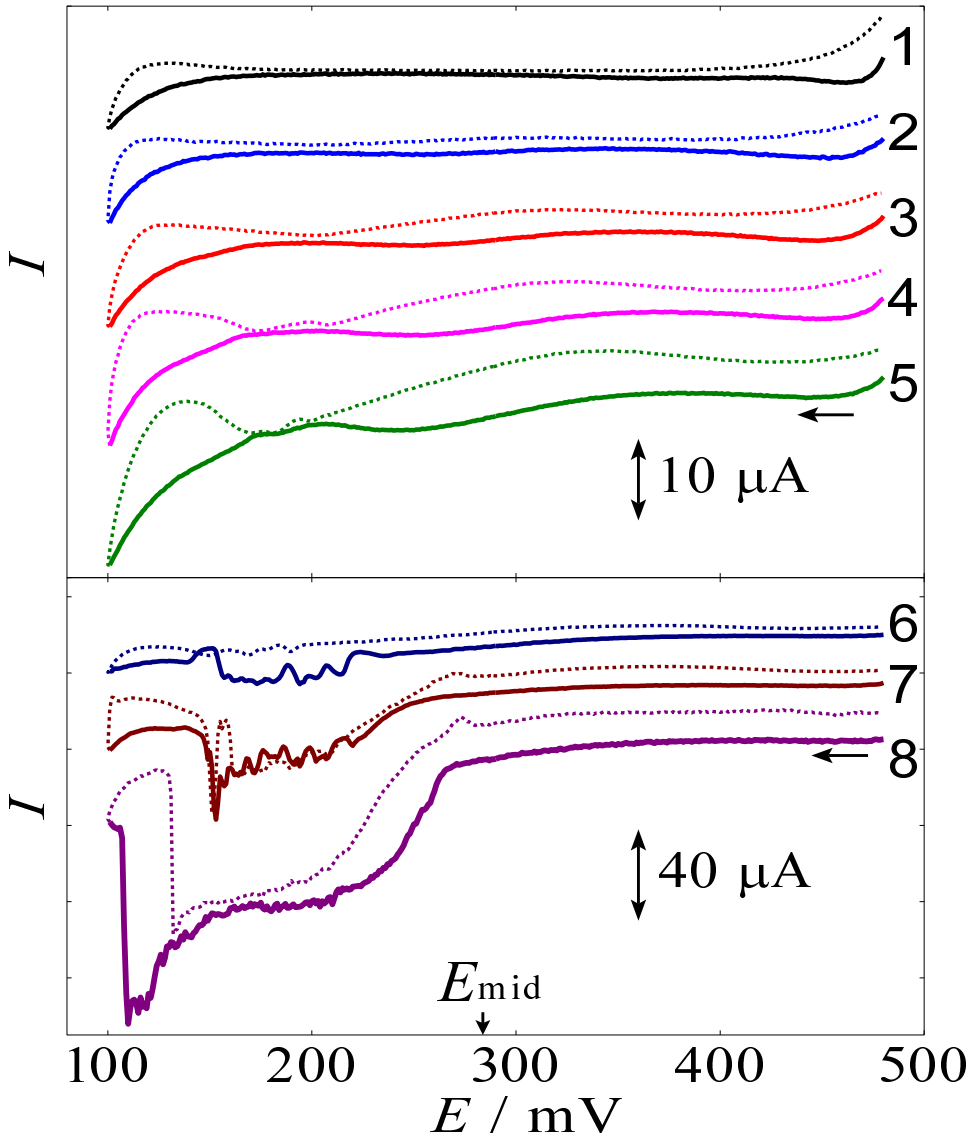

Figure 2.3: Cyclic voltammograms for the transfer of $DeSO_4^-$ across the DCE|W interface at v = 10 mV s^{-1}, $c^{b,W}_{DeSO_4^-}$ = 0 (1), 20 (2), 50 (3), 80 (4), 100 (5), 200 (6), 300 (7), 500 (8) μmol dm^{-3}. Dotted lines show the currents recorded in the reverse scans. E_{mid} indicates the mid-point potential of transfer of $DeSO_4^-$.

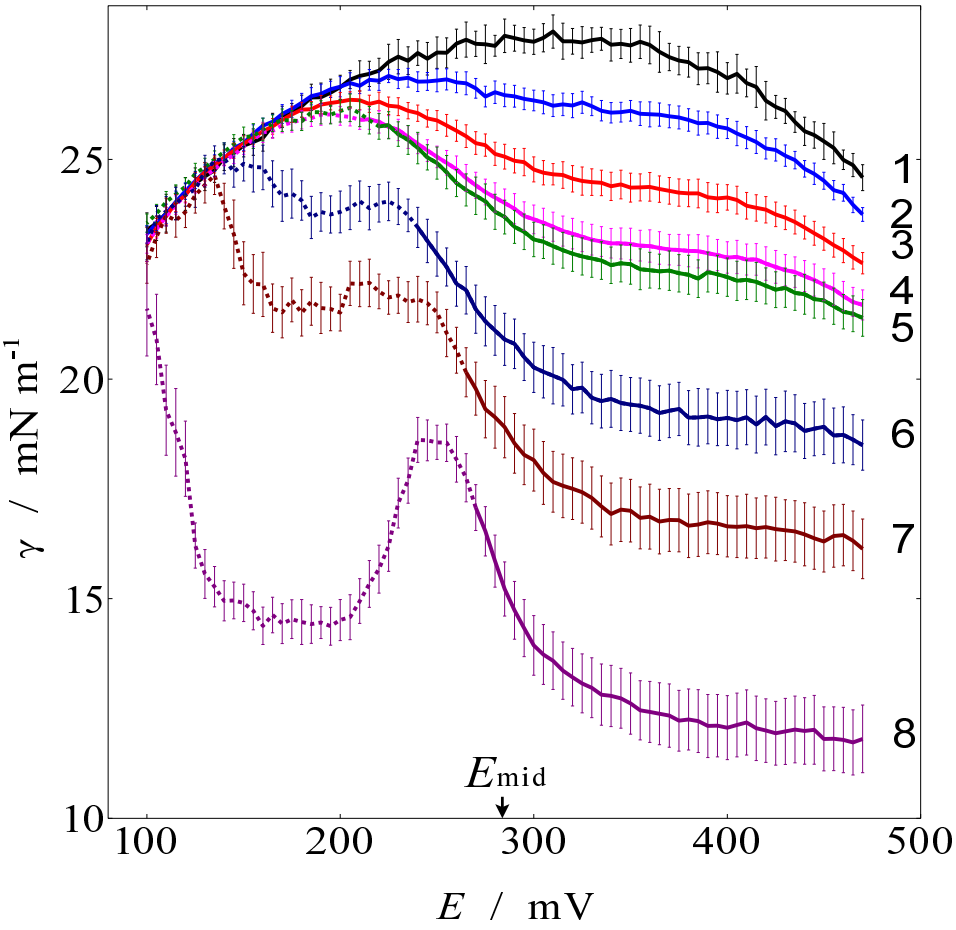

Figure 2.4: Electrocapillary curves at DCE|W interface recorded in the presence of $DeSO_4^-$ at $v = 10$ mV s^{-1}, $c^{b,W}_{DeSO_4^-} = 0$ (1), 20 (2), 50 (3), 80 (4), 100 (5), 200 (6), 300 (7), 500 (8) μmol dm^{-3}. Dotted lines of the electrocapillary curves indicate the region where γ is recorded under the irregularly increased current. Vertical bars show the 90% confidence interval for 10 independent measurements.

of the model of the electrochemical instability [1].

To estimate the adsorbed amount of $DeSO_4^-$, we need to take account of the fact that under the current flow the surface concentrations of $DeSO_4^-$ on both side of the interface, $c^{0,W}_{DeSO_4^-}$ and $c^{0,O}_{DeSO_4^-}$, are different from $c^{b,W}_{DeSO_4^-}$ and $c^{b,O}_{DeSO_4^-}$. Not $c^{b,i}_{DeSO_4^-}$ but $c^{0,i}_{DeSO_4^-}$ should be used in the Gibbs adsorption equation and an adsorption isotherm. Assuming that the ion-transfer process is electrochemically reversible and the potential is uniform throughout the interface, we calculated the distribution of $c^{0,W}_{DeSO_4^-}$ at a given value of E from E_{mid} and $c^{b,W}_{DeSO_4^-}$ based on the diffusion equation and the Nernst equation, taking account of the shape of the pendant drop, using FEMLAB 3.1 (COMSOL). The ratio of the diffusion coefficient of $DeSO_4^-$ in the W phase to that in the DCE phase was assumed to be 0.87, as deduced from the ratio of viscosity coefficients of the DCE phase to that in W phase [38]. The value of $c^{0,W}_{DeSO_4^-}$ at the bottom of the pendant drop was used for a calculation of the adsorbed amount.

The Gibbs adsorption equation in the system (cell I) under the constant temperature and pressure is

$$-\frac{1}{RT}\mathrm{d}\gamma = \frac{q^W}{RT}\mathrm{d}E + (\Gamma_{Na^+} - \frac{a_{Na^+}a_{Cl^-}}{a_W}\Gamma_W)\mathrm{d}\ln a_{Na^+} + (\Gamma_{DeSO_4^-} - 2\frac{a_{Mg^{2+}}a^2_{DeSO_4^-}}{a_W}\Gamma_W)\mathrm{d}\ln a_{DeSO_4^-} \quad (2.3)$$

where Γ_i and a_i are the surface excess and the activity of the chemical species i in the W phase, respectively, and q^W is the excess surface charge density in W. Here, we have assumed that the activities of Mg^{2+}, Cl^-, $TPnA^+$, and TPB^- are independent of $c^{b,W}_{DeSO_4^-}$, because these concentrations are much higher than $c^{b,W}_{DeSO_4^-}$ [39]. Since $a_{DeSO_4^-} << a_W$ and $a_{Na^+} << a_W$, the activity coefficient of $DeSO_4^-$ is constant over the concentration range of $DeSO_4^-$ studied. Then, from eq 2.3 we obtain

$$-\frac{1}{RT}\left(\frac{\partial\gamma}{\partial\ln c^{0,W}_{DeSO_4^-}}\right)_{P,T,\mu_i,E} = \Gamma_{DeSO_4^-} + \Gamma_{Na^+} = \Gamma_{NaDeSO_4}. \quad (2.4)$$

The adsorptivity of $DeSO_4^-$ must be higher than Na^+, and hence, $\Gamma_{DeSO_4^-} >> \Gamma_{Na}$ and $\Gamma_{NaDeSO_4} \simeq \Gamma_{DeSO_4^-}$. This equation does not contain the factor, 2, in the denominator of the left hand side

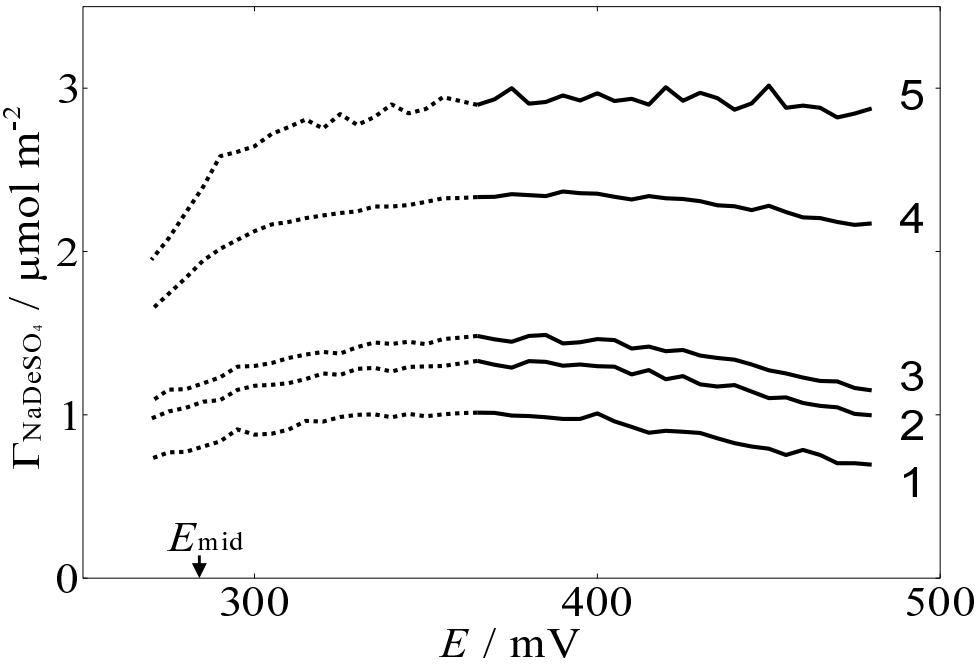

Figure 2.5: Potential-dependence of surface excess of $NaDeSO_4$ at $c^{\mathrm{b,W}}_{\mathrm{DeSO_4^-}} = 50$ (1), 80 (2), 100 (3), 200 (4), and 300 μmol dm^{-3}(5). The dotted lines represent the regions where the interface is possibly under the electrochemical instability.

of eq 2.4, because the electroneutrality at this interface is maintained by the supporting electrolytes [39]. Figure 2.5 shows the dependence of $\Gamma_{\mathrm{DeSO_4^-}}$ on E at $c^{\mathrm{b,W}}_{\mathrm{DeSO_4^-}} = 50$ (1), 80 (2), 100 (3), 200 (4), and 300 μmol dm^{-3} (5). The values of $\Gamma_{\mathrm{DeSO_4^-}}$ were obtained using a weighted three-point (curves 1 and 5) or a five-point (curves 2–4) moving average method of γ vs. $\ln c^{\mathrm{0,W}}_{\mathrm{DeSO_4^-}}$ plots. $\Gamma_{\mathrm{DeSO_4^-}}$ increases with increasing $c^{\mathrm{b,W}}_{\mathrm{DeSO_4^-}}$ and also increases with the negative shift of E from 480 to 380 mV (Figure 2.5). The dotted lines in Figure 2.5 show $\Gamma_{\mathrm{DeSO_4^-}}$ in the regions where the interface is probably under the electrochemical instability.

We estimated the values of $\Delta G^{\mathrm{W},\ominus}_{\mathrm{ads}}$ from the dependence of γ on $c^{\mathrm{0,W}}_{\mathrm{DeSO_4^-}}$. From eq 2.4, the lowering of γ with the adsorption of $DeSO_4^-$ is written as

$$\gamma_0 - \gamma = RT \int_0^{c^{\mathrm{0,W}}_{\mathrm{DeSO_4^-}}} \Gamma_{\mathrm{DeSO_4^-}} \mathrm{d} \ln c^{\mathrm{0,W}}_{\mathrm{DeSO_4^-}} \tag{2.5}$$

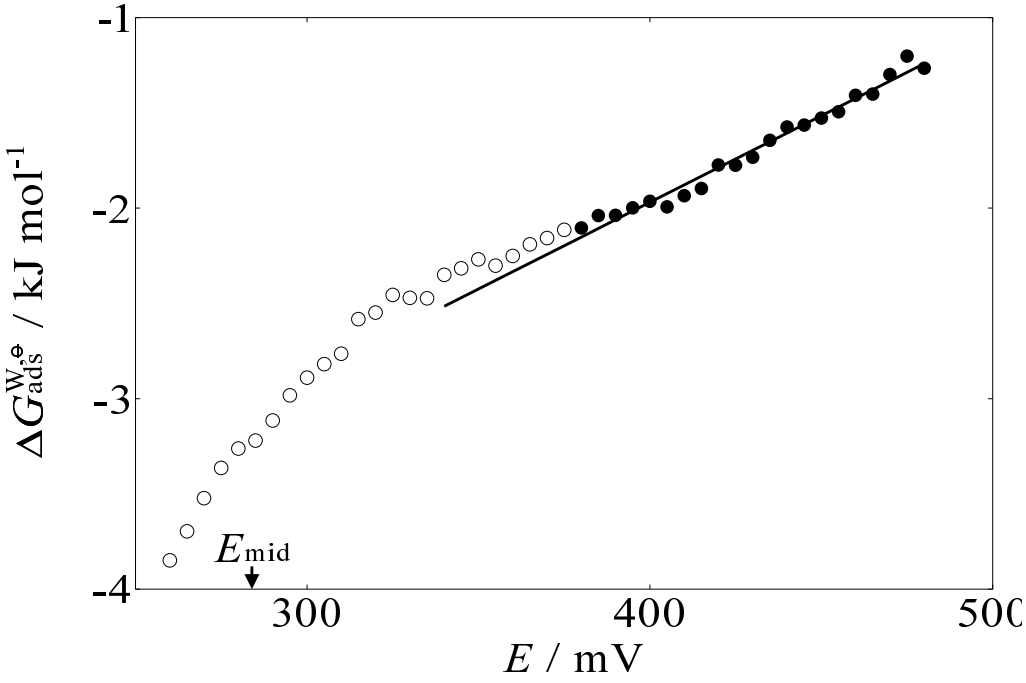

Figure 2.6: Potential-dependence of the standard Gibbs energy for the adsorption of $DeSO_4^-$ from W at the DCE|W interface. The open circles shows the regions where the interface is possibly under the electrochemical instability. The regression line is for the data between 380 mV and 480 mV.

where γ_0 is γ when $c^{b,W}_{DeSO_4^-} = 0$. In the case of the Langmuir isotherm,

$$Bc^{0,W}_{DeSO_4^-} = \frac{\Gamma_{DeSO_4^-}}{\Gamma^{max}_{DeSO_4^-} - \Gamma_{DeSO_4^-}}, \tag{2.6}$$

the dependence of γ is expressed as

$$\gamma_0 - \gamma = RT\Gamma^{max}_{DeSO_4^-} \ln\left(1 + Bc^{0,W}_{DeSO_4^-}\right) \tag{2.7}$$

where $\Gamma^{max}_{DeSO_4^-}$ and B are the maximum adsorbed amount of $DeSO_4^-$ and the adsorption coefficient $B = \exp(-\Delta G^{W,\ominus}_{ads}/RT)$, respectively. $\Gamma^{max}_{DeSO_4^-}$ was assumed to be 8.5×10^{-6} mol m^{-2}, the cross-section of all-trans alkane [40].

Figure 2.6 shows the potential-dependence of $\Delta G^{W,\ominus}_{ads}$ obtained by the weighted least-square fitting of eq 2.7 to the dependence of γ on $c^{0,W}_{DeSO_4^-}$. Open circles in Figure 2.6 indicate the values possibly affected with the electrochemical instability. It is dearly seen that $\Delta G^{W,\ominus}_{ads}$

linearly decreases with the change in E to the negative direction. It is questionable to give any physical meanings to the plot in $E < 380$ mV, because the interface is possibly in the instability condition in these regions. The straight line in Figure 2.6 is the linear regression line for the data between $E = 380$ and 480 mV. The slope of the line is 9.1 kJ mol^{-1} V^{-1}, which corresponds to $\beta = 0.91$. A simple interpretation for the departure of β from 0.5 is that the center of the charge of adsorbed ions is located in the W side of the interface, probably almost outside of the diffuse-part of the double layer in W [41].

2.3.4 Potential-dependent adsorption of $DeNH_3^+$.

Figure 2.7 shows cyclic voltammograms for the transfer of $DeNH_3^+$ across the DCE|W interface at $c^{b,W}_{DeNH_3^+} = 0$, 10, 20, 30, 40, 50, 60, 70, 80, 100, 200, 300, and 400 μmol dm^{-3} (curves 1 to 13, in this order). The dotted lines in Figure 2.7 are voltammograms recorded in the reverse scans. In Figure 2.7, the voltammograms were shown after E was corrected to have the same E_{mid} value, since the potential of the reference electrodes occasionally drifted between the measurements. In Figure 2.7, E_{mid} of the voltammograms is located at 395 mV. When $c^{b,W}_{DeNH_3^+} \geq 100$ μmol dm^{-3} , the irregularly increased currents were discerned in the voltammograms. In our previous studies [4, 6], the irregularly increased currents induced by the transfer of $DeNH_3^+$ clearly appeared in a certain potential region (instability window) in the polarized window above 500 μmol dm^{-3} of $DeNH_3^+$. In the present voltammograms, such a clear instability window was observed only at the highest concentration of $c^{b,W}_{DeNH_3^+}$, 400 μmol dm^{-3}.

Electrocapillary curves at the DCE|W interface in the presence of $DeNH_3^+$ are shown in Figure 2.8. The numbers in Figure 2.8 correspond to the numbers in Figure 2.7. Dotted line parts of the electrocapillary curves in Figure 2.8 were recorded in the regions where the irregularly increased currents clearly appeared on the voltammograms.

An increase in $c^{b,W}_{DeNH_3^+}$ reduces γ. When $E \geq 570$ mV, the γ values of all electrocapillary curves agreed with γ at $c^{b,W}_{DeNH_3^+} = 0$. This shows that the adsorbed amount of $DeNH_3^+$ at the DCE|W interface is negligible in the limiting current region. The maximum decrease in γ with

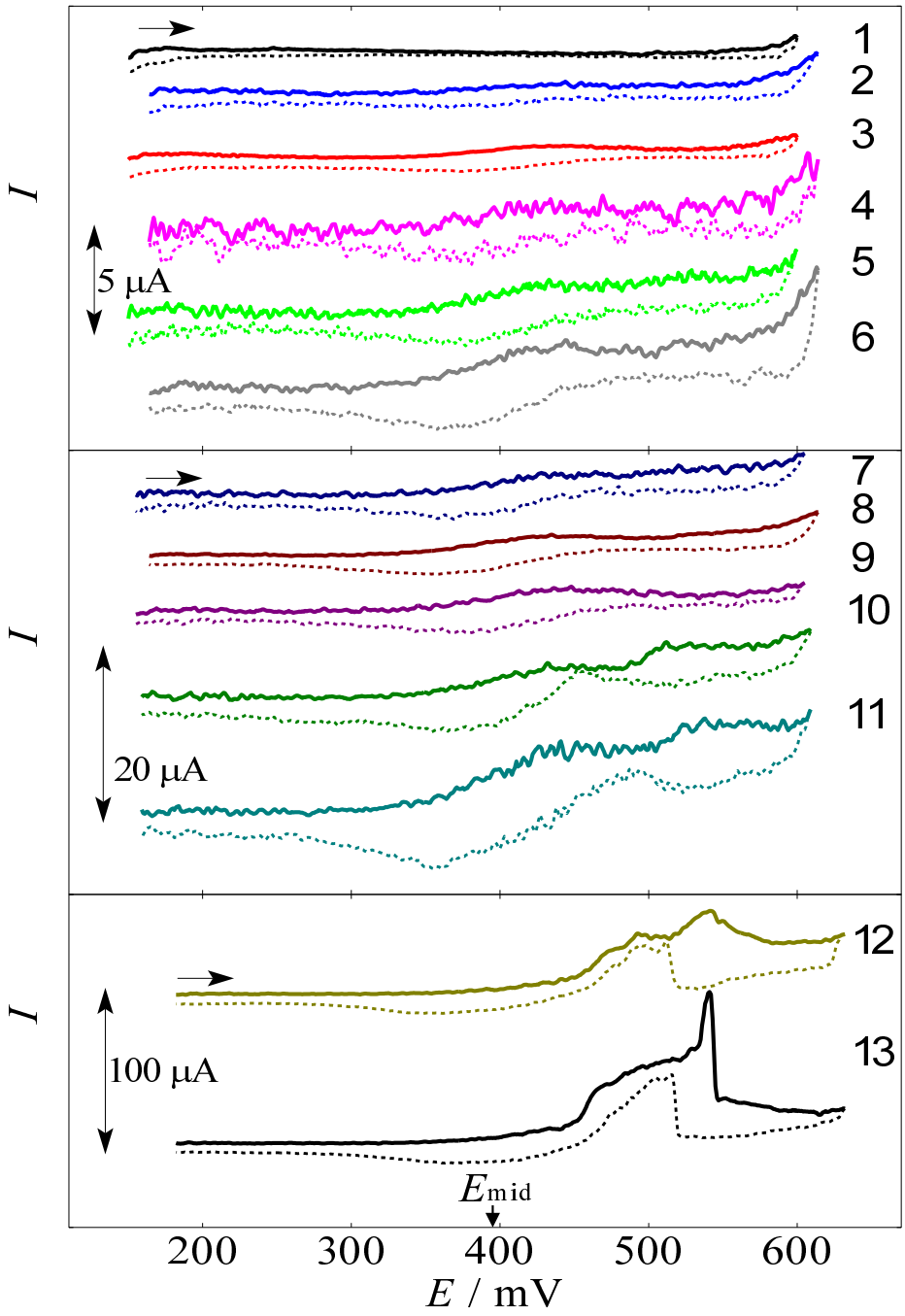

Figure 2.7: Cyclic voltammograms for the transfer of $DeNH_3^+$ across the DCE|W interface at $v = 10$ mV s^{-1} and $c^{b,W}_{DeNH_3^+} = 0$ (1), 10 (2), 20 (3), 30 (4), 40 (5), 50 (6), 60 (7), 70 (8), 80 (9), 100 (10), 200 (11), 300 (12), and 400 (13) μmol dm^{-3}. Dotted lines show the currents recorded in the reverse scans.

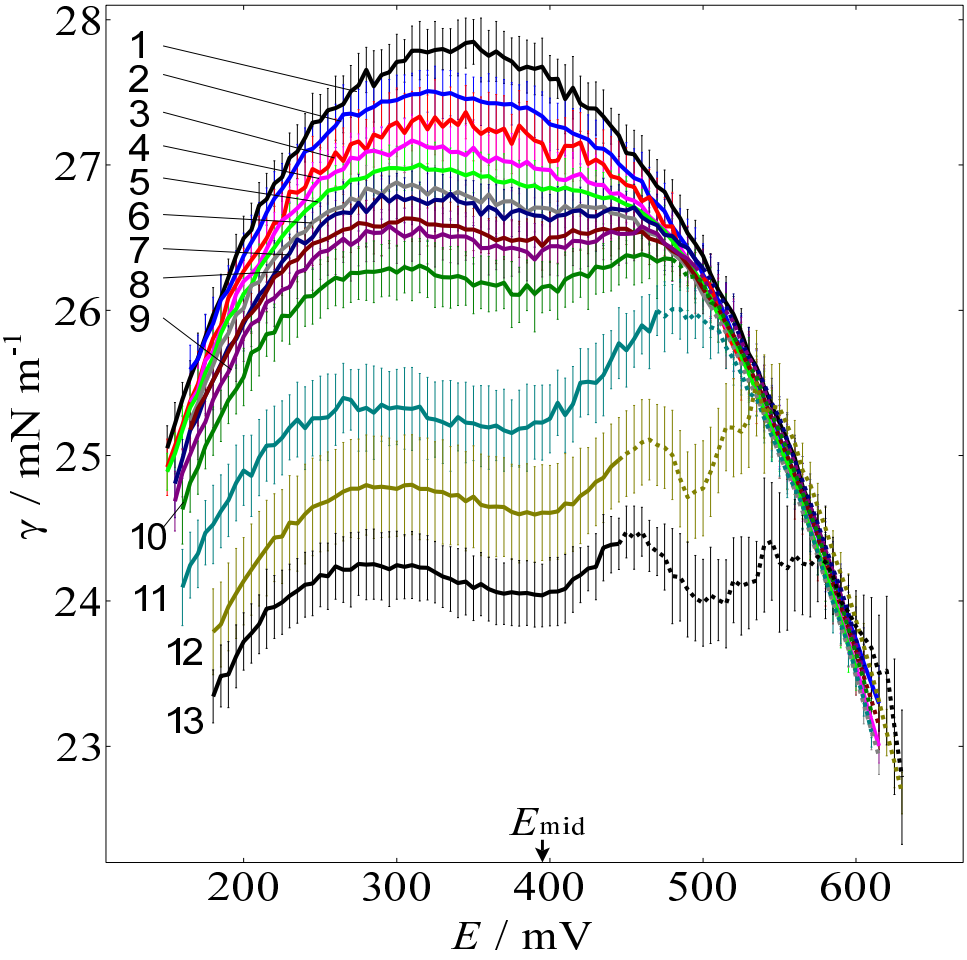

Figure 2.8: Electrocapillary curves recorded at $v = 10$ mV s^{-1} in the presence of $DeNH_3^+$. $c^{b,W}_{DeNH_3^+} = 0$ (1), 10 (2), 20 (3), 30 (4), 40 (5), 50 (6), 60 (7), 70 (8), 80 (9), 100 (10), 200 (11), 300 (12), and 400 (13) μmol dm^{-3}. Dotted parts of the curves show the data recorded with the irregularly increased current. Vertical bars show the 90% confidence interval for 10 measurements.

the increase of $c^{\mathrm{b,W}}_{\mathrm{DeNH_3^+}}$ was observed around E_{mid}. The decrease in γ in $E < E_{\mathrm{mid}}$ was greater than that in $E > E_{\mathrm{mid}}$. These electrocapillary curves indicate that $\mathrm{DeNH_3^+}$ strongly adsorbs when $\mathrm{DeNH_3^+}$ is distributed in the W phase than when $\mathrm{DeNH_3^+}$ is distributed in the DCE phase. These tendencies of the distribution and adsorption are similar to the cases of the adsorption of $\mathrm{DeSO_4^-}$ described above. The adsorptivity of $\mathrm{DeSO_4^-}$ is stronger than that of $\mathrm{DeNH_3^+}$, because at the same concentration and at E_{mid} the value of γ in the presence of $\mathrm{DeNH_3^+}$ is higher than the presence of $\mathrm{DeSO_4^-}$.

When $c^{\mathrm{b,W}}_{\mathrm{DeNH_3^+}} \geq 50$ μmol dm^{-3}, the electrocapillary curves have a positive curvature in the region around E_{mid}. In these potential regions, the DCE|W interface should be under the electrochemical instability and γ values have no thermodynamic meaning. The surface excesses of $\mathrm{DeNH_3^+}$ ($\Gamma_{\mathrm{DeNH_3^+}}$) for six different $c^{\mathrm{b,W}}_{\mathrm{DeNH_3^+}}$ were calculated using a five-point moving average method of γ vs. $\ln c^{0,\mathrm{W}}_{\mathrm{DeNH_3^+}}$ plots. From the Gibbs adsorption equation in the system (cell II) in the presence of the supporting electrolytes, we obtain

$$-\frac{1}{RT}\left(\frac{\partial\gamma}{\partial \ln c^{0,\mathrm{W}}_{\mathrm{DeNH_3^+}}}\right)_{P,T,\mu_i,E} = \Gamma_{\mathrm{DeNH_3^+}}. \tag{2.8}$$

Figure 2.9 shows the potential-dependence of $\Gamma_{\mathrm{DeNH_3^+}}$ on E at $c^{\mathrm{b,W}}_{\mathrm{DeNH_3^+}} = 40$ (curve 1), 50 (curve 2), 60 (curve 3), 70 (curve 4), 80 (curve 5), and 100 μmol dm^{-3} (curve 6). $\Gamma_{\mathrm{DeNH_3^+}}$ increases with an increase in $c^{\mathrm{b,W}}_{\mathrm{DeNH_3^+}}$. The maximum of $\Gamma_{\mathrm{DeNH_3^+}}$ appeared around 350 mV, where is about 50 mV more negative than E_{mid}. In the potential more positive than this maximum, the values of $\Gamma_{\mathrm{DeNH_3^+}}$ decreased sharply with E.

The value of $\Delta G^{\mathrm{W},\ominus}_{\mathrm{ads}}$ for the adsorption of $\mathrm{DeNH_3^+}$ at DCE|W was estimated with weighted least-square fitting of eq 2.7 to the experimental dependence of γ on $c^{0,\mathrm{W}}_{\mathrm{DeNH_3^+}}$. In this fitting, we assumed that $\Gamma^{\max}_{\mathrm{DeNH_3^+}} = 8.5 \times 10^{-6}$ mol m^{-2}. Figure 2.10 shows the potential-dependence of $\Delta G^{\mathrm{W},\ominus}_{\mathrm{ads}}$ of $\mathrm{DeNH_3^+}$. A linear relationship with the slope of -9.8 kJ mol^{-1} V^{-1} was observed between $\Delta G^{\mathrm{W},\ominus}_{\mathrm{ads}}$ of $\mathrm{DeNH_3^+}$ and E. The slope corresponds to β of 0.90. This value of β is close to the β value of $\mathrm{DeSO_4^-}$ and suggests that the center of charge of adsorbed $\mathrm{DeNH_3^+}$ is located almost outside of the diffuse-part of the electrical double layer in W. According to the model of potential-dependent adsorption, the maximum adsorption occurs at $\Delta^{\mathrm{W}}_{\mathrm{O}}\phi^{\ominus} - 57/z$ mV when

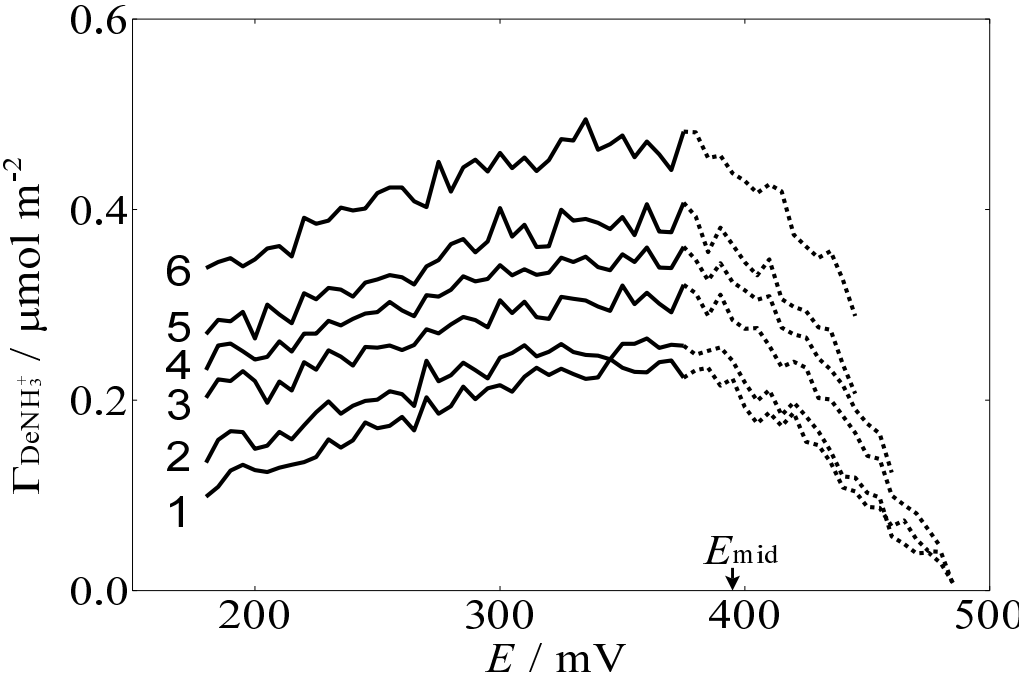

Figure 2.9: Potential-dependence of the surface excess of $DeNH_3^+$ at $c^{b,W}_{DeNH_3^+} = 40$ (1), 50 (2), 60 (3), 70 (4), 80 (5), and 100 (6) μmol dm^{-3}. The dotted lines represent the regions where are possibly affected with the electrochemical instability.

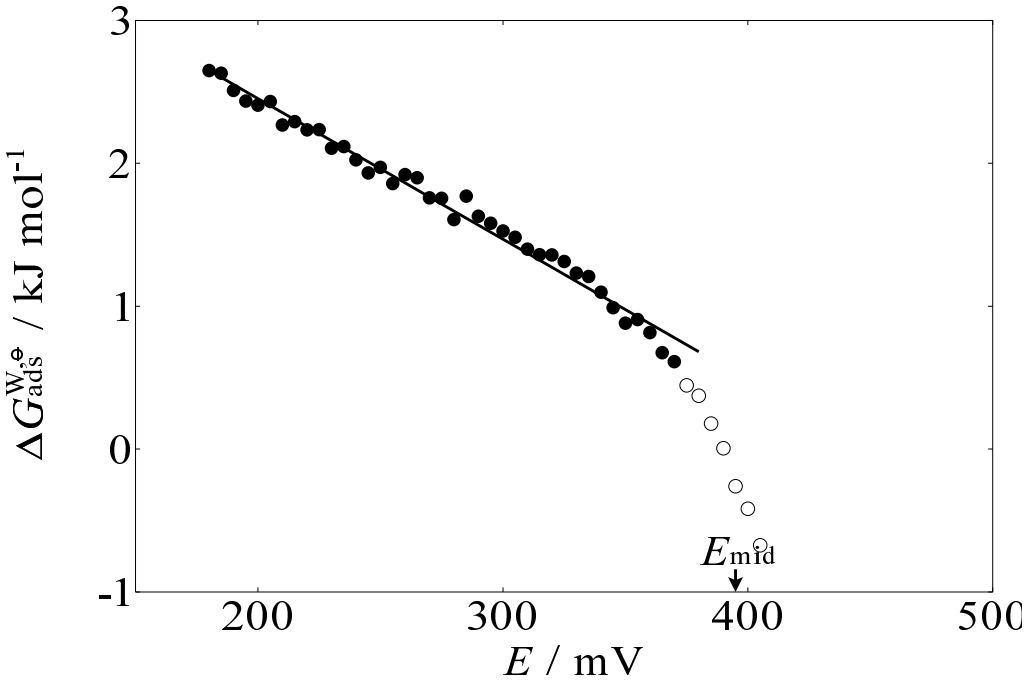

Figure 2.10: Potential dependence of the standard Gibbs energy for the adsorption of $DeNH_3^+$ from W at the DCE|W interface. The open circles shows the regions where are possibly affected with the electrochemical instability. The line shows a liner regression for the data between 180 mV and 370 mV.

$\beta = 0.9$ [8]. The location of the maximum of $\Gamma_{\mathrm{DeNH_3^+}}$ in Figure 2.9 seems to corroborate this relation.

2.4 Conclusions

The simultaneous recording of a voltammogram and an electrocapillary curve has revealed that the interface is under the electrochemical instability even in the potential region where the irregularly increased current is not discerned in the voltammogram. The potential-dependent adsorption of $\mathrm{DeSO_4^-}$ and $\mathrm{DeNH_3^+}$ at the DCE|W interface under the transfer of these ions was examined. In the potential region before the emergence of the electrochemical instability, the standard Gibbs energies for the adsorption of $\mathrm{DeSO_4^-}$ and $\mathrm{DeNH_3^+}$ are both linearly dependent on the potential, as was assumed in the simple model for the potential-dependent adsorption and partitioning of surface active ions at the liquid-liquid interface [8]. The values of β of $\mathrm{DeSO_4^-}$ and $\mathrm{DeNH_3^+}$ determined were 0.91 and 0.90, respectively. These β values suggest that the charged head groups of adsorbed $\mathrm{DeSO_4^-}$ and $\mathrm{DeNH_3^+}$ are protruded into the W phase. The large departure of β from 0.5 seems to be a property common to conventional ionic surfactant composed of a non-charged hydrophobic part and a hydrophilic charged part.

References

[1] Kakiuchi, T. *J. Electroanal. Chem.* **2002**, *536*, 63–69.

[2] Kakiuchi, T.; Chiba, M.; Sezaki, N.; Nakagawa, M. *Electrochem. Commun.* **2002**, *4*, 701–704.

[3] Kakiuchi, T.; Nishi, N.; Kasahara, T.; Chiba, M. *ChemPhysChem* **2003**, *4*, 179–185.

[4] Kasahara, T.; Nishi, N.; Yamamoto, M.; Kakiuchi, T. *Langmuir* **2004**, *20*, 875–881.

[5] Sakka, T.; Tanaka, K.; Shibata, Y.; Ogata, Y. H. *J. Electroanal. Chem.* **2006**, *591*, 168–174.

[6] Kitazumi, Y.; Kakiuchi, T. *J. Phys.: Condens. Matter* **2007**, *19*, 375104.

[7] Kakiuchi, T. *J. Electroanal. Chem.* **2004**, *569*, 287–291.

[8] Kakiuchi, T. *J. Electroanal. Chem.* **2001**, *496*, 137–142.

[9] Kakiuchi, T.; Kobayashi, M.; Senda, M. *Bull. Chem. Soc. Jpn.* **1987**, *60*, 3109–3115.

[10] Kakiuchi, T.; Kobayashi, M.; Senda, M. *Bull. Chem. Soc. Jpn.* **1988**, *61*, 1545–1550.

[11] Maeda, K.; Kihara, S.; Suzuki, M.; Matsui, M. *J. Electroanal. Chem.* **1990**, *295*, 183–201.

[12] Maeda, K.; Hyogo, W.; Nagami, S.; Kihara, S. *Bull. Chem. Soc. Jpn.* **1997**, *70*, 1505–1515.

[13] Goto, T.; Maeda, K.; Yoshida, Y. *Langmuir* **2005**, *21*, 11788–11794.

[14] Higgins, D. A.; Corn, R. M. *J. Phys. Chem.* **1993**, *97*, 489–493.

[15] Piron, A.; Brevet, P. F.; Girault, H. H. *J. Electroanal. Chem.* **2000**, *483*, 29–36.

[16] Nishi, N.; Izawa, K.; Yamamoto, M.; Kakiuchi, T. *J. Phys. Chem. B* **2001**, *105*, 8162–8169.

[17] Nishi, N.; Kakiuchi, T. *Russ. J. Electrochem.* **2003**, *39*, 125–129.

[18] Martins, M. C.; Pereira, C. M.; Girault, H. H.; Silva, F. *Electrochim. Acta* **2004**, *50*, 135–139.

[19] Lhotsky, A.; Mareček, V.; Zalis, S.; Samec, Z. *J. Electroanal. Chem.* **2005**, *585*, 269–274.

[20] Yoshida, Z.; Kihara, S. *J. Electroanal. Chem.* **1987**, *227*, 171–181.

[21] Fermin, D. J.; Ding, Z. F.; Duong, H. D.; Brevet, P. F.; Girault, H. H. *J. Phys. Chem. B* **1998**, *102*, 10334–10341.

[22] Nagatani, H.; Fermin, D. J.; Girault, H. H. *J. Phys. Chem. B* **2001**, *105*, 9463–9473.

[23] Nagatani, H.; Ozeki, T.; ; Osakai, T. *J. Electroanal. Chem.* **2006**, *588*, 99–105.

[24] Girault, H. H. J.; Schiffrin, D. J.; Smith, B. D. V. *J. Colloid Interface Sci.* **1984**, *101*, 257–266.

[25] Kakiuchi, T.; Nakanishi, M.; Senda, M. *Bull. Chem. Soc. Jpn.* **1988**, *61*, 1845–1851.

[26] Bashforth, F.; Adams, J. C. *An Attempt to Test the Theories of Capillary Action*; Cambridge University Press, 1883.

[27] Nakagawa, T.; Oyanagi, Y. Program System 'SALS' for Nonlinear Least Squares Fitting in Experimental Sciences; In *Recent Developments in Statistical Inference and Data Analysis*; Matusita, K., Ed.; North Holland Publishing Company: Amsterdam, 1980; pp 221–225.

[28] Maze, C.; Burnet, G. *Surf. Sci.* **1971**, *24*, 335–342.

[29] Ohde, H.; Uehara, A.; Yoshida, Y.; Maeda, K.; Kihara, S. *J. Electroanal. Chem.* **2001**, *496*, 110–117.

[30] Yoshida, Y.; Maeda, K.; Shirai, O. *J. Electroanal. Chem.* **2005**, *578*, 17–24.

[31] Kakiuchi, T.; Senda, M. *Bull. Chem. Soc. Jpn.* **1983**, *56*, 1322–1326.

[32] Kakiuchi, T.; Senda, M. *Bull. Chem. Soc. Jpn.* **1983**, *56*, 1753–1760.

[33] Samec, Z.; Mareček, V.; Holub, K.; Račinský, S.; Hájková, P. *J. Electroanal. Chem.* **1987**, *225*, 65–78.

[34] Roozeman, R. J.; Liljeroth, P.; Johans, C.; Williams, D. E.; Kontturi, K. *Langmuir* **2002**, *18*, 8318–8323.

[35] Kakiuchi, T.; Teranishi, Y.; Niki, K. *Electrochim. Acta* **1995**, *40*, 2869–2874.

[36] Thomson, J. *Philos. Mag.* **1855**, *10*, 330–333.

[37] Marangoni, C. *Ann. Phys. Chem.* **1871**, *143*, 337–354.

[38] Wandlowski, T.; Mareček, V.; Samec, Z. *Electrochim. Acta* **1990**, *35*, 1173–1175.

[39] Tajima, K. *Bull. Chem. Soc. Jpn.* **1970**, *43*, 3063–3066.

[40] Doucet, J.; Denicolo, I.; Craievich, A. *J. Chem. Phys.* **1981**, *75*, 1523–1529.

[41] Kakiuchi, T.; Takasu, Y. *J. Phys. Chem. B* **1997**, *101*, 5963–5968.

Chapter 3

Imaging of the liquid-liquid interface under the electrochemical instability using confocal fluorescence microscopy

The onset of the electrochemical instability has been imaged at the 1,2-dichloroethane (DCE)|water (W) interface modified with a fluorescent phospholipid using confocal fluorescence microscopy (CFM). Heterogeneously fluorescent images are recorded successively under the transfer of dodecylsulfate ions (DS^-) across the interface, which induces the irregularly increased current in a voltammogram. The commencement of the hydrodynamic movement of the solutions due to the electrochemical instability has been detected as the appearance of dark domains at the edge of the interface, that is, the three-phase contact of the DCE-W-glass wall confining the interface. In the potential region around the mid-point potential of the transfer of DS^-, the area of the dark domains fluctuates and gradually grows with time. These locally confined unstable domains give rise to slightly augmented current in the simultaneously recorded voltammogram. The interface in this potential range appears to be globally stable at the expense of small unstable domains. In the potential region where the irregularly increased current is visible in the voltammogram, the entire interface becomes unstable and the dark and bright regions move vertiginously due to the Marangoni convection of the adjacent solution phases.

3.1 Introduction

The electrochemical instability is a thermodynamically unstable condition of the liquid-liquid interface [1] caused by the potential-dependent adsorption of surface-active ions [2], and induces irregular currents on ion-transfer voltammograms of surface-active ions [3–7]. The irregular current corresponds to the turbulence near the interface due to the interfacial-tension-driven convection or the Marangoni convection. The electrochemical instability is conditioned by the phase-boundary potential ($\Delta_{\mathrm{O}}^{\mathrm{W}}\phi$) and appears only in the limited range of $\Delta_{\mathrm{O}}^{\mathrm{W}}\phi$, that is, in the instability potential window [1]. The stable and unstable states are switched by $\Delta_{\mathrm{O}}^{\mathrm{W}}\phi$. It is interesting to see microscopically how the interface enters into the mode of the electrochemical instability.

Uredat and Findenegg observed the phase transition and the formation of the domain structure in the Gibbs monolayer of octadecanol and 1,1,2,2-tetrahydroperfluorododecanol at the hexane|water interface using Brewster angle microscopy (BAM) [8] and showed the usefulness of BAM to study the temperature-induced phase transition of the Gibbs monolayer films at the liquid-liquid interface. At the air-water interface, the phase transition and the domain formation of the phospholipid films have been observed by epifluorescence microscopy [9, 10]. Dale and Unwin employed CFM to see the movement of the liquid-liquid interface, responding to the applied voltage [11]. However, the two-dimensional imaging of the liquid-liquid interface under the control of $\Delta_{\mathrm{O}}^{\mathrm{W}}\phi$ has not been reported. It is highly likely that the electrochemical instability is accompanied by the microscopic domain formation at the liquid-liquid interface, because the hydrodynamic movement of the liquid phase caused by the Marangoni effect, where the local change in the interfacial tension is the driving force of the movement, is responsible to the irregular current. The microscopic structure at the liquid-liquid interface at the incipient stage of the electrochemical instability may then be observed with microscopic techniques. Confocal fluorescence microscopy (CFM) has a potential to observe adsorbed molecules at the liquid-liquid interface with high sensitivity and selectivity [12], because CFM has a higher depth resolution than conventional fluorescence microscopy and is suitable to observe the fluorophore-adsorbed

liquid-liquid interface in the presence of the fluorophore in the adjacent bulk phase. In the present work, we successfully imaged the inhomogeneity at the 1,2-dichloroethane (DCE)|water (W) interface caused by the transfer of dodecylsulfate (DS^-) across the interface using CFM and a probe, a fluorescent phospholipid, which is zwitterionic and stays adsorbed in the entire range of the applied potential across the interface, unless disturbed by the electrochemical instability.

3.2 Experimental section

DCE was washed with concentrated sulfuric acid, water, an aqueous solution of Na_2CO_3, and water, successively. After being dried with $CaCl_2$, the DCE was distilled and washed with copious water three times before use. Water employed was purified with a Milli-Q system (Milli-Q Gradient, Millipore). Tetrapentylammonium tetraphenylborate (TPnATPB) was synthesized as described elsewhere [13]. Tetrapentylammonium chloride (TPnACl), LiCl, $MgCl_2$, sorbitan monooleate (SMO), sodium dodecylsulfate (NaDS), 2-(4,4-difluoro-5,7-diphenyl-4-bora-3a,4a-diaza-*s*- indacene-3-pentanoyl)-1-hexadecanoyl- *sn*-glycero-3- phosphocholine (D3815, Molecular Probes) were used without further purification.

$\Delta^{\mathrm{W}}_{\mathrm{O}}\phi$ of the polarized DCE|W interface was controlled using the electrochemical cell:

Ag	AgCl	5 mmol dm^{-3} TPnACl 10 mmol dm^{-3} $MgCl_2$	50 mmol dm^{-3} TPnATPB 0.3 μmol dm^{-3} D3815	100 mmol dm^{-3} LiCl 1 mmol dm^{-3} NaDS	AgCl	Ag	(I)
		W_{ref}	DCE	W			

The potential of the right-hand-side terminal with respect to the left is hereafter denoted as E. The current (I) due to the flow of the positive charge from W to DCE was taken to be positive.

The configuration of the cell is illustrated in Figure 3.1. A glass plate of 1.7 mm thickness having a center hole of 2 mm diameter was used to support the DCE|W interface. The

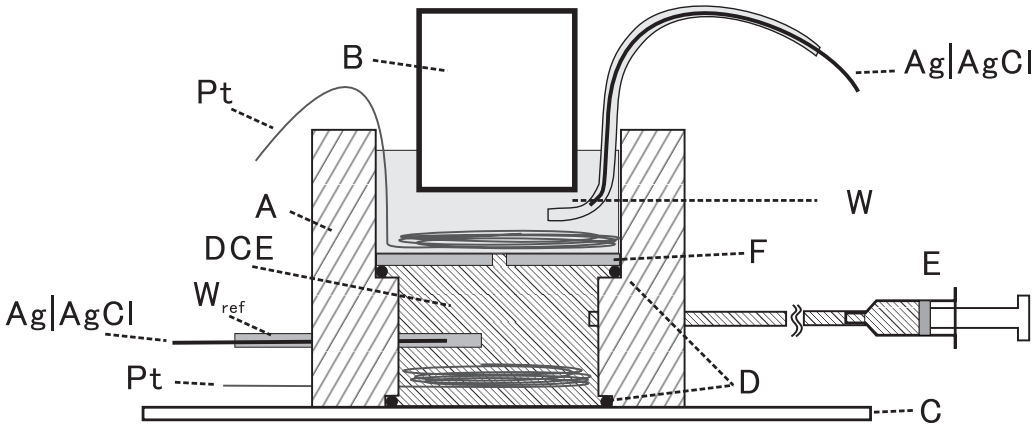

Figure 3.1: Shematic representation of the experimental cell, A: Teflon body, B: objective, C: slide glass, D: O rings, E: micro injector, and F: glass plate with a hole of 2 mm diameter.

position of the interface was adjusted to be located at the upper orifice of the hole. A four-electrode potentiostat equipped with ohmic drop compensation (HA10100mM, Hokuto Denko) was employed to control the potential drop across the DCE|W interface.

A confocal unit (CSU10, Yokogawa), which is capable of collecting 360 images per second, and a high sensitivity camera (C7190, Hamamatsu), which collects 30 frames per second, were attached to a fixed stage upright microscope (BX51WI, Olympus) on a vibration isolation stage. The flatness of the DCE|W interface was checked by the homogeneity of the fluorescence. To set the focal plane at the DCE|W interface, the focus was adjusted to have the highest fluorescence intensity [12]. A water-immersion objective lens with 10x magnification and the numerical aperture of 0.3 was employed. A home-made program was used for synchronized recording of I and fluorescence microscopy images and for controling of E. The accuracy of the synchronization between setting a value of E and an image recording was at least 33 ms, which corresponds to the precision of 3 mV in the setting of E at the scan rate (v) of 100 mV s^{-1}. A home-made program was employed for the analysis of CFM images.

3.3 Results and discussion

3.3.1 CFM imaging under the potential sweep.

Two voltammograms in Figure 3.2A were recorded in the presence of 1 mmol dm^{-3} DS^- in W and 0.3 μmol dm^{-3} D3815 in DCE at $v = 100$ mV s^{-1}. The solid and the dotted lines in Figure 3.2A are the voltammograms recorded in the absence and presence of 1 mmol dm^{-3} SMO in DCE, respectively. The addition of SMO suppresses the irregularly increased current on the ion-transfer voltammogram due to the electrochemical instability [3–7]. The forward scan starting from 500 mV to the negative direction of E gives rise to the negative current due to the transfer of DS^- from W to DCE. The dotted line shows a diffusion-limited-like ion transfer with a negative peak in the forward scan and a positive peak in the reverse scan, giving the mid-point potential (E_{mid}) of 355 mV. The irregularly increased current appeared in the potential regions between 300 and 140 mV in the forward scan and between 160 and 380 mV in the reverse scan (the solid line in Figure 3.2A). The currents outside of this region agree with the dotted line, as has been observed in previous works of the electrochemical instability [3–7].

The intensity of the fluorescence at the DCE|W interface in the absence of DS^- was uniform and independent of E in the polarized window of $100 < E < 500$ mV. When $E = 500$ mV, there was no visible difference in the fluorescent intensities at the DCE|W interface in the absence and presence of DS^-. The adsorption of DS^- should be appreciable [14], but does not seem to appreciably affect the adsorption of D3815. Figure 3.2B shows a series of the confocal fluorescence images of the DCE|W interface recorded simultaneously with recording the solid line in Figure 3.2A. The alphabetical label in each panel of the images corresponds to the same label in the voltammogram in Figure 3.2A at the potential indicated. The lower right corners of the images in Figure 3.2B are the edge of the glass plate supporting the DCE|W interface. The bright circle at the lower right corner is a drop of the DCE phase attached on the glass plate while the handling of the cell.

From $E = 500$ to 370 mV in the forward scan, the DCE|W interface was homogeneously

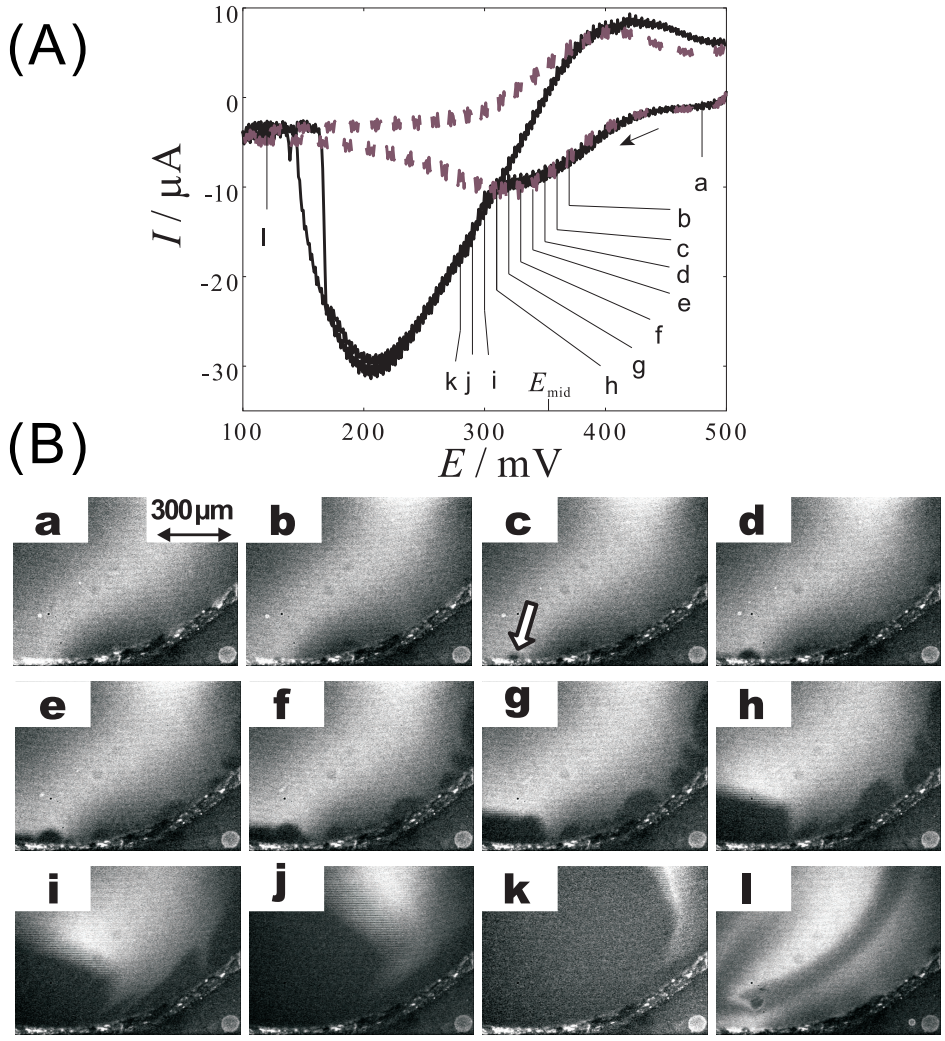

Figure 3.2: Voltammograms for the transfer of DS^- across the DCE|W interface modified with D3815 at v = 100 mV s^{-1} (A) and simultaneously recorded fluorescent images of the interface (B). The solid and dotted lines indicate the voltammograms recorded in the absence and presence of 1 mmol dm^{-3} SMO in the DCE phase, respectively. E_{mid} indicates the mid-point potential of the transfer of DS^-. The arrow in image c points the appeared dark domain.

fluorescent (Figure 3.2B, (a, b)). At $E = 360$ mV, the domain with weaker fluorescence or a darker domain appeared at the interface, as pointed by the arrow in Figure 3.2B, (c). The dark domains grew slowly with scanning of E (Figure 3.2B, (d–h)). When $E \leq 300$ mV, the dark domain at the lower left grew rapidly and the movement of the dark domain continued while the irregularly increased current was recorded on the voltammogram. In this potential region, the dark domains grown at the interface were flushed out from the field of view because of the vigorous lateral flow of the interface (Figure 3.2B, (i–k)). The irregularly increased current on the cyclic voltammogram disappeared in concurrence with the disappearance of the movement when $E < 140$ mV. The trace of the turbulence persisted as inhomogeneous fluorescence at the DCE|W interface (Figure 3.2B, (l)).

There must be a depletion of D3815 in the dark domain. The instability caused by the adsorption and partition of DS^- carried away adsorbed D3815 from the interface in the region, $140 < E < 360$ mV. Since the adsorption of DS^- in this potential range is thermodynamically unstable, adsorbed DS^- ions should also be absent or significantly reduced in the dark domains [14]. The fluorescent probe is carried away hydrodynamically with the desorption of DS^-.

It is notable that the irregularly increased current was not observed in the region, $310 < E < 370$ mV (Figure 3.2B, (b–h)). In our previous studies of the electrochemical instability accompanied by the transfer of surface-active ions, we noticed in voltammograms of ion transfer a small but appreciable current increase in E_{mid} in comparison with the diffusion-limited current [3, 4, 14]. These observations demonstrate that the irregularly increased current is not the only phenotype of the electrochemical instability at the liquid-liquid interface and the locally confined unstable regions coexist with the stable part of the interface.

The appearance and growth of dark domains with the scanning of E was imaged around E_{mid} at different values of v studied. The existence of the dark domain is therefore conditioned by E and is independent of I, that is, the concentration gradient of DS^- at the DCE|W interface. This corroborates the thermodynamic nature of the electrochemical instability [1]. In the present system, all the dark domains appeared at the edge of the DCE|W interface or the

DCE-W-glass wall boundary. The heterogeneous current density at the meniscus may catalyze the emergence of the electrochemical instability. While the electrochemical instability emerged at the boundary remains to be locally confined to the dark domains, the global stability of the entire DCE|W interface is maintained. The dark domains may be likened to a sacrificed anode in corrosion of metals.

3.3.2 Evolution of the dark domains under the potentiostatic condition.

To see the evolution of the dark domains at a given value of E, the CFM images of the interface were recorded under the potentiostatic condition. Figure 3.3A shows a potential-step chronoamperogram for the transfer of 1 mmol dm^{-3} DS^{-} in W when E was stepped from 400 to 340 mV at $t = 0$ and further stepped from 340 to 320 mV at $t = 5$ s. Figure 3.3B shows the time-dependence of the area of the dark domain (S) appeared at the bottom-right corner on the view-field. Figure 3.3C shows a series of CFM images of the DCE|W interface recorded simultaneously with Figure 3.3A. The alphabetical labels in the images correspond to the alphabets on Figure 3.3B, showing the values of t when the images were acquired.

At $E = 400$ mV, the interface was homogeneously fluorescent (Figure 3.3C, (a)). When E was stepped from 400 to 340 mV ($t = 0$), the current similar to the diffusion-limited current was recorded, but a dark domain appeared in Figure 3.3C at $t = 0.2$ s, (b). Then S increased slowly with time (Figure 3.3C, (c–e)) and seemed to reach a quasi-stationary value, while E was kept at 340 mV. In Figure 3.3C, the shape of the dark domain at 340 mV was not deformed extremely as the dark domain in Figure 3.2B, (f–i). The presence of the slowly growing dark domain in Figure 3.3C, (b–e) corresponds to a slightly augmented current in comparison with that for the diffusion-limited case. When E was stepped from 340 to 320 mV at $t = 5$ s, S decreased abruptly (Figure 3.3C, (f, g)). This conspicuous change of S may correspond to the emergence of another dark domain out of the view-field. In Figure 3.3C, (h), another dark domain is seen over the top edge of the view-field. When E was kept at 320 mV, the dark

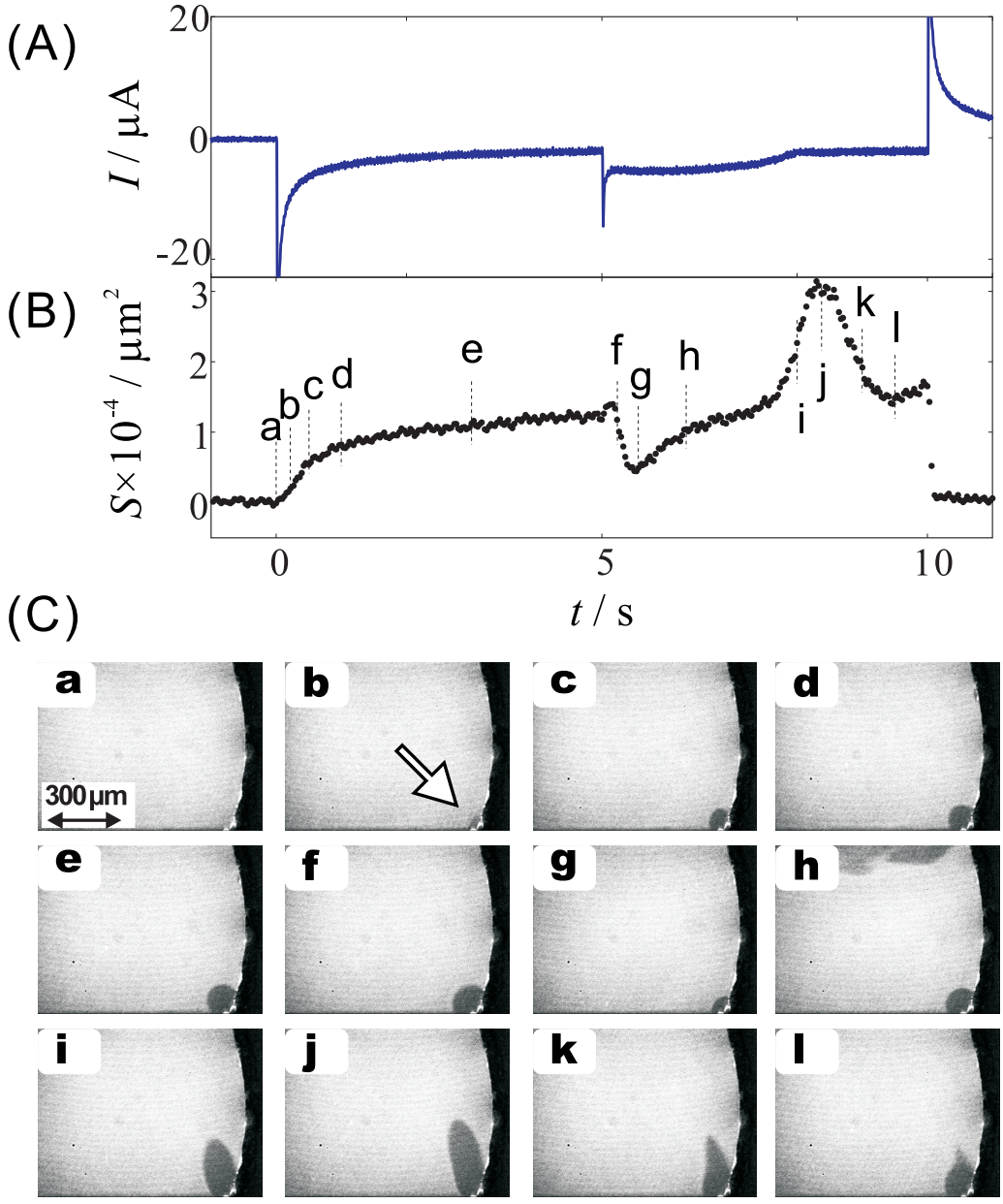

Figure 3.3: A potential-step chronoamperogram for the transfer of DS^- across the D3815 modified DCE|W interface (A), a time-dependence of the area of a dark domain (B), and simultaneously recorded fluorescent images of the interface (C) when E was stepped from 400 to 340 mV at $t = 0$, from 340 to 320 mV at $t = 5$ s, and from 320 to 400 mV at $t = 10$ s. The alphabets in the images correspond to the alphabets in B. The arrow in image b points the appeared dark domain.

domain at the lower right corner of the view-field showed stretching or elongating motion Figure 3.3C, (h–l).

At both $E = 340$ and 320 mV, the interface is under the electrochemically unstable condition. However, the motion of the dark domain at $E = 320$ mV was more vigorous than that at $E = 340$ mV. The degree of the Marangoni effect or the driving force of the hydrodynamic movement of the adjacent solutions thus depends on E. The global stability of the interface in the presence of the dark domains when E is in the instability window implies that the local value of $\Delta_{\mathrm{O}}^{\mathrm{W}}\phi$ may be different from place to place, though the global $\Delta_{\mathrm{O}}^{\mathrm{W}}\phi$ is maintained at a constant value by the potentiostat. The locally confined domain, which is under the electrochemically unstable condition, in effect maintains the global stability of the interface, as described above. The existence of such a domain in the interface should cause the local enhancement of the mass transfer in the vicinity of the interface and augment the current, which is, otherwise, diffusion-limited.

When the interface is under the global stability in spite of the electrochemical instability, the interface often shows a kind of rhythmic motion. Figure 3.4A shows potential-step chronoamperograms for the transfer of 1 mmol dm^{-3} DS^- in W when E was stepped from 400 to 330 mV at $t = 0$. The dotted line in Figure 3.4A was recorded in the presence of 1 mmol dm^{-3} SMO in the DCE phase. Figure 3.4B shows the time-dependence of S when the solid line in Figure 3.4A was recorded.

The negative current in Figure 3.4A decreased monotonically when $t > 0$. The current shows the interface at $E = 330$ mV is under the global stability. Appeared dark domains in CFM images showed an oscillatory deformation like as Figure 3.3C, (h–l) when $t > 0.15$ s. The estimated period of the deformation in the case shown in Figure 3.4 is about 1.4 s. The period seems to be affected by several factors, such as E, the concentration of DS^-, and the shape of the interface. This rhythmic motion at the interface is quasi-two-dimensional and should be distinguished from the oscillation phenomena at the liquid-liquid interface where the interface is globally unstable [15–18].

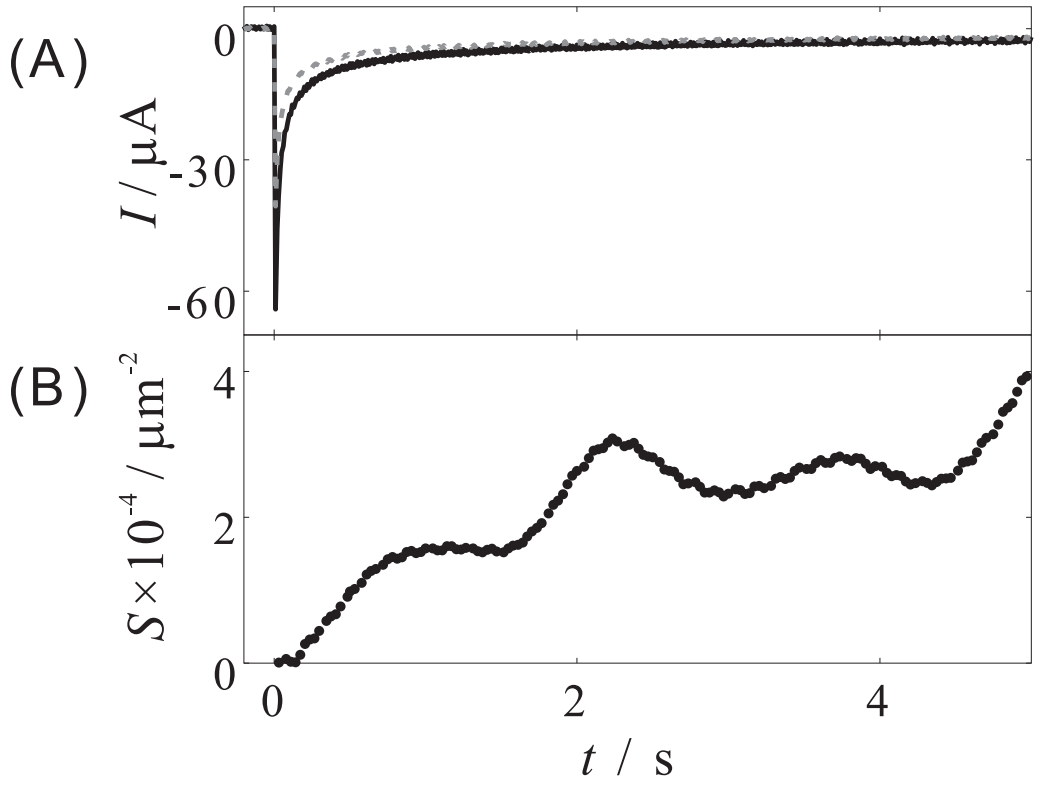

Figure 3.4: A potential-step chronoamperogram for the transfer of DS^- across the D3815 modified DCE|W interface (A) and a time-dependence of the area of a dark domain (B) when E was stepped from 400 to 330 mV at $t = 0$. The dotted line in (A) shows the chronoamperogram recorded in the presence of 1 mmol dm^{-3} SMO in the DCE phase.

3.3.3 CFM imaging under the globally unstable conditions.

We examined the evolution of the dark domains when E was stepped to 300 mV, where the interface was globally unstable and the irregularly increased current appeared in Figure 3.2A. The solid line in Figure 3.5A shows a chronoamperogram recorded when E was stepped from 400 to 300 mV at $t = 0$ in the presence of 1 mmol dm^{-3} DS^{-} in W. Images in Figure 3.5B show the CFM images of the DCE|W interface from $t = 0$ to $t = 0.33$ s with the interval of 1/30 s. The number in each image shows the time when the image was recorded.

The negative current, which is the convolution of the charging current and ion-transfer current due to the transfer of DS^{-}, initially decreases with time, as is usual in potential-step chronoamperometry. However, at $t = 0.09$ s, the current reached a minimum and, when $t > 0.09$ s, the negative current of the solid line fluctuated irregularly (See inset of Figure 3.5A). In contrast, the current recorded in the presence of 3 mmol dm^{-3} SMO in DCE (dotted line) monotonically decreased with time. The magnitude of the current in the solid line is much greater than that of the dotted line, suggesting the hydrodynamic movement of the solution bulk.

In CFM images in Figure 3.5B, the dark domain appeared right after the step of E (the arrow in the image at $t = 0.03$ s) and grew rapidly (images when $0.03 \leq t \leq 0.13$ s). When $t \leq 0.13$ s, the irregular movement of the interface was not observed. When $t > 0.13$ s, the growing dark domain from the upper left in the images drove the other dark domain in the lower right corner. The disagreement between the augmentation of the current at $t = 0.09$ s and this pushing out of the dark domain suggests that the irregular movement of the interface has emerged outside of the view-field. Once the irregularly increased current or the turbulence near the DCE|W interface appeared, the motion of the CFM image was too fast to follow the details of the evolution or movement of the unstable domains.

The addition of SMO is known to be effective to suppress the irregularly increased current and the vigorous movement of the interface [3–7, 14]. Figure 3.5C show the CFM images recorded simultaneously with the dotted line in Figure 3.5A. When $t > 0$, the dark domain

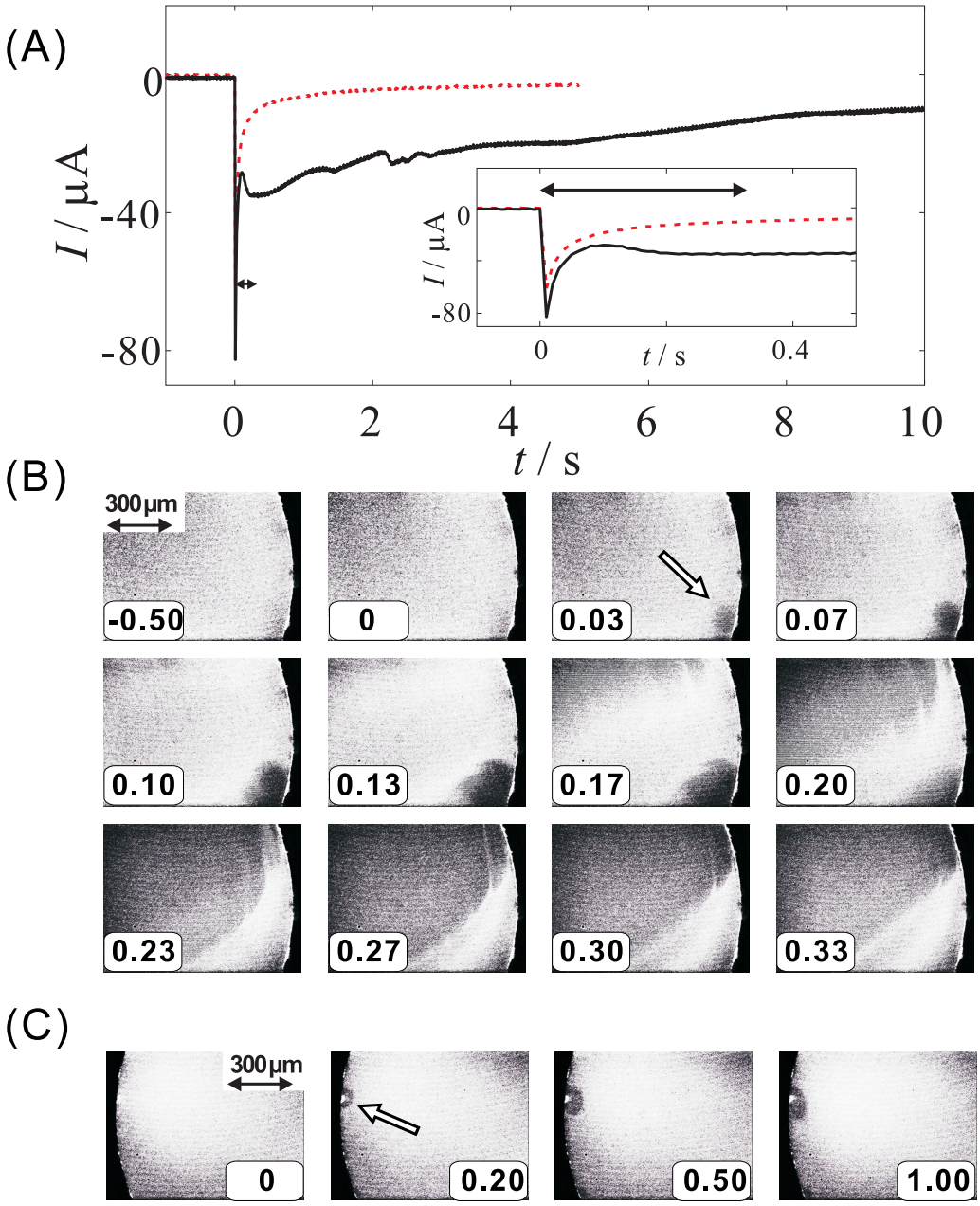

Figure 3.5: Potential-step chronoamperograms for the transfer of DS^- across the D3815 modified DCE|W interface (A) and simultaneously recorded CFM images of the interface (B and C) when E was stepped from 400 to 300 mV at $t = 0$. The images in (B) were recorded simultaneously with the solid line in (A) from $t = 0$ to $t = 0.33$ s with the interval of 1/30 s. The dotted line in (A) and images in (C) are recorded in the presence of 3 mmol dm^{-3} SMO in the DCE phase. The inset in (A) shows the magnified chronoamperograms. The numbers in each image show the times when the images were recorded. The arrow in (A) shows the region where images in (B) are recorded. The arrows in images (B) at $t = 0.03$ s and (C) $t = 0.20$ s point the emerged dark domains.

appeared in the CFM images of the DCE|W interface even in the presence of SMO (the arrow in the image at $t = 0.20$ s). This demonstrates that the electrochemical instability does develop even in the presence of 3 mmol dm^{-3} SMO in DCE. The rapid expansion and the deformation of the dark domain were not observed. The addition of SMO thus suppresses the global movement of the interface, and, it is effective only to that extent to contain the irregularly increased current on a voltammogram.

3.4 Conclusions

Simultaneous recording of a cyclic voltammogram or a potential-step chronoamperogram and a series of CFM images demonstrates that a slightly augmented current in a cyclic voltammogram prior to the onset of irregularly increased currents is caused by the locally confined instability due to the presence of unstable domains, which emerge at the edge of the interface. The abnormally large irregular current is not the only phenotype of the electrochemical instability. The coexistence of such unstable small domains and the large stable regions in the interface creates a sort of a globally metastable state. Such inhomogeneity of the interface is probably responsible to the apparent potential dependence of the degree of instability, which should follow the all-or-none law, if it is of thermodynamically nature.

References

[1] Kakiuchi, T. *J. Electroanal. Chem.* **2002**, *536*, 63–69.

[2] Kakiuchi, T. *J. Electroanal. Chem.* **2001**, *496*, 137–142.

[3] Kakiuchi, T.; Chiba, M.; Sezaki, N.; Nakagawa, M. *Electrochem. Commun.* **2002**, *4*, 701–704.

[4] Kakiuchi, T.; Nishi, N.; Kasahara, T.; Chiba, M. *ChemPhysChem* **2003**, *4*, 179–185.

[5] Kasahara, T.; Nishi, N.; Yamamoto, M.; Kakiuchi, T. *Langmuir* **2004**, *20*, 875–881.

[6] Sakka, T.; Tanaka, K.; Shibata, Y.; Ogata, Y. H. *J. Electroanal. Chem.* **2006**, *591*, 168–174.

[7] Kitazumi, Y.; Kakiuchi, T. *J. Phys.: Condens. Matter* **2007**, *19*, 375104.

[8] Uredat, S.; Findenegg, G. H. *Langmuir* **1999**, *15*, 1108–1114.

[9] Weis, R. M.; McConnell, H. M. *Nature* **1984**, *310*, 47–49.

[10] Lösche, H.; Möhwald, H. *Colloids Surf.* **1984**, *10*, 217–224.

[11] Dale, S. E. C.; Unwin, P. R. *Electrochem. Commun.* **2008**, *10*, 723–726.

[12] Zheng, X. Y.; Harata, A. *Anal. Sci.* **2001**, *17*, 131–135.

[13] Nishi, N.; Izawa, K.; Yamamoto, M.; Kakiuchi, T. *J. Phys. Chem. B* **2001**, *105*, 8162–8169.

[14] Kitazumi, Y.; Kakiuchi, T. *Langmuir* **2009**, *25*, 8062–8068.

[15] Dupeyrat, M.; Michel, J. *Experientia. Suppl.* **1971**, *18*, 269–273.

[16] Dupeyrat, M.; Nakache, E. *Bioelectrochem. Bioenerg.* **1978**, *5*, 134–141.

[17] Yoshikawa, K.; Matsubara, Y. *J. Am. Chem. Soc.* **1984**, *106*, 4423–4427.

[18] Kihara, S.; Maeda, K. *Prog. Surf. Sci.* **1994**, *47*, 1–54.

Chapter 4

Emergence of the electrochemical instability in transfer of decylammonium ion across the 1,2-dichloroethane|water interface formed at the tip of a micropipette

The effect of the size of a liquid|liquid interface on the electrochemical instability (EI) has been studied voltammetrically for the transfer of decylammonium ions ($DeNH_3^+$) across the 1,2-dichloroethane|water interface formed at the tip of a micropipette. An abnormally increased irregular current (AIIC) reproducibly appears on the voltammogram without the positive-feedback for the iR compensation. This fact confirms that the AIIC is not an artifact associated with the positive-feedback usually employed for the iR compensation at the liquid|liquid interface of conventional size. The emergence of the AIIC at the micro liquid|liquid interface supported at the tip of the micropipette is suppressed by either a decrease in the concentration of $DeNH_3^+$ or a decrease in the diameter of the interface. The concentration of $DeNH_3^+$ required to induce the AIIC at the micro liquid|liquid interface is significantly higher than that at the

interface of conventional size. The effect of the diameter of the micropipette on the AIIC is in line with the case of the aspect-ratio effect on the formation of cellular convection of Marangoni instability.

4.1 Introduction

The electrochemical instability (EI) of a liquid|liquid interface [1] is a thermodynamic instability that takes place when

$$\left[\frac{\partial^2\gamma}{\partial\left(\Delta_{\mathrm{O}}^{\mathrm{W}}\phi\right)^2}\right]_{T,P,\mu_i} > 0 \tag{4.1}$$

where γ is the interfacial tension and $\Delta_{\mathrm{O}}^{\mathrm{W}}\phi$ is the phase-boundary potential. This condition may be fulfilled through the interplay of the potential-dependent adsorption and partition of surface-active ions between the two phases [2]. The EI explains the characteristic features of the instability experimentally found at the liquid|liquid interface when surface-active ions move across the interface [3–7]. Three main features of the EI are the existence of the instability window of the phase-boundary potential, the location of the instability window close to the half-wave potential, and a positive finite value of γ when the interface becomes unstable.

When a liquid-liquid two-phase system falls in the state of the EI due to the transfer of surface-active ions across the liquid|liquid interface, the Marangoni convection is induced owing to the heterogeneity of the interfacial tension. Because the convection enhances the mass-transfer of surfactant ions to the interface, the abnormally increased irregular current (AIIC) emerges in the ion-transfer voltammogram [3–5, 7, 8].

The area of the liquid|liquid interface where the EI has so far been found is relatively large, ca. 0.1 [3–6, 8] or 50 cm^2 [7]. Since the EI is a thermodynamic concept as expressed in equation (1), it is supposed to be independent of the dimension and the shape of the interface, as has been found previously [3–5, 7, 8]. However, when the area of the liquid|liquid interface is very small, the appearance of the EI can be different. It is known that the interface is stabilized with a decrease in the interfacial area in case of the thermally induced Marangoni convection [9–11].

The ion transfer across the micro liquid|liquid interface has been studied [12–14] at the tip of a micropipette, where the aspect ratio (ratio of diameter of the pipette to the depth) is very small. In the Marangoni convection in a cylinder caused by the temperature gradient [9, 10], the convective motion is suppressed due to the presence of the wall of the cylinder when the aspect ratio is small. Then, it is natural to expect that the Marangoni convection due to the

EI can also be suppressed at the interface formed at tip of the micropipette.

Aside from the hydrodynamic constraint due to the aspect ratio, a decrease in the interfacial area may bring about other consequences. If the turbulence of the interface occurs in a way similar to the nucleation and growth mechanism, that is, the initial formation of unstable micro domains at the interface followed by the growth of these domains, the onset of the EI should be proportional to the interfacial area, provided that the frequency of the nucleation per unit area and unit time is constant. Then, with decreasing the area of the interface, a stochastic nature of the EI would become surfaced. The effect of the edge of the interface on the EI may also become appreciable at a nm-sized pipette because of the electrical double layer on the surface of a glass pipette.

The present paper reports a study of the EI at the micro liquid|liquid interface supported at the tip of a micropipette [12–14]. An advantage of using a micro liquid|liquid interface is that the positive-feedback for the iR compensation is not required. At the liquid|liquid interface of conventional size, we can not rule out the the possibility that the positive-feedback which is mandatory in recording voltammograms causes the EI. In this work, we demonstrate that the EI appears without the iR compensation. We also describe some new features of the EI at the micro liquid|liquid interface supported at the tip of a micropipette.

4.2 Experimental

Tetrapentylammonium tetraphenylborate (TPnATPB) used as the supporting electrolyte in the 1,2-dichloroethane (DCE) phase was prepared from tetrapentylammonium iodide (Tokyo Kasei Kogyo, 98%) and sodium tetraphenylborate (NaTPB, Dojindo Lab., 99.5%), as described elsewhere [15]. Lithium chloride monohydrate (Wako Chemical Industries, 99.9%), magnesium chloride (Merck, pro analysis), and sorbitan monooleate (Span80, Wako Chemical Industries) were used without further purification. DCE (Wako Chemical Industries, 99.5%) was washed with water three times before use. A stock solution containing 10 mmol dm^{-3} decylamine (Tokyo Kasei Kogyo, 95%), 12 mmol dm^{-3} HCl, and 0.1 mol dm^{-3} LiCl was diluted with

a 0.1 mol dm^{-3} LiCl aqueous solution to prepare test solutions at desired concentrations of decylammonium ions ($DeNH_3^+$). The electrochemical cell employed in the present study is represented as:

		5 mM NaTPB	20 mM	100 mM LiCl			
Ag	AgCl	10 mM $MgCl_2$	TPnATPB	HCl	AgCl	Ag	(I)
				$c^{W,0}_{DeNH_3^+}$ mM $DeNH_3^+$			
		(W_{ref})	(DCE)	(W)			

where M stands for mol dm^{-3}, W_{ref} is the aqueous phase for the reference of the potential in DCE, W is the aqueous phase containing $DeNH_3^+$, and $c^{W,0}_{DeNH_3^+}$ is the initial concentration of $DeNH_3^+$ in the W phase. The potential of right-hand-side terminal with respect to the left is hereafter denoted as E. The current, I, corresponding to the flow of the positive charge from W to DCE is taken to be positive.

Micropipettes were made from borosilicate glass capillaries (G-1, Narishige, o.d./i.d.=1.0 mm/ 0.6 mm) using a pipette puller (PC-10, Narishige). An optical microscope (BX-60, x200-x1000, Olympus) was used to observe the tip of a pipette for determining the inner diameter of the tip, d, prior to an electrochemical measurement. A micropipette filled with the W phase was immersed in the DCE phase to form a micro liquid|liquid interface. The interface supported at the tip of a micropipette was confirmed using a digital camera (C7190-20, Hamamatsu Photonics) equipped with a long-working-distance objective (x100, LMPlanFL, Olympus).

Electrochemical measurements were made using either a microelectrode potentiostat (HECS-972C, Fusou Electro Chemical System) without Ohmic drop compensation or a four-electrode potentiostat (HA1010mM1A, Hokuto Denko Co.) with a positive feedback for the iR drop compensation in the cases when d was 580 μm and 5 mm. Cyclic voltammograms were recorded with a homemade computer-controlled system.

4.3 Results and discussion

In previous studies, the abnormally increased irregular currents (AIIC) in voltammograms, that is, the irregular currents whose magnitude far exceeds the diffusion-limited current, were taken as evidence of the EI [3–5]. In the present study, we found that the emergence of the AIIC in voltammograms for the transfer of $DeNH_3^+$ across the micro liquid|liquid interface supported at the tip of a micropipette was dependent on the concentration of $DeNH_3^+$ ($c^{W,0}_{DeNH_3^+}$), d , and the scan rate of the applied voltage (v). In the following, we first describe typical voltammograms that exhibit the AIIC. We then describe the effects of the concentration of $DeNH_3^+$, the area of the interface formed at the tip of the micropipette, and v on the emergence of the AIIC.

4.3.1 AIIC at the micro liquid|liquid interface

Curve 1 in Figure 4.1 shows a voltammogram for the transfer of $DeNH_3^+$ across the micro liquid|liquid interface supported at the tip of the micropipette when $d = 25$ μm, $v = 100$ mV s^{-1}, and $c^{W,0}_{DeNH_3^+} = 10$ mmol dm^{-3}. The solid line and the broken line represent the traces in the forward and reverse scans, respectively. In the forward scan, the potential where the AIIC begun (E_1) was -340 mV and the potential where the AIIC ended (E_2) was -230 mV. Thus, the instability window that was seen in the transfer of $DeNH_3^+$ at the conventional liquid|liquid interface [5] appeared also at the micro liquid|liquid interface without the positive feedback for iR compensation. The AIIC was also seen in the reverse scan. The potential where the AIIC resurged was close to E_2 and subsided at ca. -300 mV. The current was large positive in the AIIC region in both forward and reverse scans. The width of the AIIC region in the reverse scan was narrower than that in the forward scan.

Curve 2 in Figure 4.1 shows the voltammogram recorded when the DCE phase contained 6 mmol dm^{-1} Span80, which is a nonionic surfactant and is known to suppress the AIIC [3–5,7,8]. The shape of this voltammogram reflects the diffusion-controlled transfer of $DeNH_3^+$ in the micropipette [16], which is characterized by the appearance of a peak caused by the linear diffusion in the forward scan and a sigmoidal voltammogram in the reverse scan. The AIIC is

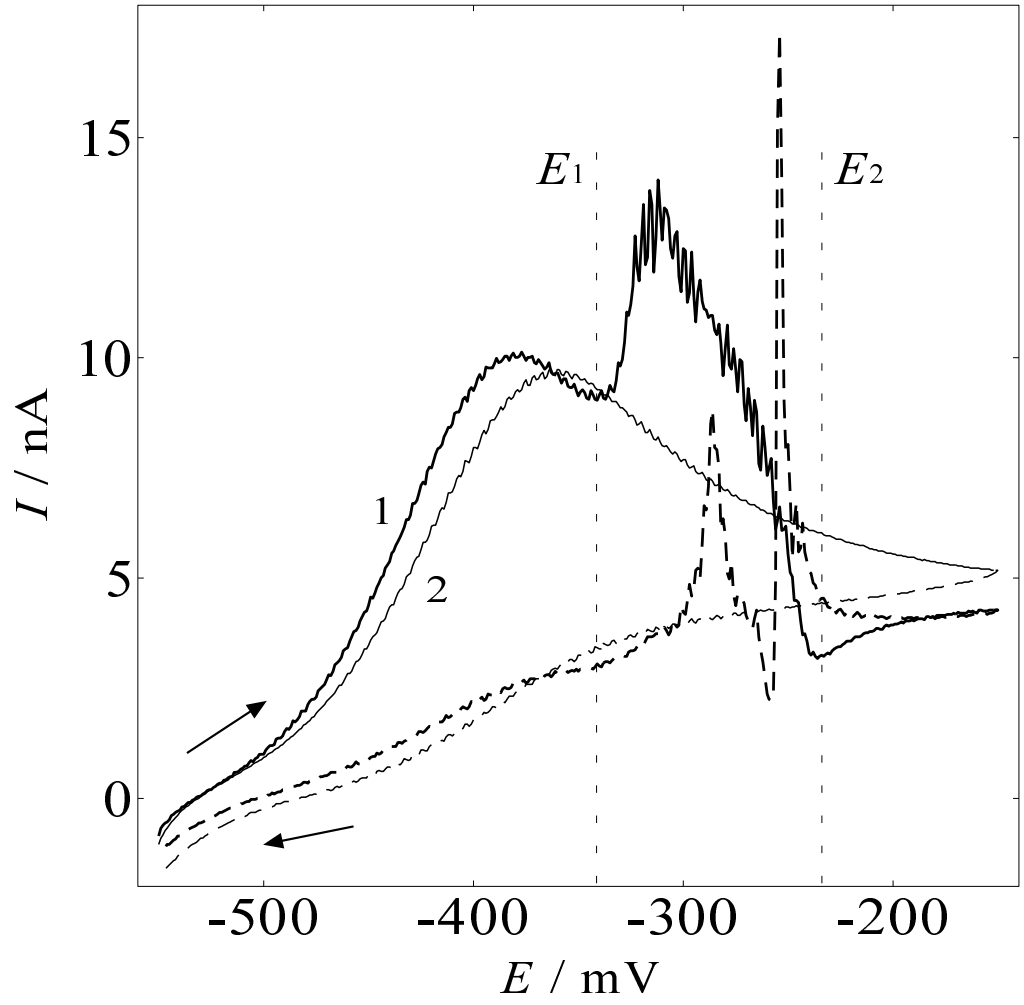

Figure 4.1: Cyclic voltammograms for the transfer of $DeNH_3^+$ across the DCE|W interface supported at the tip of a micropipette, when the W phase filled in the pipette contained 10 mmol dm^{-3} $DeNH_3^+$, d was 25 μm and v was 100 mV s^{-1} (curve 1). Curve 2 is a voltammogram recorded when the DCE phase contained 6 mmol dm^{-3} Span80. Solid and broken lines show the forward and backward scans, respectively. E_1 and E_2 represent potentials of the beginning and the end of the AIIC respectively.

thus suppressed in the voltammograms in the presence of Span80.

The determination of the half-wave potential of $DeNH_3^+$ transfer based on the voltammogram using the micropipette is not straightforward because of the asymmetric diffusion of $DeNH_3^+$ on both sides of the interface, that is, the approximately linear diffusion inside the pipette and the radial diffusion in the DCE phase [13, 17, 18]. We therefore fitted numerically simulated voltammograms, taking account of the shape of the micropipette [16], to experimental voltammograms for determining the formal potential of the transfer of $DeNH_3^+$ ($E^{0\prime}$). The obtained value, $E^{0\prime} = -380$ mV, is close to the point of inflection in the voltammogram in the reverse scan in Figure 4.1.

All features of the AIIC found at the micro liquid|liquid interface, that is, the existence of the AIIC as an instability window, the location of the instability window being close to $E^{0\prime}$, and the disappearance of the AIIC by addition of Span80 in DCE, are similar to the features of the EI reported at the liquid|liquid interface of conventional size [5]. The emergence of the AIIC at the micro liquid|liquid interface supported at the tip of the micropipette thus ascertains the generality of the EI. The fact that, the AIIC was confirmed without applying the positive-feedback for the iR compensation demonstrates that the EI is not an artifact caused by the positive-feedback.

Curve 1 in Figure 4.1 shows significantly larger currents than the diffusion-limited current (curve 2) between the initial potential of the voltammogram and E_1, before the onset of the AIIC. According to the electrocapillary curve reported by Kasahara et al. [5], $DeNH_3^+$ adsorbs at the interface in this potential range. The increase in the current in the absence of Span80 when $E < E_1$ is probably attributable to the desorption of $DeNH_3^+$, as is the case of voltammograms in the presence of weakly adsorbed reactants on an electrode [19]. At the potentials more positive than E_2, the current of curve 1 was considerably lower than that of curve 2. This reflects the exhaustion of $DeNH_3^+$ inside the pipette after the AIIC.

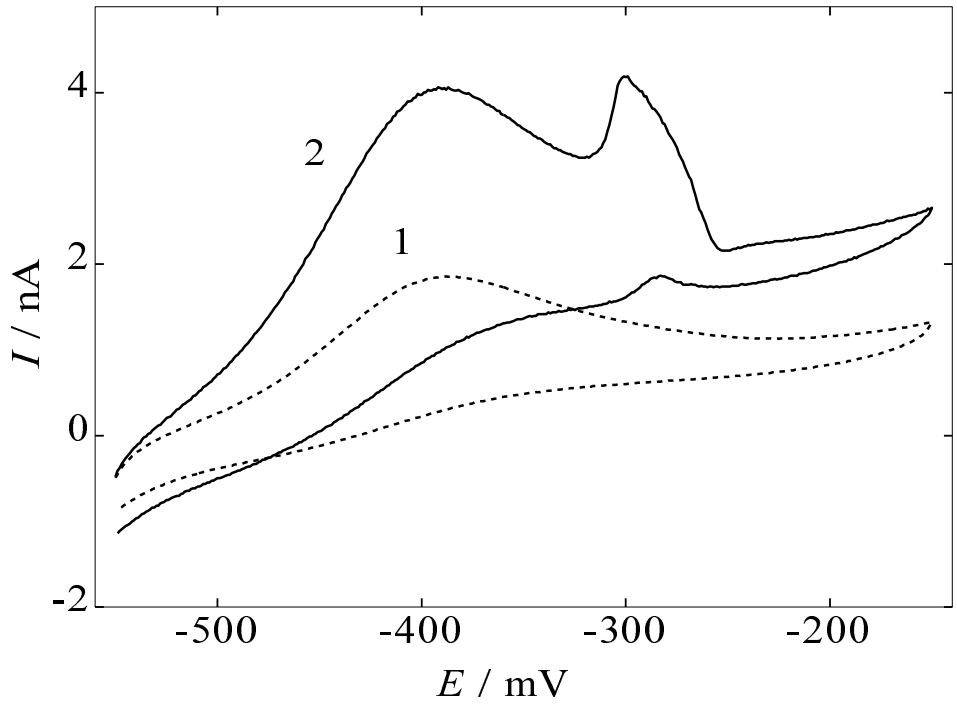

Figure 4.2: Effect of the bulk concentration of $DeNH_3^+$ in W on the shape of the voltammograms. $c^{W,0}_{DeNH_3^+}$: 2 (curve 1) and 5 (curve 2) mmol dm^{-3}. d : 25 μm. v : 100 mV s^{-1}.

4.3.2 Effect of the concentration and the interfacial area on the AIIC

Although the AIIC was confirmed in Figure 4.1, the value of $c^{\mathrm{W},0}_{\mathrm{DeNH_3^+}}$ 10 mmol dm^{-3}, is at least ten times higher than that required to cause the AIIC at the interface of a conventional size. Figure 4.2 shows voltammograms for two different concentrations of $c^{\mathrm{W},0}_{\mathrm{DeNH_3^+}}$, 2 mmol dm^{-3} (curve 1) and 5 mmol dm^{-3} (curve 2), recorded at $v = 100$ mV s^{-1} and $d = 25$ μm. Surprisingly, the AIIC was not detected at $c^{\mathrm{W},0}_{\mathrm{DeNH_3^+}} = 2$ mmol dm^{-3} as shown in the voltammogram (curve 1). By raising the concentration to 5 mmol dm^{-3}, the AIIC did appear between $E_1 = -320$ mV and $E_2 = -260$ mV (curve 2). The threshold level for the AIIC at this interface resides between 2 and 5 mmol dm^{-3}. This is in marked contrast with the case of AIIC at the DCE|W interface of conventional size, where the AIIC was detected at $c^{\mathrm{W},0}_{\mathrm{DeNH_3^+}} = 0.5$ mmol dm^{-3} [5]. The decrease in the area of the interface apparently stabilizes the interface against the AIIC; the occurrence of the AIIC depends on the size of the interface and $c^{\mathrm{W},0}_{\mathrm{DeNH_3^+}}$.

We systematically examined the influence on the AIIC of three factors d, v, and $c^{\mathrm{W},0}_{\mathrm{DeNH_3^+}}$. The results are summarized in Figure 4.3 at two values of v, 10 (a) and 200 mV s^{-1} (b). The AIIC always appeared when $c^{\mathrm{W},0}_{\mathrm{DeNH_3^+}}$ was high and d was large (•). The AIIC never appeared when $c^{\mathrm{W},0}_{\mathrm{DeNH_3^+}}$ was low and d was small (∘). Between these two cases, the AIIC occasionally emerged (△) for multiple measurements. In each set of the experimental conditions, voltammograms were recorded at least twice. There seems to be a demarcation line shown as a dashed line in each panel of Figure 4.3 that divides the experimental conditions into two groups, that is, the conditions that make the interface AIIC-prone and those AIIC-resistant.

According to the studies of the thermally induced Marangoni convection in a cylinder, the convection is suppressed when the aspect ratio is small [9, 10]. Since the aspect ratio of the pipette decreases with the decrease in d, the inner space of the pipette is probably too small to allow the formation of rolls. In other words, the suppression of the AIIC at small values of d in Figure 4.3 is likely to be explained by the effect of the aspect ratio on the Marangoni convection.

It is known that, the driving force of the surfactant induced Marangoni convection is pro-

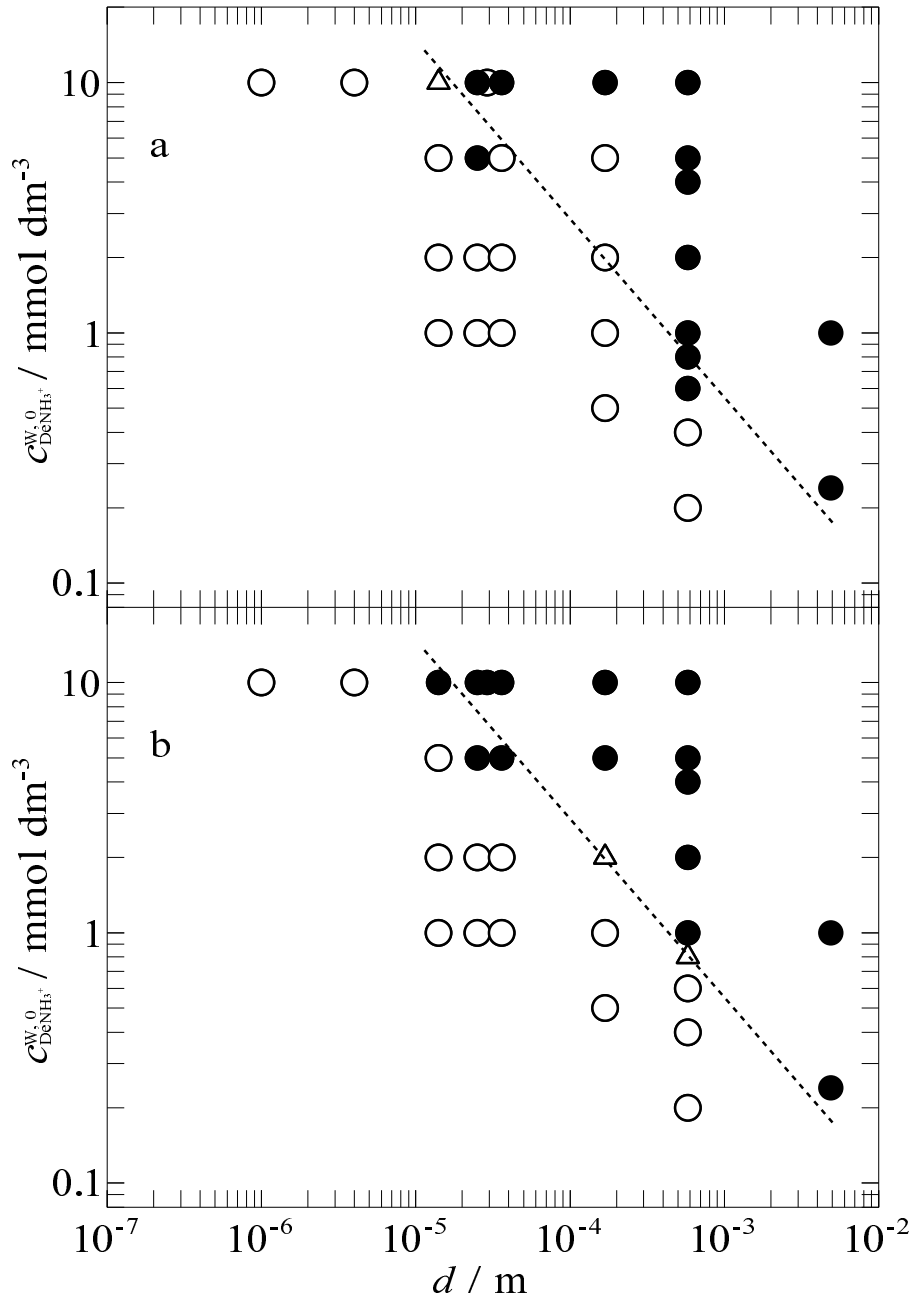

Figure 4.3: Effect of the inner diameter of the pipette orifice and the concentration of $DeNH_3^+$ on the appearance of the AIIC on voltammograms. v : 10 (a) and 200 mV s^{-1} (b). Filled circle, open triangle, and open circle show the case when the AIIC was observed, occasionally observed, and not observed, respectively. Dashed lines show the demarcation between the filled circles and the open circles.

portional to the concentration gradient of the surfactant normal to the interface [20,21]. In the present case of the EI-induced Marangoni convection, the slopes of the dashed line in Figure 4.3 at both scan rates have the same value, -0.7. This suggests that for the AIIC to occur, c^3 is approximately equivalent to d^2, i.e., the concentration is more effective than the increase in the size of the interface.

Another possible factor that can cause the observed dependence (dashed line in Figures 4.3a and 4.3b) is the edge effect due to the double layer of the wall of the pipette, which can be responsible to possible nonuniform distribution of the potential at the interface, nonuniform flow of $DeNH_3^+$, and streaming potential. However, this edge effect is expected to be small because the thickness of the double layer is thin in comparison with the size of the tip of the micropipette.

If the probability of the occurrence of electrochemically unstable domains in the interface is proportional to $c^{\mathrm{W},0}_{\mathrm{DeNH_3^+}}$ and the area of the interface, the dashed line in Figure 4.3 is expected to have a slope of -2. However, the experimental slope is considerably smaller, about -0.7 as described above. The nucleation-and-growth-type process, if any, does not seem to be a determining factor of the AIIC under the present experimental conditions.

4.3.3 Depletion of $DeNH_3^+$ in pipette due to the AIIC

One thing we should be aware of in studying the EI using micropipette is the depletion of surfactant ions inside the pipette during recording a voltammogram, as exemplified in the positive end of curve 1 in Figure 4.1. Since the depletion depends on the total amount of surfactant ions transferred across the interface, it should also depend on v. We therefore examined the effect of v on the appearance of the AIIC in voltammograms.

Effect of the scan rate on the AIIC

Figure 4.4 shows voltammograms recorded at three different values of v, 10 (a), 50 (b), and 200 mV s^{-1} when $d = 25$ μm and $c^{\mathrm{W},0}_{\mathrm{DeNH_3^+}} = 5$ mmol dm^{-3}. In Figure 4.4a, the AIIC was barely

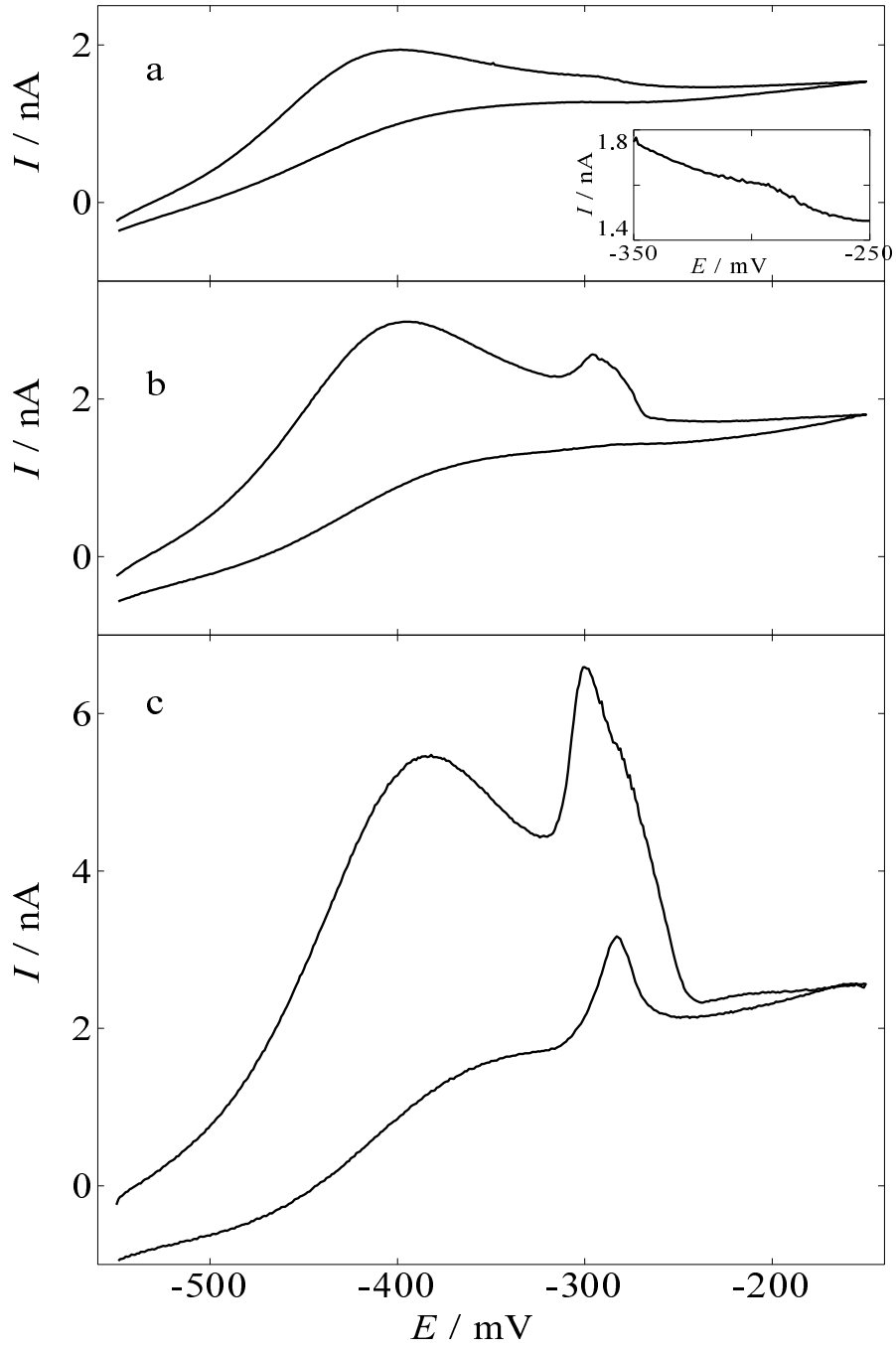

Figure 4.4: Effect of the scan rate on the shape of the voltammograms. v : 10 (a), 50 (b), and 200 mV s^{-1}(c). $c^{W,0}_{DeNH_3^+}$: 5 mmol dm^{-3} and d : 25 μm. The inset in a shows magnified view of the forward scan where the AIIC emerged.

visible around $E = -300$ mV. In Figures 4.4b and 4.4c, the AIIC was clear. The degree of AIIC judged from the magnitude of the AIIC thus depends on v. A decrease in the peak area of the AIIC with a decrease in v means that the charge transported across the interface due to the AIIC reduces with decreasing v.

This dependence indicates that the diffusion-layer thickness for the transfer of $DeNH_3^+$ or the concentrations gradient of $DeNH_3^+$ inside the pipette affects the degree of AIIC. Since this type of scan rate dependence is not observed at the interface of conventional size, the depletion of $DeNH_3^+$ inside the pipette is likely to be responsible to the dependence of the degree of the AIIC on v.

Moreover, the shape of the voltammogram during the AIIC recorded at the micro liquid|liquid interface is different from that recorded at the liquid|liquid interface of conventional size. The shape of all voltammograms exhibiting the AIIC (Figures 4.1, 4.2, and 4.4) is triangle. In contrast, at the interface of conventional size, the magnitude of the AIIC is almost independent of v; the shape of the voltammogram during the AIIC is trapezoidal [5]. The steady current during the AIIC means that the convective transport of $DeNH_3^+$ is independent of time. In contrast, the AIIC of a triangle shape in the present case indicates that the transport of $DeNH_3^+$ by the convection inside the capillary decreases with time because of the depletion of $DeNH_3^+$.

AIIC in the multiple cyclic voltammogram

To further demonstrate the exhaustion of $DeNH_3^+$ in the vicinity of the tip of the pipette , we recorded voltammograms with consecutive scans of the applied voltage. Figure 4.5 shows the voltammograms recorded at $v = 50$ mV s^{-1} when $d = 33$ μm and $c^{\mathrm{W},0}_{\mathrm{DeNH_3^+}} = 10$ mmol dm^{-3}. The number indicated by each curve indicates the number of cycles of the voltage scan, n. The AIIC clearly appeared in the first cycle, but was narrower and smaller in curve 2 and was even smaller in curve 3. The AIIC completely disappeared in curve 4. E_1 shifted to the positive potentials with n. Obviously, the concentration of $DeNH_3^+$ in the pipette decreases with n. In the fourth cycle, the concentration of $DeNH_3^+$ in the vicinity of the tip of the pipette is estimated

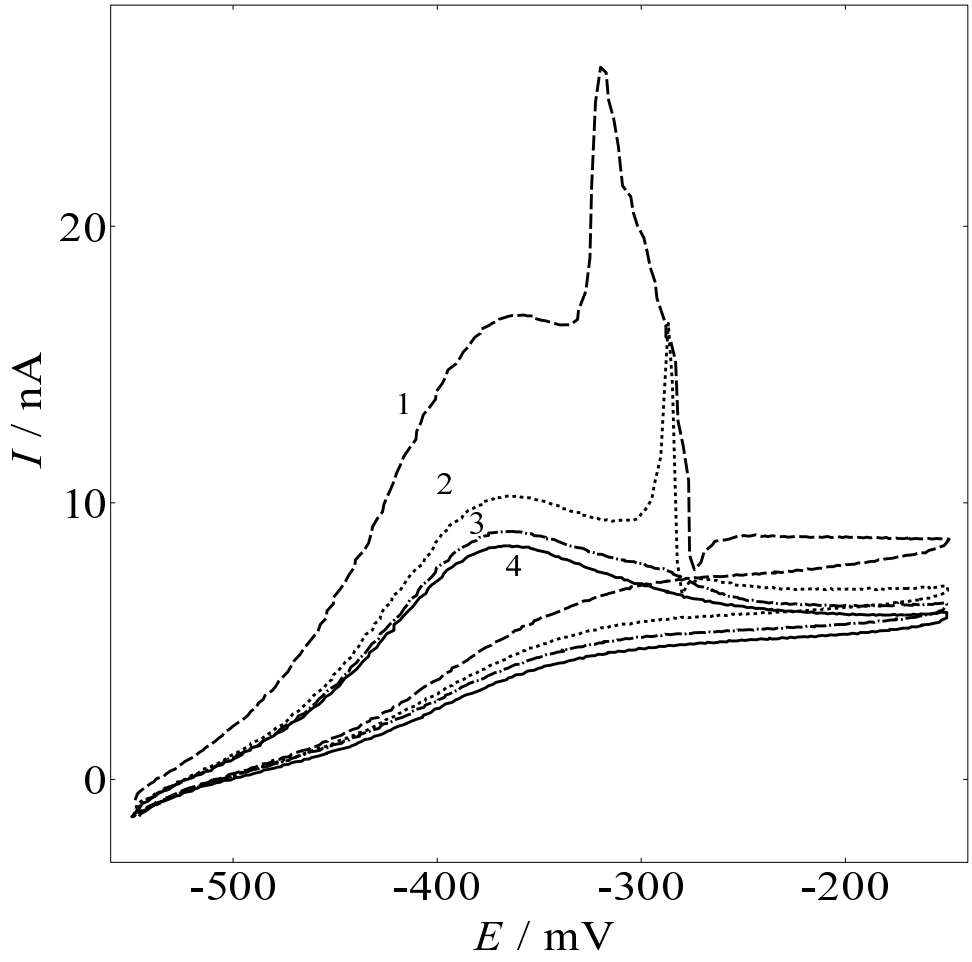

Figure 4.5: Effect of the cycles on the cyclic voltammograms of the transfer of the $DeNH_3^+$. v : 50 mV s^{-1}, $c^{W,0}_{DeNH_3^+}$: 10 mmol dm^{-3} and d : 33 μm. The numbers show the number of cycles.

to be 4 mmol dm^{-3} from the diffusion-limited peak current (curve 4). This concentration is within the stable region in Figure 4.3.

The results in Figure 4.4 and 4.5 raise a concern that at smaller values of d and $c^{W,0}_{DeNH_3^+}$ the EI may not be detected as AIIC, because of the depletion of $DeNH_3^+$ inside the capillary.

One of the methods free from this depletion problem is the employment of a liquid|liquid interface formed at a micro-hole [22] in a thin membrane separating two immiscible electrolyte solutions. Since the two semi-infinite bulk phase assures the supply of $DeNH_3^+$ even under the AIIC, there should be no depletion problem unlike micropipette experiments above. We plan to conduct experiments using a micro liquid|liquid interface at the micro-hole to examine the effect of interfacial area on the AIIC.

4.4 Conclusion

The AIIC caused by EI has been shown to take place in the transfer of $DeNH_3^+$ across the DCE|W interface formed at the tip of the micropipette. The AIIC without the positive-feedback for the iR compensation confirmed that the EI is not an artifact caused by the positive-feedback. The effect of the size of the pipette and the concentration of $DeNH_3^+$ on the AIIC is in accordance with other Marangoni instabilities. Care must be exercised in studying the EI at the micro liquid|liquid interface formed at the tip of the micropipette because of the problem of the depletion of ions in the vicinity of the interface.

References

[1] Kakiuchi, T. *J. Electroanal. Chem.* **2002**, *536*, 63–69.

[2] Kakiuchi, T. *J. Electroanal. Chem.* **2001**, *496*, 137–142.

[3] Kakiuchi, T.; Chiba, M.; Sezaki, N.; Nakagawa, M. *Electrochem. Commun.* **2002**, *4*, 701–704.

[4] Kakiuchi, T.; Nishi, N.; Kasahara, T.; Chiba, M. *ChemPhysChem* **2003**, *4*, 179–185.

[5] Kasahara, T.; Nishi, N.; Yamamoto, M.; Kakiuchi, T. *Langmuir* **2004**, *20*, 875–881.

[6] Goto, T.; Maeda, K.; Yoshida, Y. *Langmuir* **2005**, *21*, 11788–11794.

[7] Sakka, T.; Tanaka, K.; Shibata, Y.; Ogata, Y. H. *J. Electroanal. Chem.* **2006**, *591*, 168–174.

[8] Kakiuchi, T. *J. Electroanal. Chem.* **2004**, *569*, 287–291.

[9] Vrentas, J. S.; Narayanan, R.; Agrawal, S. S. *Int. J. Heat Mass Transf.* **1981**, *24*, 1513–1529.

[10] Rosenblat, S.; Davis, S. H.; Homsy, G. M. *J. Fluid Mech.* **1982**, *120*, 91–122.

[11] Rosenblat, S.; Homsy, G. M.; Dabis, S. H. *J. Fluid Mech.* **1982**, *120*, 123–138.

[12] Taylor, G.; Girault, H. H. J. *J. Electroanal. Chem.* **1986**, *208*, 179–183.

[13] Stewart, A. A.; Taylor, G.; Girault, H. H.; Mcaleer, J. *J. Electroanal. Chem.* **1990**, *296*, 491–515.

[14] Shao, Y. H.; Mirkin, M. V. *Anal. Chem.* **1998**, *70*, 3155–3161.

[15] Nishi, N.; Izawa, K.; Yamamoto, M.; Kakiuchi, T. *J. Phys. Chem. B* **2001**, *105*, 8162–8169.

[16] Nishi, N.; Imakura, S.; Kakiuchi, T. *J. Electroanal. Chem.* **2008**, *621*, 297–303.

[17] Tsujioka, N.; Imakura, S.; Nishi, N.; Kakiuchi, T. *Anal. Sci.* **2006**, *22*, 667–671.

[18] Nishi, N.; Imakura, S.; Kakiuchi, T. *Anal. Chem.* **2006**, *78*, 2726–2731.

[19] Wopschal, R.; Shain, I. *Anal. Chem.* **1967**, *39*, 1514–.

[20] Brian, P. L. T. *AICHE J.* **1971**, *17*, 765–772.

[21] Brian, P. L. T.; Smith, K. A. *AICHE J.* **1972**, *18*, 231–233.

[22] Campbell, J. A.; Girault, H. H. *J. Electroanal. Chem.* **1989**, *266*, 465–469.

Chapter 5

Spontaneous emulsification under the electrochemically unstable condition

The phase-boundary potential ($\Delta_{\mathrm{O}}^{\mathrm{W}}\phi$) across the 1,2-dichloroethane (DCE)|water interface in the presence of dodecyl sulfates is controlled by the distribution potential determined by selection of the composition of the electrolytes dissolved in either one or both of the two phases. When tetraethylammonium dodecyl sulfate, tetrapropylammonium dodecyl sulfate, and tetrabutylammonium dodecyl sulfate exist in the system, $\Delta_{\mathrm{O}}^{\mathrm{W}}\phi$ is in the potential region where the interface is under the electrochemical instability due to the potential-dependent adsorption of dodecyl sulfate. In this system, the spontaneous emulsification and oscillation of the interfacial tension develop in the vicinity of the interface. On the other hand, in the presence of tetrapentylammonium dodecyl sulfate in DCE, $\Delta_{\mathrm{O}}^{\mathrm{W}}\phi$ is out of the potential region and the spontaneous emulsification is not observed.

5.1 Introduction

The electrochemical instability (EI) [1] defines the condition when a liquid-liquid interface becomes thermodynamically unstable due to the potential-dependent adsorption of surface-active ions and can explain salient features of various unstable phenomena at the liquid-liquid interface, such as the spontaneous emulsification [2–13] and the oscillation of the interfacial tension (γ) or the phase-boundary potential ($\Delta_{\mathrm{O}}^{\mathrm{W}}\phi$) [14–18, 18–26]. EI defines the condition when a liquid-liquid interface become thermodynamically unstable due to the potential dependent adsorption at the electrified interface [27]. The emergence of the EI has been observed for various surface-active ions [28–36] in the certain potential region around the standard ion transfer potential ($\Delta_{\mathrm{O}}^{\mathrm{W}}\phi^{\ominus}$) of these ions. These observations have been carried out under the external control of the potential. However, the EI is a general concept which is independent of the way how $\Delta_{\mathrm{O}}^{\mathrm{W}}\phi$ is controlled. In fact, many of the studies of the oscillation phenomena at the liquid-liquid interface have been conducted without externally applying the potential across the interface. An important point to obtain a consistent understanding of the instability at both polarized and nonpolarized liquid-liquid interface is to apprehend the fact that the $\Delta_{\mathrm{O}}^{\mathrm{W}}\phi$ value can be controlled also by the partition of ions [37–39]. When a single 1:1 electrolyte distributes in an oil-water two-phase system, $\Delta_{\mathrm{O}}^{\mathrm{W}}\phi$ under the partition equilibrium is determined by the distribution of the ions and is given by the equation [37, 39] :

$$\Delta_{\mathrm{O}}^{\mathrm{W}}\phi = \frac{\Delta_{\mathrm{O}}^{\mathrm{W}}\phi_{\mathrm{C}^+}^{\ominus} + \Delta_{\mathrm{O}}^{\mathrm{W}}\phi_{\mathrm{A}^-}^{\ominus}}{2}, \tag{5.1}$$

where $\Delta_{\mathrm{O}}^{\mathrm{W}}\phi_{\mathrm{C}^+}^{\ominus}$ and $\Delta_{\mathrm{O}}^{\mathrm{W}}\phi_{\mathrm{A}^-}^{\ominus}$ are the standard ion-transfer potentials of the cation, C^+, and anion, A^-, respectively. The $\Delta_{\mathrm{O}}^{\mathrm{W}}\phi$ of the system in the presence of a single ionic surfactant can be turned by the selection of the counterion for a given ionic surfactant. Therefore, the emergence of the EI in the presence of surface-active ions can be controlled with the selection of those counterions. The purpose of the recent work is to demonstrate that $\Delta_{\mathrm{O}}^{\mathrm{W}}\phi$ determined by the composition of ionic component in both phases in nonpolarized liquid-liquid systems does play a central role in developing the instability and resting a stable state.

In this work, we employ dodecyl sulfate (DS) as a surface-active ion, because the EI induced by the transfer of DS is well documented [29, 30, 36]. To control $\Delta_{\mathrm{O}}^{\mathrm{W}}\phi$, we employed tetraalkylammonium as the counter ion, because the values of $\Delta_{\mathrm{O}}^{\mathrm{W}}\phi^{\circ}$ are available in the literature [40–42]. We found that the spontaneous emulsification and the oscillation of γ at the 1,2-dichloroethane (DCE)| water (W) interface take place only in a certain range of $\Delta_{\mathrm{O}}^{\mathrm{W}}\phi$.

5.2 Experimental

DCE was washed with concentrated sulfuric acid, water, an aqueous solution of Na_2CO_3, and water, successively. After being dried with $CaCl_2$, the DCE was distilled and washed with water three times before use. Water was purified with a Milli-Q system (Milli-Q Gradient, Millipore). Water and DCE were mutually saturated before preparation of the solutions. Tetraethylammonium chloride (TEACl), tetrapropylammonium chloride (TPrACl), tetrabutylammonium chloride (TBACl), tetrapentylammonium chloride (TPnACl), and sodium dodecylsulfate (SDS) were used without further purification. Tetraethylammonium dodecyl sulfate (TEADS) was prepared by extraction with chloroform from the mixture of TEACl and SDS. Then the chloroform solution was evaporated under the vacuum. TEADS is a hygroscopic white powder. Tetrapropylammonium dodecyl sulfate (TPrADS), tetrabutylammonium dodecyl sulfate (TBADS), and tetrapentylammonium dodecyl sulfate (TPnADS) were prepared by extraction with dichloromethane form the aqueous solution of TPrACl and SDS, TBACl and SDS, and TPnACl and SDS, respectively. The dichloromethane solution was washed with water three times, and then, dichloromethane was evaporated under the vacuum. TPrADS is a hygroscopic waxy solid. TBADS and TPnADS are viscous transparent liquids.

Video imaging of the interface was carried out by using a CCD video camera. To form the interface, the aqueous solution was slowly poured onto the DCE phase in a glass cuvette with 1 cm width, 4.5 cm height, and 1 cm optical length. A pendant drop method was employed for the γ measurement. A drop of the DCE solution was formed at the tip of a grass capillary tube dipped into the aqueous solution. The detail of the apparatus has been described elsewhere [35].

All the measurements were made at 25.0±0.1 °C.

5.3 Results and discussion

Figure 5.1 shows the voltammogram for the transfer of DS across the DCE|W interface in the absence of (broken line) and in the presence of 10 μmol dm^{-3} 2-(4,4- difluoro-5,7- diphenyl- 4-bora-3a,4a- diaza-s- indacene-3- pentanoyl)-1- hexadecanoyl- *sn*-glycero-3- phosphocholine in DCE phase for a suppression of the irregularly increased current (solid line) at the scan rate of 50 mV s^{-1}. In Figure 5.1, $E_{\mathrm{mid,TEA}}$ denotes the mid-point potential of voltammogram for the transfer of TEA across the DCE|W interface. The irregularly increased current was observed in the potential range, $-150 < E < 35$ mV vs $E_{\mathrm{mid,TEA}}$. This potential range of instability agrees with our previous observation for the transfer of DS [29, 30, 36]. This potential region, may be called the instability potential window. In the voltammograms, $E_{\mathrm{mid,DS}}$ was 70 mV more positive than $E_{\mathrm{mid,TEA}}$. The reported values of $\Delta_{\mathrm{O}}^{\mathrm{W}}\phi^{\ominus}$ of TEA, TPrA, TBA and TPnA are 44 , -91, -225, and -360 mV, respectively [40]. Assuming that $E_{\mathrm{mid,DS}} - E_{\mathrm{mid,TEA}} = \Delta_{\mathrm{O}}^{\mathrm{W}}\phi_{\mathrm{DS}}^{\ominus} - \Delta_{\mathrm{O}}^{\mathrm{W}}\phi_{\mathrm{TEA}}^{\ominus}$, the value of $\Delta_{\mathrm{O}}^{\mathrm{W}}\phi_{\mathrm{DS}}^{\ominus}$ is determined as 114 mV. The potentials at A, B, C, and D in Figure 5.1 show the locations of $\Delta_{\mathrm{O}}^{\mathrm{W}}\phi$ at the DCE|W interface in the presence of TEADS, TPrADS, TBADS, and TPnADS deduced using equation 5.1, respectively. The locations of $\Delta_{\mathrm{O}}^{\mathrm{W}}\phi$ for TEADS, TPrADS, and TBADS are within the instability window. In the case of TPnADS, the location of $\Delta_{\mathrm{O}}^{\mathrm{W}}\phi$ is out of the instability window. It is therefore expected that the EI at the DCE|W interface would develop in the presence of TEADS, TPrADS, and TBADS but would not in the presence of TPnADS.

Figure 5.2 shows the successive images of the side view of DCE|W interface after the DCE solution of 20 mmol dm^{-3} TEADS was contacted with the DCE saturated water in a glass cuvette. The time elapsed after the contact for each image in Figure 5.2 is 0 (A), 2 (B), 5 (C), 10 (D), 20 (E), 40 (F), 60 (G), 120 (H), and 300 minutes (I). The contact of two liquids immediately induced the convective motion in both bulk phases. The upper W phase and the lower DCE phase gradually became clouded (Figures 5.2B to 5.2G). The cloud was due to the

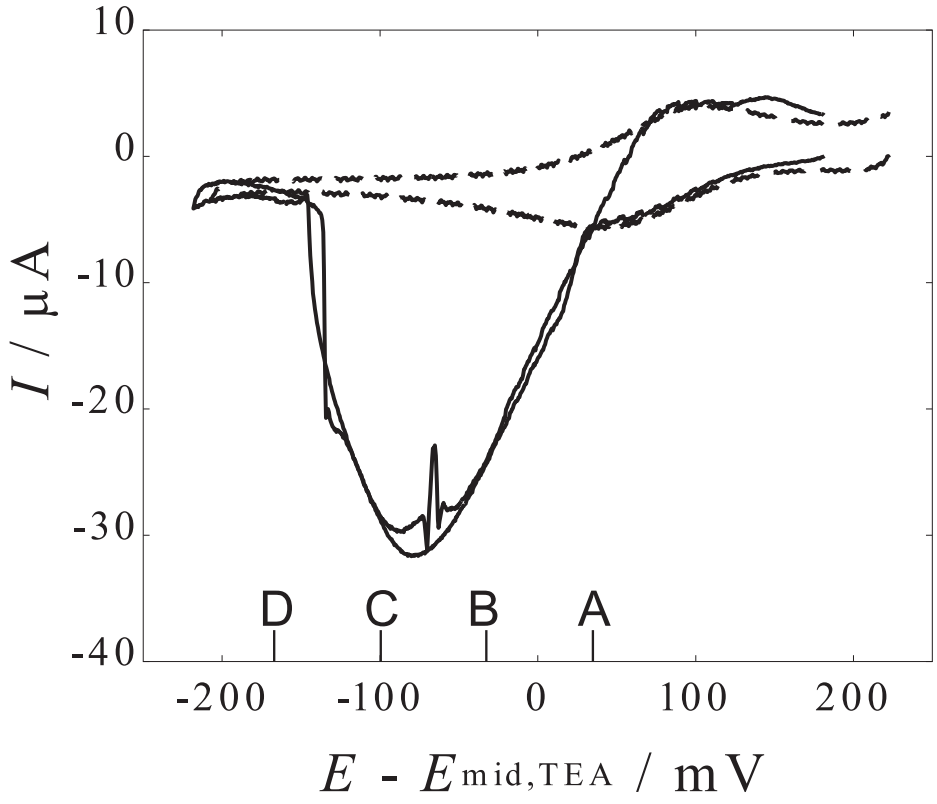

Figure 5.1: Cyclic voltammograms for the transfer of DS across the DCE|W interface when its concentration in the W phases is 1 mmol dm^{-3} at the scan rate of 50 mV s^{-1}. The DCE phase contains 50 mmol dm^{-3} tetrapentylammonium tetraphenylborate and the W phase contains 100 mmol dm^{-1} LiCl as the supporting electrolytes. Broken line was voltammogram suppressed the irregularly current increase. A, B, C, and D show the locations of $\Delta_{\mathrm{O}}^{\mathrm{W}}\phi$ in the presence of TEADS, TPrADS, TBADS, and TPnADS.

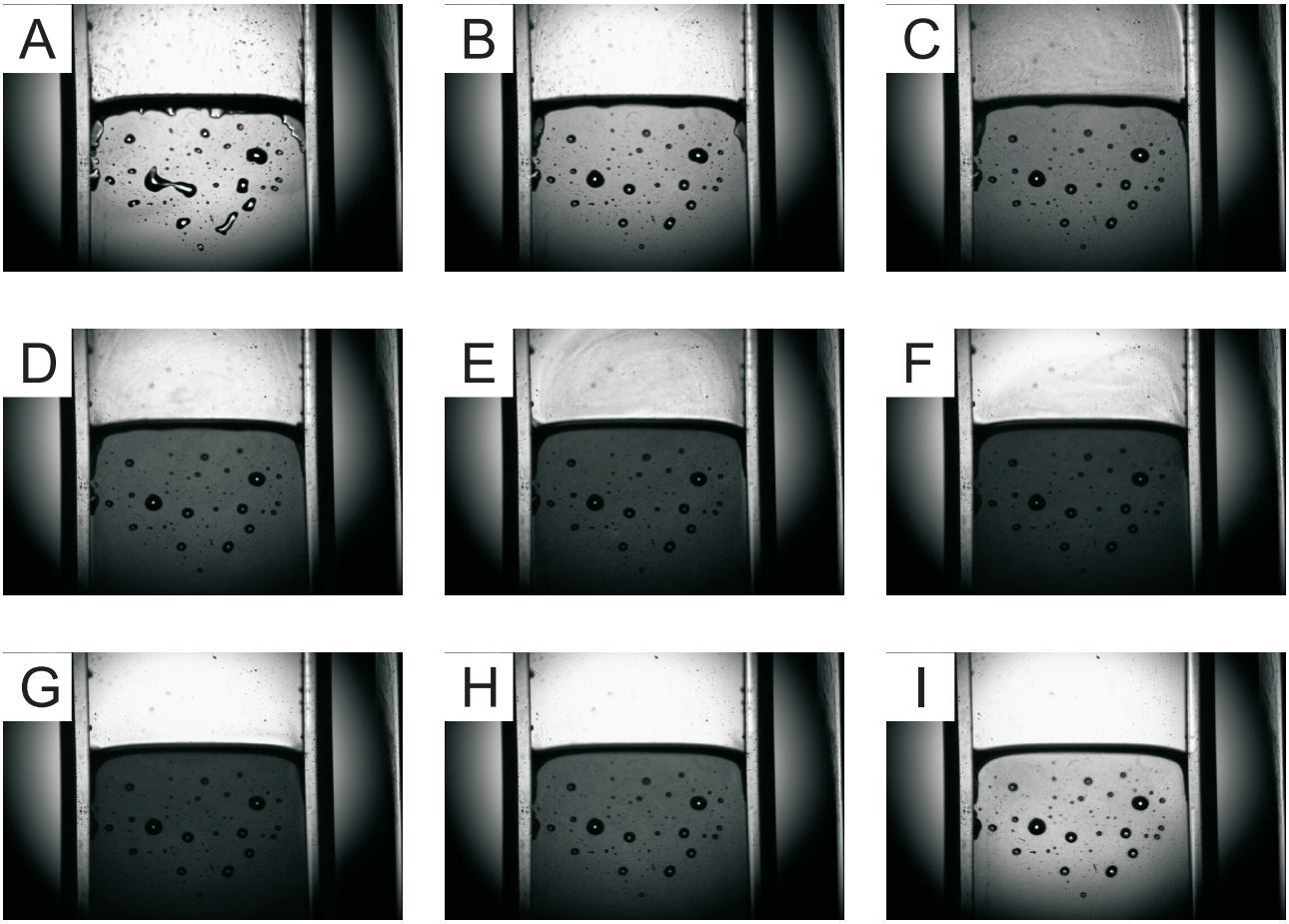

Figure 5.2: Spontaneous emulsification when the DCE solution of 20 mmol dm^{-3} TEADS contacts with water at 0 (A), 2 (B), 5 (C), 10 (D), 20 (E), 40 (F), 60 (G), 120 (H), and 300 minutes (I).

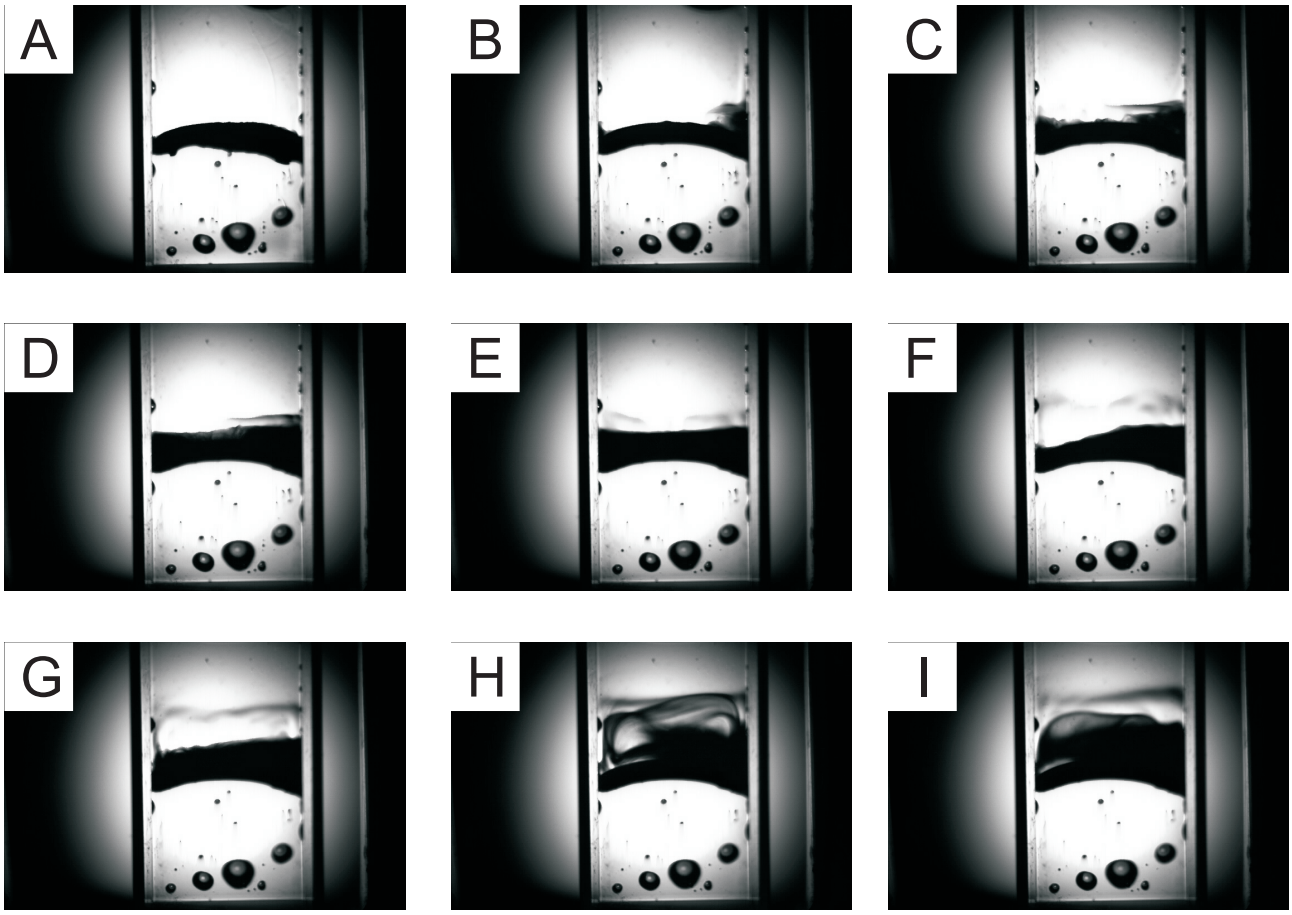

Figure 5.3: Spontaneous emulsification when the aqueous solution of 25 mmol dm^{-3} TPrADS contacts with DCE at 0 (A), 2 (B), 5 (C), 10 (D), 20 (E), 30 (F), 40 (G), 50 (H), and 60 minutes (I).

dispersion into the bulk of the emulsion formed at the interface by the interfacial turbulence. After one hour, the cloud became thinner (Figures 5.2G to 5.2I). Eventually, the both phases became transparent and the convective motion rested. In contrast, the emulsification and interfacial convection were not observed when the aqueous solutions of 10 and 70 mmol dm^{-3} TEADS were contacted with DCE.

The contact of the DCE solution of 20 mmol dm^{-3} TPrADS with water did not induce the emulsification nor the visible motion of the interface. On the other hand, the contact of the aqueous solution of 25 mmol dm^{-3} TPrADS with the water saturated DCE induced the emulsification. Figure 5.3 shows the images of the DCE|W interface in the presence of 25 mmol

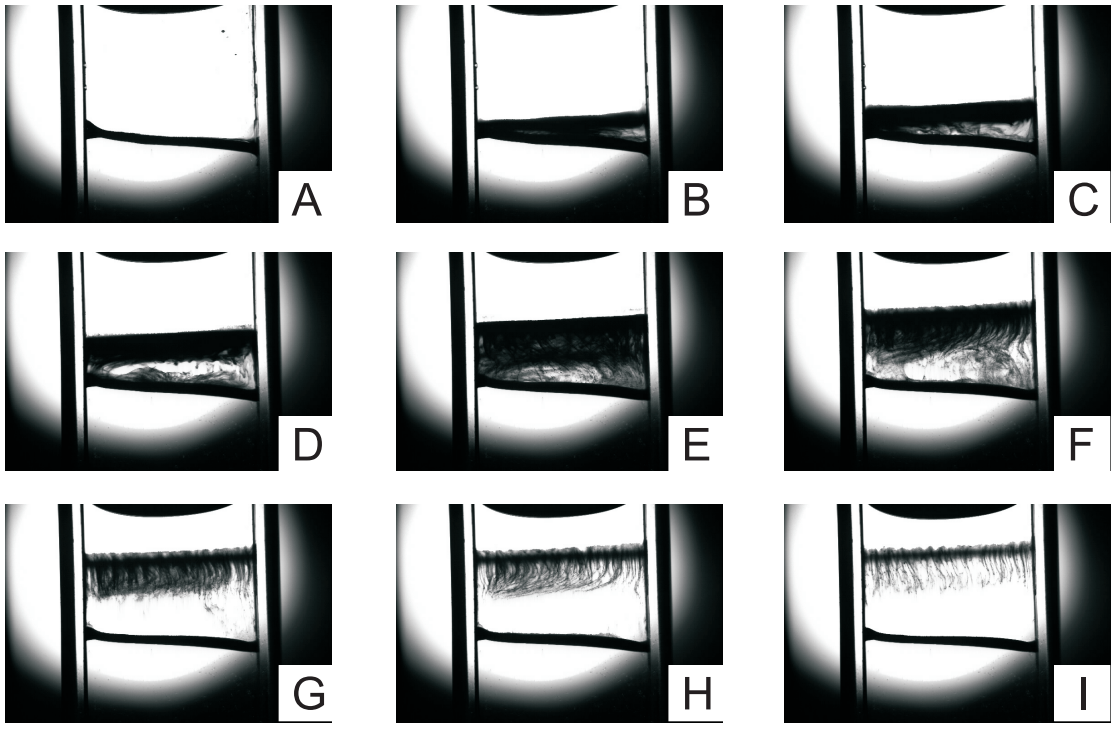

Figure 5.4: Spontaneous emulsification when the aqueous solution of 2.5 mmol dm^{-3} TBADS contacts with DCE at 0 (A), 2 (B), 5 (C), 10 (D), 30 (E), 60 (F), 90 (G), 120 (H), and 180 minutes (I).

dm^{-3} TPrADS in the W phase taken at 0 (A), 2 (B), 5 (C), 10 (D), 20 (E), 30 (F), 40 (G), 50 (H), and 60 minutes (I) after the contact. The emulsion was formed in the upper W phase and remained near the DCE|W interface in contrast with the emulsification induced TEADS. The eruptive motion at the interface was occasionally observed (Figures 5.3H and 5.3I) instead of the continuous convection in the bulk phases.

The spontaneous emulsification was observed when the aqueous solution of TBADS with DCE. Figure 5.4 shows the images of the DCE|W interface in the presence of 2.5 mmol dm^{-3} TBADS in the W phase taken at 0 (A), 2 (B), 5 (C), 10 (D), 30 (E), 60 (F), 90 (G), 120 (H), and 180 minutes (I) after the contact. The emulsion was formed in the upper W phase and

the twitching motion at the interface was observed. After one hour, the emulsion disappeared gradually. While the emulsification occured, the DCE phase remained clear.

The spontaneous emulsification was not observed when the DCE solution of 10 to 50 mmol dm^{-3} TPnADS was contacted with the water saturated with DCE and when DCE was contacted with the TPnADS saturated aqueous solution.

The fact that the spontaneous emulsification was observed at the DCE|W interface in the presence of TEADS, TPrADS, and TBADS and not observed for TPnADS demonstrates that the emergence of the EI is conditioned by $\Delta_{\mathrm{O}}^{\mathrm{W}}\phi$. This demonstrates the controllability of the spontaneous emulsification induced by a single ionic surfactant based on the EI. In a typical ionic surfactant, sodium bis(2-ethylhexyl)sulfosuccinate (Na^+ $BEHSS^-$) which is known to induce the spontaneous emulsification [9, 12, 43–45], the distribution potential created by the distribution of Na^+ and $BEHSS^-$ would be within the instability window that is determined by the potential-dependent adsorption of bis(2-ethylhexyl)sulfosuccinate ion. This prediction is supported by the observed value of $E_{\mathrm{mid,BEHSS^-}}$ was 0.12 V vs $E_{\mathrm{mid,TEA}}$, the observed instability window was located between 0.1 and 0.4 V vs $E_{\mathrm{mid,TEA}}$ when the concentration of $BEHSS^-$ was 0.3 mmol dm^{-3} (unpublished data), and the reported value of $\Delta_{\mathrm{O}}^{\mathrm{W}}\phi^{\ominus}_{\mathrm{Na^+}}$ is 0.59 V [46].

It seems necessary to distinguish two phenotypes of EI, the emulsification in one or both phases and the oscillation of γ and/or the movement of the interface. The spontaneous emulsification induced by TEADS was observed when the concentration of TEADS in the DCE phase is higher than 4 mmol dm^{-3}. When the concentration is lower than 4 mmol dm^{-3}, the oscillation of γ was observed at the drop-shaped interface. In producing mayonnaise, it is successful only when sufficiently vigorous stirring is given to the mixture of egg yolk, vinegar, and oil. In this analogy, it is expected that the greater the value of $\Delta G_{\mathrm{dissol}}$ the stronger the Marangoni effect is to cause the emulsification. The only during force for the spontaneous emulsification is the energy of the dissolution of the salt compared of an ionic surfactant and its counterion. It is interesting to estimate semiquantitatively the dissolution energy in such cases.

The distribution equilibrium of an ionic surfactant is described by

$$\Delta_{\mathrm{O}}^{\mathrm{W}}\phi_{\mathrm{C}^+}^{\ominus} - \Delta_{\mathrm{O}}^{\mathrm{W}}\phi_{\mathrm{A}^-}^{\ominus} = \frac{RT}{F}\ln\frac{c_{\mathrm{C}^+}^{\mathrm{W}}c_{\mathrm{A}^-}^{\mathrm{W}}}{c_{\mathrm{C}^+}^{\mathrm{O}}c_{\mathrm{A}^-}^{\mathrm{O}}}, \tag{5.2}$$

where R, T, and F are the gas constant, the temperature, and the Faraday constant, respectively. c_j^i (i = W and O, j = C^+ and A^-) is shown the concentration of ion j in the phase i. The values of the concentration ratio $c_{\mathrm{C}^+}^{\mathrm{W}}c_{\mathrm{A}^-}^{\mathrm{W}}/\left(c_{\mathrm{C}^+}^{\mathrm{O}}c_{\mathrm{A}^-}^{\mathrm{O}}\right)$ for TEADS, TPrADS, and TBADS at equilibrium are 0.07, 3.4×10^{-4}, and 1.8×10^{-6}, respectively. Upon contact of the two phases, the surfactant dissolved in one of the phases starts to dissolve into the other phase. In this process the system may be under the non-equilibrium condition if the $\Delta_{\mathrm{O}}^{\mathrm{W}}\phi$ is within the instability window. The energy change for the dissolution of the surfactant ($\Delta G_{\mathrm{dissol}} = RT\ln c_{\mathrm{C}^+}^{\mathrm{W}}c_{\mathrm{A}^-}^{\mathrm{W}} - RT\ln c_{\mathrm{C}^+}^{\mathrm{W}\ominus}c_{\mathrm{A}^-}^{\mathrm{W}\ominus}$), where the superscript $^{\ominus}$ on c indicates the value at equilibrium, acts presumably as the driving force for the emulsification at the interface. The fact that 4 mmol dm^{-3} is the threshold for the spontaneous emulsification by TEADS suggest that $\Delta G_{\mathrm{dissol}} = 1.2$ kJ mol^{-1} is required for the present case of the area of the interface1 cm^2. It is important to note that during the transfer of the salt from one phase to the other $\Delta_{\mathrm{O}}^{\mathrm{W}}\phi$ is equal to $\left(\Delta_{\mathrm{O}}^{\mathrm{W}}\phi_{\mathrm{C}^+}^{\ominus} + \Delta_{\mathrm{O}}^{\mathrm{W}}\phi_{\mathrm{A}^-}^{\ominus}\right)/2$ under such a non-steady state, provided that C+ and A^- are the only charged components in both phases, when the interface is planar and the mean transport of ions follows with the semi-infinite linear diffusion regime [47].

Figure 5.5 shows the time-dependence of γ at the DCE|W interface when the water was made contact with the DCE solutions of 2 mmol dm^{-3} TEADS (solid line) or TPrADS (broken line). Dotted line shows the case when the aqueous solution of TPrADS with water saturated DCE. γ increases with time in the presence of the salts in the DCE phase. In the case of TEADS, γ almost reached the value for the neat DCE|W interface [35, 48, 49]. This reflects that the volume of the DCE drop (about 30 mm^3) is distinctly smaller than the volume of the W phase (about 10^4 mm^3)in this measurement.

Oscillation of γ and $\Delta_{\mathrm{O}}^{\mathrm{W}}\phi$ at the dichloromethane |water interface due to the extraction of TEADS and TPrADS has been reported [19]. In this work, the weak oscillation of γ was observed in the presence of TEADS. However, no oscillation was observed in the presence of

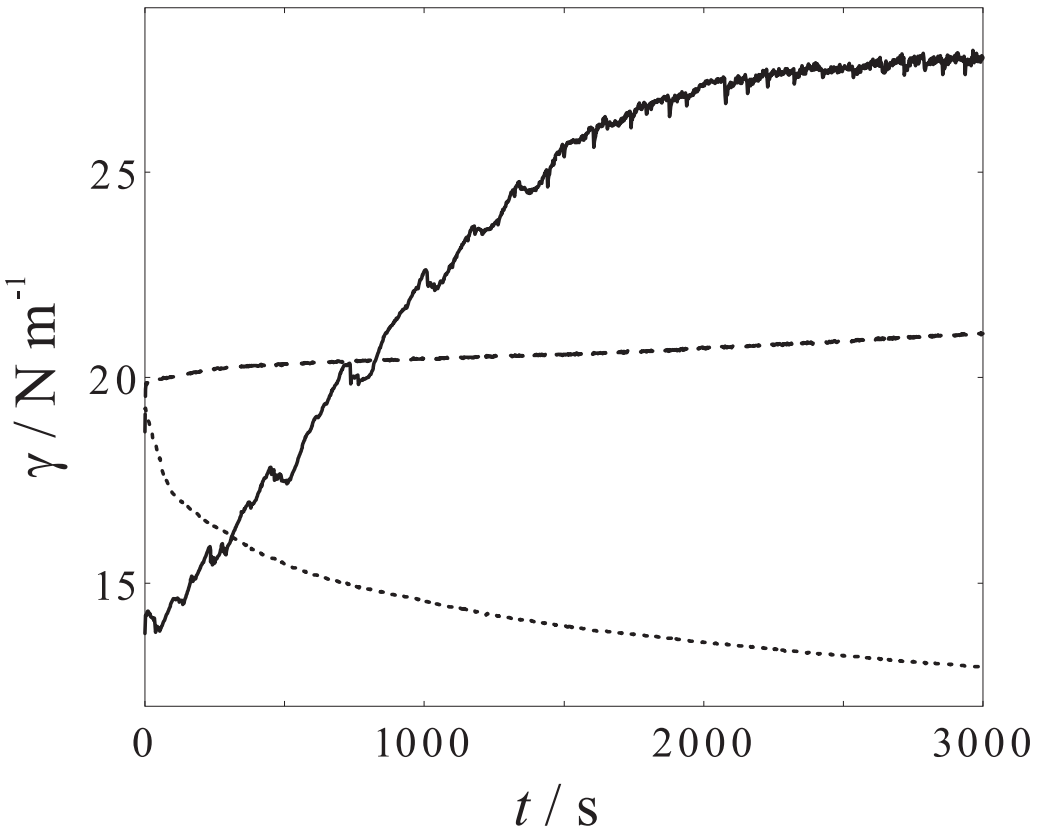

Figure 5.5: Time-dependences of γ after the water was made contact with the DCE solution of 2 mmol dm^{-3} TEADS (solid line) or TPrADS (broken line) and the pure DCE was made contact with the aqueous solution of 2 mmol dm^{-3} TPrADS (dotted line).

TPrADS.

5.4 Conclusion

The existence of TEADS TPrADS, TBADS brings the DCE|W interface unstable, because the distribution potential enters in the instability window determined by the potential-dependent adsorption of DS and the partition of its salts, TEADS and TPrADS. When the TEADS transfers from DCE to W and when TPrADS and TBADS transfer from W to DCE, the spontaneous emulsification occurs at the DCE|W interface. When the concentration of TEADS is low, the oscillation of γ at the DCE|W interface takes place. The EI emerges regardless of the way of controlling the potential. The spontaneous emulsification due to the emergence of the EI can be controlled by the selection of the counter ion in the ionic surfactant.

References

[1] Kakiuchi, T. *J. Electroanal. Chem.* **2002**, *536*, 63–69.

[2] Gad, J. *Arch. Anat. Physiol., Lpz.,* **1878**, 181–205.

[3] Quincke, G. *Ann. Phys., Lpz.,* **1904**, *15*, 1–54.

[4] McBain, J. W.; Woo, T.-M. *Proc. Roy. Soc. A* **1937**, *163*, 182–188.

[5] Kaminski, A.; McBain, J. W. *Proc. Roy. Soc. A* **1949**, *198*, 447–454.

[6] Groves, M. J. *Chem. Ind.* **1978**, *17*, 417–423.

[7] Greiner, R. W.; Evans, D. F. *Langmuir* **1990**, *6*, 1793–1796.

[8] Rang, M. J.; Miller, C. A. *Prog. Colloid Polym. Sci.* **1998**, *109*, 101–117.

[9] Nishimi, T.; Miller, C. A. *Langmuir* **2000**, *16*, 9233–9241.

[10] Forgiarini, A.; Esquena, J.; González, C.; Solans, C. *Langmuir* **2001**, *17*, 2076–2083.

[11] López-Montilla, J. C.; Herrera-Morales, P. E.; Pandey, S.; Shah, D. O. *J. Disp. Sci. Tech.* **2002**, *23*, 219–268.

[12] Srivastava, V. K.; Kini, G.; Rout, D. *J. Colloid Interface Sci.* **2006**, *304*, 214–221.

[13] Daikhin, L. I.; Urbakh, M. *J. Chem. Phys.* **2008**, *128*, 014706.

[14] Dupeyrat, M.; Nakache, E. *Bioelectrochem. Bioenerg.* **1978**, *5*, 134–141.

[15] Shioi, A.; Sugiura, Y.; Nagaoka, R. *Langmuir* **2000**, *16*, 8383–8389.

[16] Yui, H.; Ikezoe, Y.; Takahashi, T.; Sawada, T. *J. Phys. Chem. B* **2003**, *107*, 8433–8438.

[17] Kovalchuk, N. A.; Vollhardt, D. *J. Phys. Chem. B* **2005**, *109*, 15037–15047.

[18] Kovalchuk, N. M.; Vollhardt, D. *Adv. Colloid Interface Sci.* **2006**, *120*, 1–31.

[19] Pradines, V.; Tadmouri, R.; Lavabre, D.; Micheau, J. C.; Pimienta, V. *Langmuir* **2007**, *23*, 11664–11672.

[20] Teorell, T. *J. Gen. Physiol* **1959**, *42*, 831–845.

[21] Mueller, P.; Rudin, D. O. *J. Theoret. Biol.* **1968**, *18*, 222–258.

[22] Pant, H. C.; Rosenberg, B. *Biochim. Biophys. Acta* **1971**, *225*, 379–381.

[23] Yoshikawa, K.; Matsubara, Y. *J. Am. Chem. Soc.* **1984**, *106*, 4423–4427.

[24] Kihara, S.; Maeda, K. *Prog. Surf. Sci.* **1994**, *47*, 1–54.

[25] Sutou, S.; Yoshihisa, H.; Miyamura, K.; Gohshi, Y. *J. Colloid Interface Sci.* **1997**, *187*, 544–546.

[26] Pimienta, V.; Etchenique, R.; Buhse, T. *J. Phys. Chem. A* **2001**, *105*, 10037–10044.

[27] Kakiuchi, T. *J. Electroanal. Chem.* **2001**, *496*, 137–142.

[28] Vanýsek, P. *J. Electroanal. Chem.* **1981**, *121*, 149–152.

[29] Kakiuchi, T.; Chiba, M.; Sezaki, N.; Nakagawa, M. *Electrochem. Commun.* **2002**, *4*, 701–704.

[30] Kakiuchi, T.; Nishi, N.; Kasahara, T.; Chiba, M. *ChemPhysChem* **2003**, *4*, 179–185.

[31] Kasahara, T.; Nishi, N.; Yamamoto, M.; Kakiuchi, T. *Langmuir* **2004**, *20*, 875–881.

[32] Goto, T.; Maeda, K.; Yoshida, Y. *Langmuir* **2005**, *21*, 11788–11794.

[33] Sakka, T.; Tanaka, K.; Shibata, Y.; Ogata, Y. H. *J. Electroanal. Chem.* **2006**, *591*, 168–174.

[34] Kitazumi, Y.; Kakiuchi, T. *J. Phys.: Condens. Matter* **2007**, *19*, 375104.

[35] Kitazumi, Y.; Kakiuchi, T. *Langmuir* **2009**, *25*, 8062–8068.

[36] Kitazumi, Y.; Kakiuchi, T. *Langmuir* **2009**, *25*, 10829–10833.

[37] Hung, L. Q. *J. Electroanal. Chem.* **1980**, *115*, 159–174.

[38] Hung, L. Q. *J. Electroanal. Chem.* **1983**, *149*, 1–14.

[39] Kakiuchi, T. *Anal. Chem.* **1996**, *68*, 3658–3664.

[40] Samec, Z.; Homolka, D.; Mareček, V.; Kavan, L. *J. Electroanal. Chem.* **1983**, *145*, 213–218.

[41] Osakai, T.; Ebina, K. *J. Phys. Chem. B* **1998**, *102*, 5691–5698.

[42] Katano, H.; Tatsumi, H.; Senda, M. *Talanta* **2004**, *63*, 185–193.

[43] Zulauf, M.; Eicke, H. F. *J. Phys. Chem.* **1979**, *83*, 480–486.

[44] Shahidzadeh, N.; Bonn, D.; Meunier, J. *Europhys. Lett.* **1997**, *40*, 459–464.

[45] Nakagawa, M.; Sezaki, N.; Kakiuchi, T. *J. Electroanal. Chem.* **2001**, *501*, 260–263.

[46] A. Sabela, V. Mareček, Z. S.; Fuoco, R. *Electrochimica Acta* **1992**, *37*, 231–235.

[47] Kakiuchi, T.; Senda, M. *Bull. Chem. Soc. Jpn.* **1983**, *56*, 1322–1326.

[48] Girault, H. H.; Schiffrin, D. J.; Smith, B. D. V. *J. Electroanal. Chem.* **1982**, *137*, 207–217.

[49] Kakiuchi, T.; Nakanishi, M.; Senda, M. *Bull. Chem. Soc. Jpn.* **1988**, *61*, 1845–1851.

Chapter 6

Adsorption characteristics of aerophobic surfactants having a charged hydrophobic part and an uncharged hydrophilic part

Novel surface-active ions, (6-(methyl(2,3,4,5,6-pentahydroxyhexyl)amino)-6-oxohexyl)tripropylphosphonium (G3P) and tributyl(6-(methyl(2,3,4,5,6-pentahydroxyhexyl)amino)-6-oxohexyl)phosphonium (G4P), having a quaternary phosphonium as a charged hydrophobic part and a glucamide as an uncharged hydrophilic part, show adsorption characteristics distinctively different from those of conventional ionic surfactant having a charged hydrophilic part and an uncharged hydrophobic part. G3P and G4P, which are moderately hydrophobic, hardly adsorb at the air|water interface, whereas do strongly at the oil|water interface. The dependence of adsorption on the phase-boundary potential at the 1,2-dichloroethane (DCE)|water interface makes a sharp contrast with that of conventional ionic surfactants in that G3P and G4P strongly adsorb from the DCE side of the interface, whereas conventional ionic surfactants strongly adsorb from the aqueous phase. The dependency of the adsorption of surface-active ions on the phase-boundary potential at the liquid-liquid interface can be reversed by replac-

ing the charged moiety in hydrophilic part with the charged hydrophobic part and nonpolar uncharged part with hydrophilic charged part.

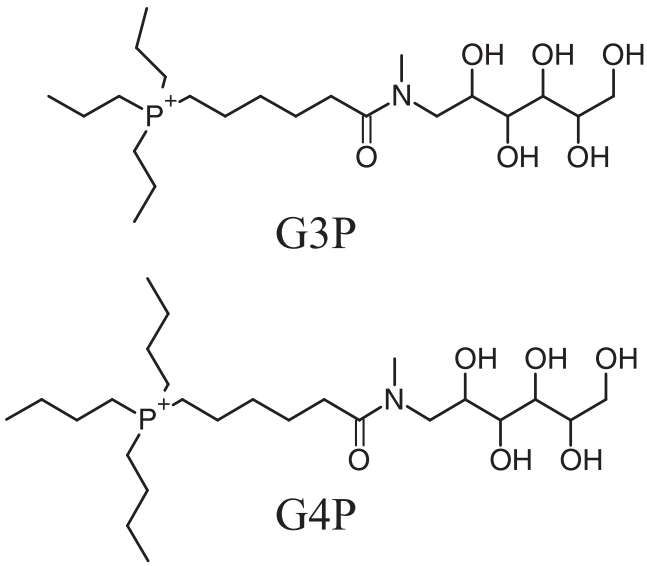

Figure 6.1: Structures of G3P and G4P.

6.1 Introduction

Conventional surfactants show high affinity to both air|water and oil|water interfaces. We report herein novel ionic surfactants that are almost aerophobic, showing little surface activity at the air|water interface, but are highly surface active at the oil|water interface, as are conventional surfactants. Novel surface-active ions we synthesized are (6-(methyl(2,3,4,5,6-pentahydroxyhexyl)amino)-6-oxohexyl)tripropylphosphonium (G3P) and tributyl(6-(methyl(2,3,4,5,6-pentahydroxyhexyl)amino)-6-oxohexyl)phosphonium (G4P), (Figure 6.1) having a charged hydrophobic part and an uncharged hydrophilic part. The uniqueness of these novel surfactants has been quantitatively characterized by measuring the interfacial tension at the air|water, heptane|water, and 1,2-dichloroethane (DCE)|water interfaces. The dependence of the surface activity of the surfactants on the phase-boundary potential across the oil-water interface ($\Delta_{\mathrm{O}}^{\mathrm{W}}\phi$) has also been studied the case of the DCE|W interface.

The dependence of adsorption of surface-active ions on $\Delta_{\mathrm{O}}^{\mathrm{W}}\phi$ is of fundamental importance in understanding the behavior of ionic surfactants at the liquid-liquid interface, in general [1], and also from the viewpoint of the electrochemical instability [2]. The adsorption Gibbs energies of surface-active ions from the water phase (W) and from the oil phase (O) depend on $\Delta_{\mathrm{O}}^{\mathrm{W}}\phi$.

A simple model [1] to describe the linear dependence of the standard adsorption Gibbs energy for an ion from one side of the interface, $\Delta G_{\mathrm{ads}}^{\alpha,\ominus}$ (α = W or O), is

$$\Delta G_{\mathrm{ads}}^{\mathrm{W},\ominus} = \Delta G_{\mathrm{ads}}^{\ominus} - zF(1-\beta)\left(\Delta_{\mathrm{O}}^{\mathrm{W}}\phi - \Delta_{\mathrm{O}}^{\mathrm{W}}\phi^{\ominus}\right) \tag{6.1}$$

and

$$\Delta G_{\mathrm{ads}}^{\mathrm{O},\ominus} = \Delta G_{\mathrm{ads}}^{\ominus} + zF\beta\left(\Delta_{\mathrm{O}}^{\mathrm{W}}\phi - \Delta_{\mathrm{O}}^{\mathrm{W}}\phi^{\ominus}\right), \tag{6.2}$$

where z, β, $\Delta_{\mathrm{O}}^{\mathrm{W}}\phi^{\ominus}$ and $\Delta G_{\mathrm{ads}}^{\ominus}$ are the charge of the ion normalized to the electronic charge, the coefficient which is independent of $\Delta_{\mathrm{O}}^{\mathrm{W}}\phi$ ($0 \leq \beta \leq 1$), the standard ion-transfer potential of the ion, and the standard adsorption Gibbs energy at $\Delta_{\mathrm{O}}^{\mathrm{W}}\phi^{\ominus}$, respectively [1].

In the case of the adsorption of decylammonium and decylsulfate at the DCE|W interface [3], β parameter of these ions are about 0.9. Electrocapillary curves of the DCE|W interface recorded in the presence of bis-quaternary ammoniums [4] indicate that the β values of the ions are close to unity. These ions consist of a charged hydrophilic part and an uncharged hydrophobic part. When these ions are adsorbed at the DCE|W interface, the charged parts of these ions are likely to be located on the aqueous side of the interface. The values of β would reflect the positions of the charged parts of the surface-active ions at the liquid-liquid interface. If so, the value of β may be altered by properly designing the structure of surface-active ions. It is expected that G3P and G4P could have β values significantly different from those of conventional ionic surfactants.

In this chapter, the author describes the adsorption properties of G3P and G4P at the air|water, the heptane|W, and the DCE|W interfaces.

6.2 Experimental

6.2.1 Chemicals.

6-Bromo-*N*-methyl-*N*-(2,3,4,5,6-pentahydroxyhexyl)hexanamide (G6Br) was synthesized using a mixed anhydride reaction from *N*-methyl-D-glucamine and 6-bromohexanoic acid with ethyl

chloroformate [5]. 6-Bromohexanoic acid (Aldrich) 30 g (0.152 mol) was added to a 200 ml of diethylether containing 15 ml pyridine. Ethyl chloroformate 20.6 g (0.19 mol) was added in the diethylether solution on ice. The mixture was then filtrated into a A solution of 30.9 g (0.158 mol) of *N*-methyl-D-glucamine (Acros) in 250 ml of methanol with a glass filter. The filter cake was washed twice with 50 ml of diethylether. The mixture was retained at 50 °C for 150 min. The solvent was removed from the mixture with a rotary evaporator under the reduced pressure. The residue was washed with 50 ml of diethylether three times and then washed with 50 ml of hexane three times. The product was dissolved into water, and extracted with dichloromethane. The evaporation of dichloromethane from the extract gave a white waxy solid (G6Br) with the yield of 18 g (32%) .

The reaction of G6Br(0.94 g, 2.5 mmol) with tripropylphosphine (0.5 ml, 2.5 mmol) was carried out in 12 ml of 2-butanol by reflux for 13 h under nitrogen atmosphere. 2-Butanol was removed from the reaction mixture, and then the mixture was washed with hexane. The product was purified by HPLC similarly. The obtained bromide salt was viscous liquid. HRMS (FAB+) 452.3125, $C_{22}H_{47}O_6NP$ requires 452.3136, deviation 2.4 ppm. (6-(methyl(2,3,4,5,6-pentahydroxyhexyl)amino)-6-oxohexyl)tripropylphosphonium chloride (G3PCl) was obtained from the ion exchange of Br^- to Cl^- by Amberlite resin (IRA-900, Organo) in methanol.

The reaction of G6Br (2.9 g, 7.7 mmol) with tributylphosphine (2.0 ml, 8.0 mmol, Wako) was carried out in 35 ml of 2-butanol by reflux for 13 h under nitrogen atmosphere. The product was purified with HPLC using an aminopropyl silica column (Unison UK-Amino, Imtakt) eluting with acetonitrile / 60 mM NH_4CO_3 aq = 40/3. The obtained bromide salt was viscous liquid. HRMS (FAB+) 494.3628, $C_{25}H_{53}O_6NP$ requires 494.3605, deviation 4.7 ppm. Tributyl(6-(methyl(2,3,4,5,6-pentahydroxyhexyl)amino)-6-oxohexyl)phosphonium chloride (G4PCl) was obtained from the ion exchange of Br^- to Cl^- by methathesis with silver chloride in aqueous solution.

6.2.2 Interfacial tension measurements.

Water was purified with a Milli-Q system (Milli-Q Gradient, Millipore). DCE was washed with concentrated sulfuric acid, water, an aqueous solution of Na_2CO_3, and water, successively. After being dried with $CaCl_2$, the DCE was distilled and washed with water three times before use. Heptane was washed with water four times before use. Tetrapentylammonium tetrakis-[3,5-bis(trifluoromethyl)phenyl]borate (TPnATFPB) was synthesized as described elsewhere [6]. Tetrapentylammonium chloride (TPnACl), $MgCl_2$, and LiCl were all reagent grades and used without further purification.

The electrochemical cell employed in the present study is

$$\begin{array}{ccc|c|c|c|c|c|c} & & & & & 100\text{ mM LiCl} & & & \\ \text{Ag} & \text{AgCl} & \text{5 mM TPnACl} & \text{50 mM} & c^{\text{b,W}}_{\text{G3PCl}}\text{ G3PCl or} & \text{AgCl} & \text{Ag} & \text{(I)} \\ & & \text{10 mM } MgCl_2 & \text{TPnATFPB} & c^{\text{b,W}}_{\text{G4PCl}}\text{ G4PCl} & & & \\ & & W_{\text{ref}} & \text{DCE} & \text{W} & & & \end{array}$$

where M stands for mol dm^{-3} and W_{ref} designates the aqueous phase for the reference of the potential in the DCE phase. The bulk concentrations of G4PCl and G3PCl in the W phase are represented by $c^{\text{b,W}}_{\text{G4PCl}}$ and $c^{\text{b,W}}_{\text{G3PCl}}$, respectively. The potential of the right-hand-side terminal with respect to the left is hereafter denoted as E. The current (I) due to the flow of the positive charge from W to DCE was taken to be positive. A four-electrode potentiostat equipped with a positive-feedback circuit (HA10100mM1A, Hokuto Denko, Japan) was used to control the phase-boundary potential across the DCE|W interface.

A pendant drop method was employed to measure the interfacial tension (γ). A homemade program was used for synchronised recording of video images of a drop and I. The detail of the apparatus has been described elsewhere [3]. All the measurements were made at 25.0±0.1 °C.

6.3 Results and discussion

Figure 6.2 shows γ at the interface between the aqueous solutions of G3PCl (triangles) or G4PCl (circles) and the air. The open square in Figure 6.2 indicates γ at the neat water|air

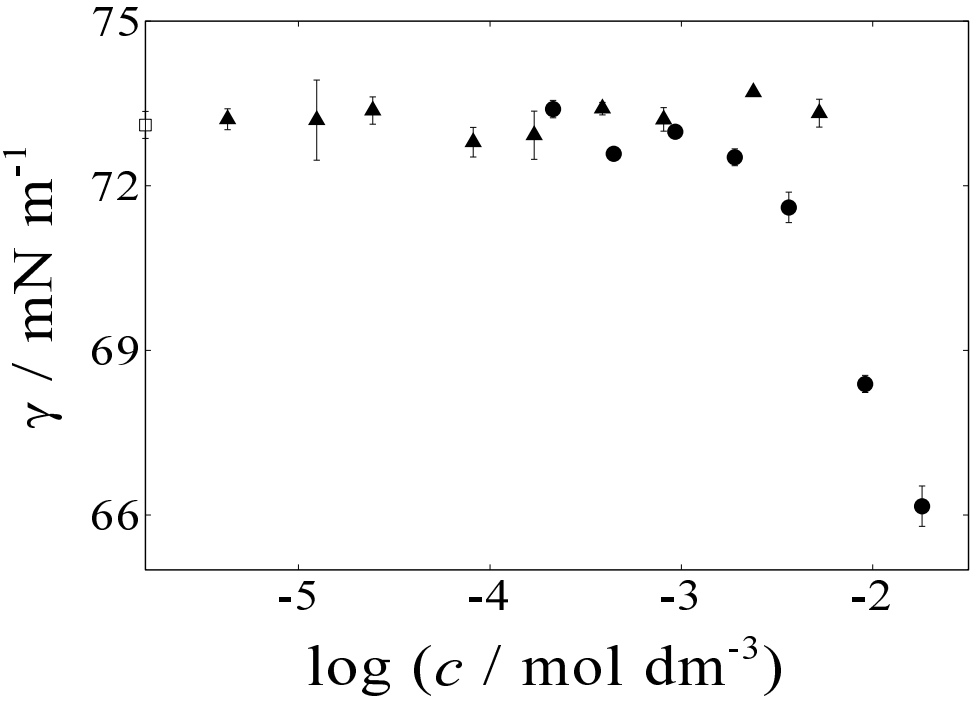

Figure 6.2: Surface tension of the aqueous solution of G3PCl (triangles) and G4PCl (circles) at 25 °C. The surface tension at pure water is shown in open square.

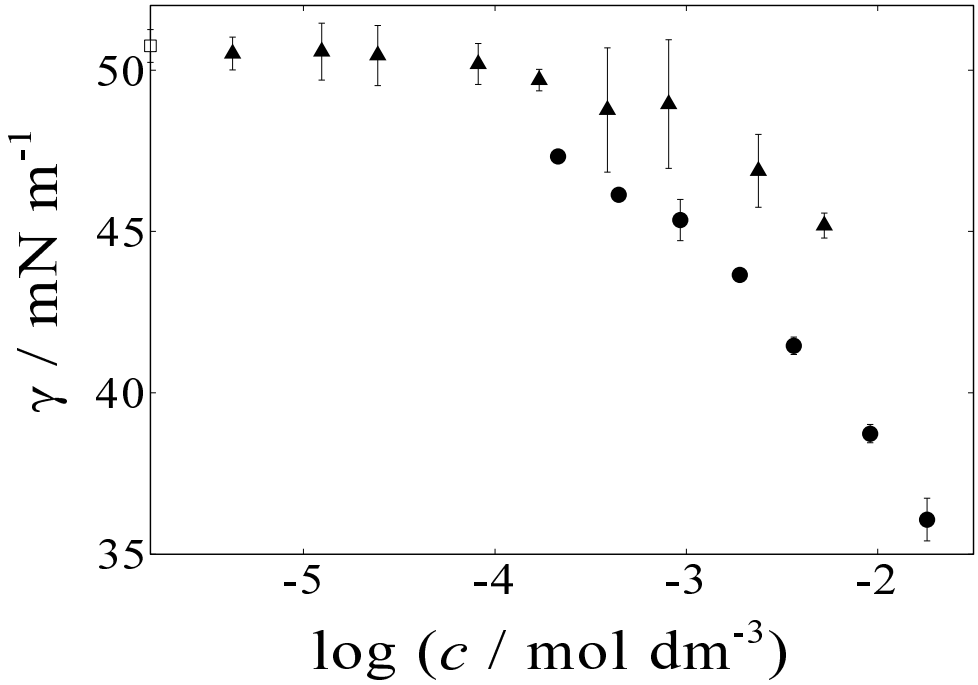

Figure 6.3: Interfacial tension at the heptane|W interface in the presence of G3PCl (triangles) and G4PCl (circles) in W at 25 °C. Open square shows γ at the pure heptane|water interface.

interface of 73.1 ± 0.3 mN m^{-1} (literature value 72.1 ± 0.3 [7], 72.00 ± 0.07 [8] mN m^{-1}). In present experimental conditions employed, the adsorption of G3P at the air|W interface was not observed up to 5 mmol dm^{-3}. This indicates that G3P has little surface activity at the air|W interface and may hence be called aerophobic. Adsorption of G4P at the air|W interface was observed when $c^{\mathrm{b,W}}_{\mathrm{G4PCl}} > 1$ mmol dm^{-3}. However, the surface activity of G4P at the air|W interface is much weaker than that of a typical cationic surfactant, decylammonium chloride, because the drop of γ at the air|W interface at $c^{\mathrm{b,W}}_{\mathrm{G4PCl}} = 10$ mmol dm^{-3} is smaller than that reported in the presence of decylammonium chloride at the same concentration ($\gamma = 64$ mN m^{-1}) [9]. The critical micelle concentration (CMC) of G4PCl was not observed in this concentration region by γ measurements up to 18 mmol dm^{-3}, whereas decylammonium has the CMC at 67 mmol dm^{-3}.

Figure 6.3 shows γ at the heptane|W interface in the presence of G3PCl (triangles) and G4PCl (circles) in W. The open squares in Figure 6.3 indicate γ of 50.7 ± 0.5 mN m^{-1} at

the pure heptane|pure water interface (literature value 50.2 mN m^{-1} [10]). The γ at the heptane|W interface decreases with the increase in $c^{b,W}_{G3PCl}$ and $c^{b,W}_{G4PCl}$. The adsorption of G3P at the heptane|W interface was discernible when $c^{b,W}_{G3PCl} > 0.1$ mmol dm^{-3}. Therefore, G3P does adsorb at the heptane|W interface, unlike the case at the air|W interface. The adsorption of G4P at the heptane|W interface is also stronger than that at the air|W interface. The critical concentration for the formation of micelles or aggregates was not observed for both G3P and G4P in the concentration range studied.

Generally, zwitterionic surfactants and conventional ionic surfactants having a charged hydrophilic part and an uncharged hydrophobic part are adsorbed both at the air|W interface and at the alkane|W interface [9, 11–15]. On the other hand, G3P and G4P are unique in that the adsorption of the ions at the air|W interface is much weaker than that at the oil|W interface. This interesting feature of G3P and G4P is probably ascribed to the fact that the hydrophobic part is also aerophobic because of its charge. In the adsorption of conventional ionic surfactants at the air|W interface, the hydrophobic moiety, such as a long-chain alkyl group, is protruded in the air. In the case of G3P, the hydrophobic moiety is charged and it is energetically unfavoured to be in the air.

Figure 6.4 shows the voltammograms for the transfer of G3P (solid line) and G4P (broken line) across the drop shaped DCE|W interface at the scan rate (v) of 10 mV s^{-1}. The dotted line in Figure 6.4 shows the voltammogram recorded in the absence of the surface-active ions. The mid-point potentials (E_{mid}) determined from the voltammograms are 455 mV for G3P and 360 mV for G4P. Under the same cell configuration, E_{mid} values of tetraethylammonium and decylammonium were observed 300 mV and 395 mV, respectively. E_{mid} values of G3P and G4P suggest that the hydrophobic-lipophilic balance of G3P and G4P is close to that of decylammonium. Although the total carbon number of G3P and G4P are large (22 for G3P and 25 for G4P), these ions are moderately hydrophilic owing to five hydroxyl groups in G3P and G4P. From a comparison with the transfer Gibbs energies of tetraalkylammoniums [16,17], the estimated effect of the addition of a hydroxyl group into an ion on its transfer Gibbs energy

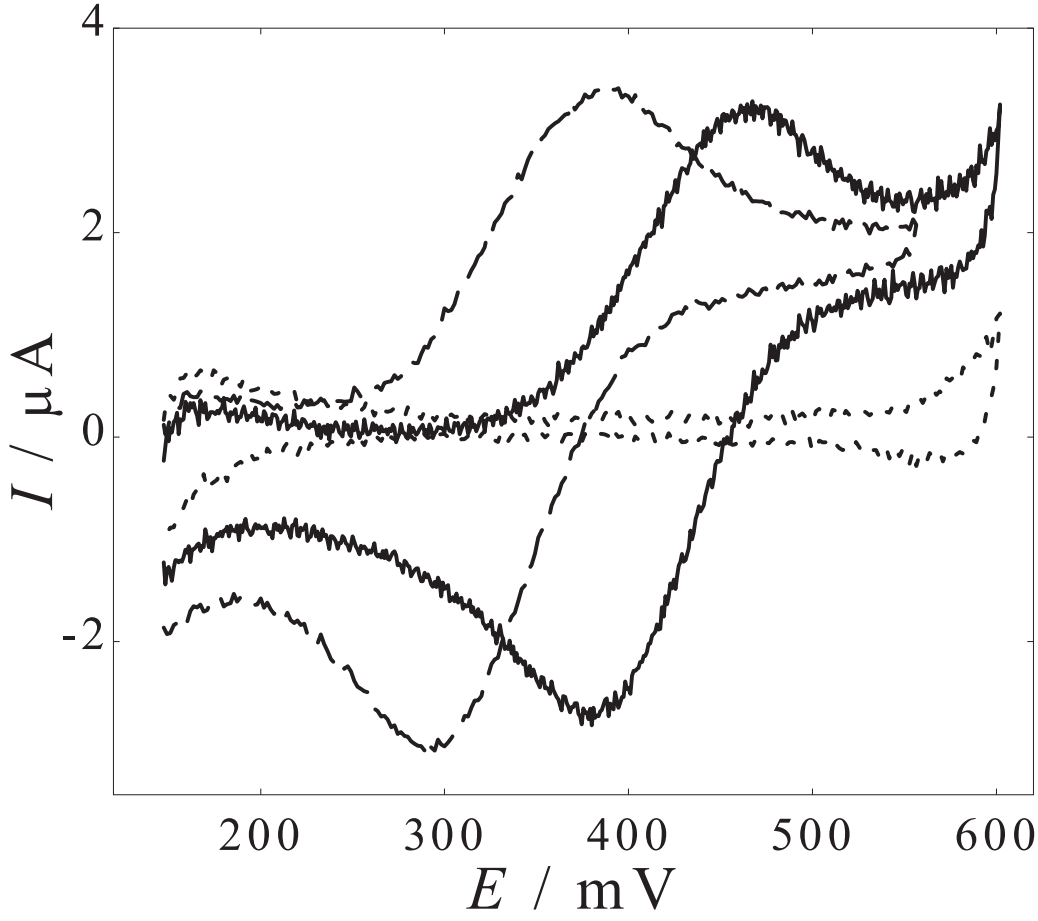

Figure 6.4: Cyclic voltammograms for the transfer of G3P (solid line) and G4P (broken line) across the drop-shaped DCE|W interface at 10 mV s^{-1}, when $c^{b,W}_{G4PCl}$ and $c^{b,W}_{G4PCl}$ are 100 μmol dm^{-3}. The dotted line shows the voltammogram in the absence of the surfactant.

is -12 kJ mol^{-1}.

Usually, the spherical shape of the interface on the DCE drop (the equatorial diameter of 3 mm) decreases the threshold concentration for the appearance of the electrochemical instability on voltammograms [3]. However, the transfer of G3P and G4P across the interface does not induce the irregular increased current due to the electrochemical instability [18–23] nor the irregular motion of the drop [3].

It is clearly seen that the electrocapillary curves at the DCE|W interface is shown in Figure 6.5 when $c^{\mathrm{b,W}}_{\mathrm{G3PCl}}$ = 0 (1), 5 (2), 10 (3), 21 (4), 27 (5), 41 (6), 50 (7), 60 (8), 79 (9), 102 (10), 150 (11), and 200 μmol dm^{-3} (12) at v = 10 mV s^{-1}. γ decreased with $c^{\mathrm{b,W}}_{\mathrm{G3PCl}}$. The adsorptivity of G3P at the DCE|W interface, where γ decreases even at $c^{\mathrm{b,W}}_{\mathrm{G3PCl}} = 5$ μmol dm^{-3}, is thus stronger than that at the air|W interface, where γ does not decrease at $c^{\mathrm{b,W}}_{\mathrm{G3PCl}} = 5$ mmol dm^{-3}. G3P is adsorbed at the DCE|W interface in the entire range of E. The adsorption of G3P in the positive branch ($\Delta^{\mathrm{W}}_{\mathrm{O}}\phi > 400$ mV) is stronger than that in the negative branch ($\Delta^{\mathrm{W}}_{\mathrm{O}}\phi < 400$ mV). This potential-dependence is distinctly different from that of conventional cationic surfactants [3]. The maximum depression of γ showing the maximum adsorption of G3P occurs around $E = 500$ mV, which is more negative than $E_{\mathrm{mid,G3P}}$ (455 mV).

Figure 6.6 shows the electrocapillary curves recorded in the presence of G4P at $c^{\mathrm{b,W}}_{\mathrm{G4PCl}}$ = 0 (1), 10 (2), 20 (3), 40 (4), 50 (5), 60 (6), 80 (7), 100 (8), 150 (9), 200 (10), and 250 μmol dm^{-3} (11). G4P is adsorbed at the DCE|W interface in whole potential region. The maximum adsorption appeared around 400 mV is more negative than $E_{\mathrm{mid,G4P}}$ (360 mV).

The electrocapillary curves have a positive curvature around 400 mV. In this region, the interface should be under the electrochemical instability [2], as are the cases of conventional ionic surfactants [3, 18–23] However, neither convective motion of the liquid nor vibration of the pendant drop was observed in recording electrocapillary curves. G4P appears to have little ability to induce the macroscopically observable convective motion in the vicinity of the interface. The Marangoni convection is caused by the regional heterogeneity of γ. G3P and G4P adsorption at the DCE|W interface is seen in the entire range of E. It is therefore likely

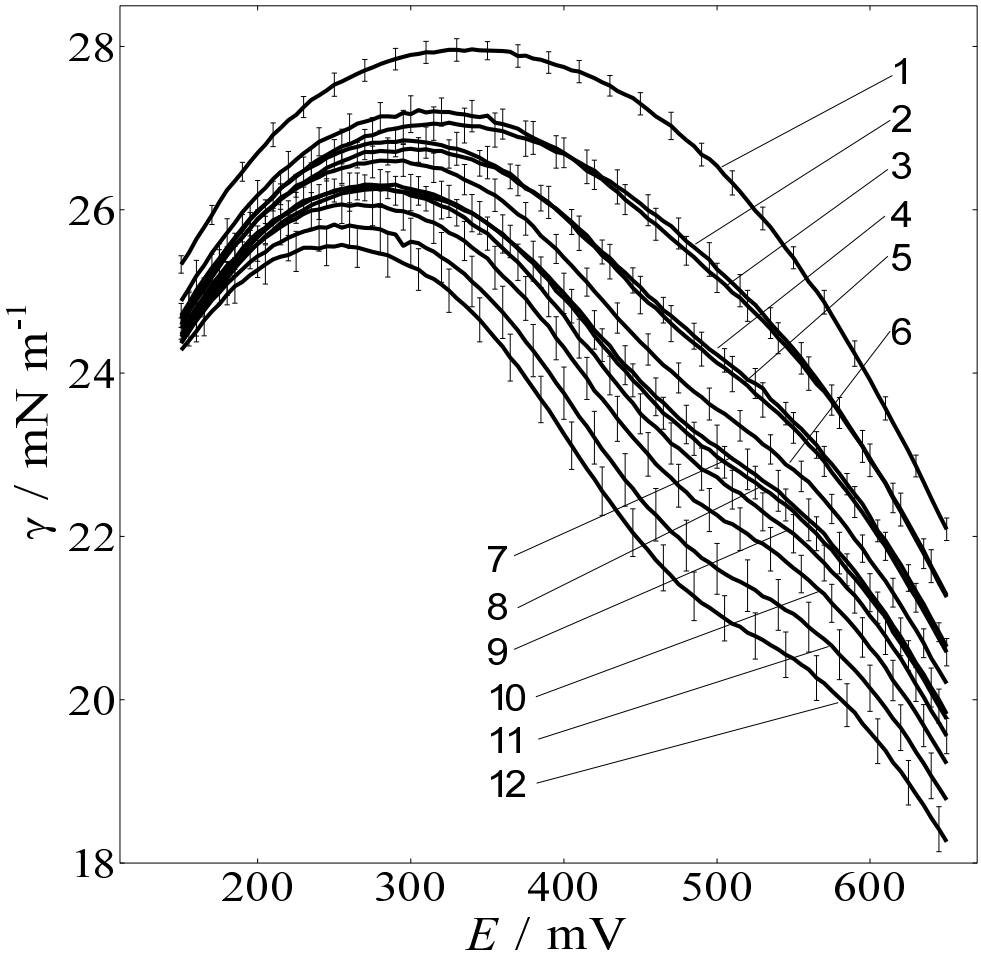

Figure 6.5: Electrocapillary curves at DCE|W interface recorded in the presence of G3PCl at $v = 10$ mV s^{-1}, $c^{\mathrm{b,W}}_{\mathrm{G3PCl}} = 0$ (1), 5 (2), 10 (3), 21 (4), 27 (5), 41 (6), 50 (7), 60 (8), 79 (9), 102 (10), 150 (11), and 200 (12) μmol dm^{-3}. Vertical bars show the 90% confidence interval for 10 independent measurements.

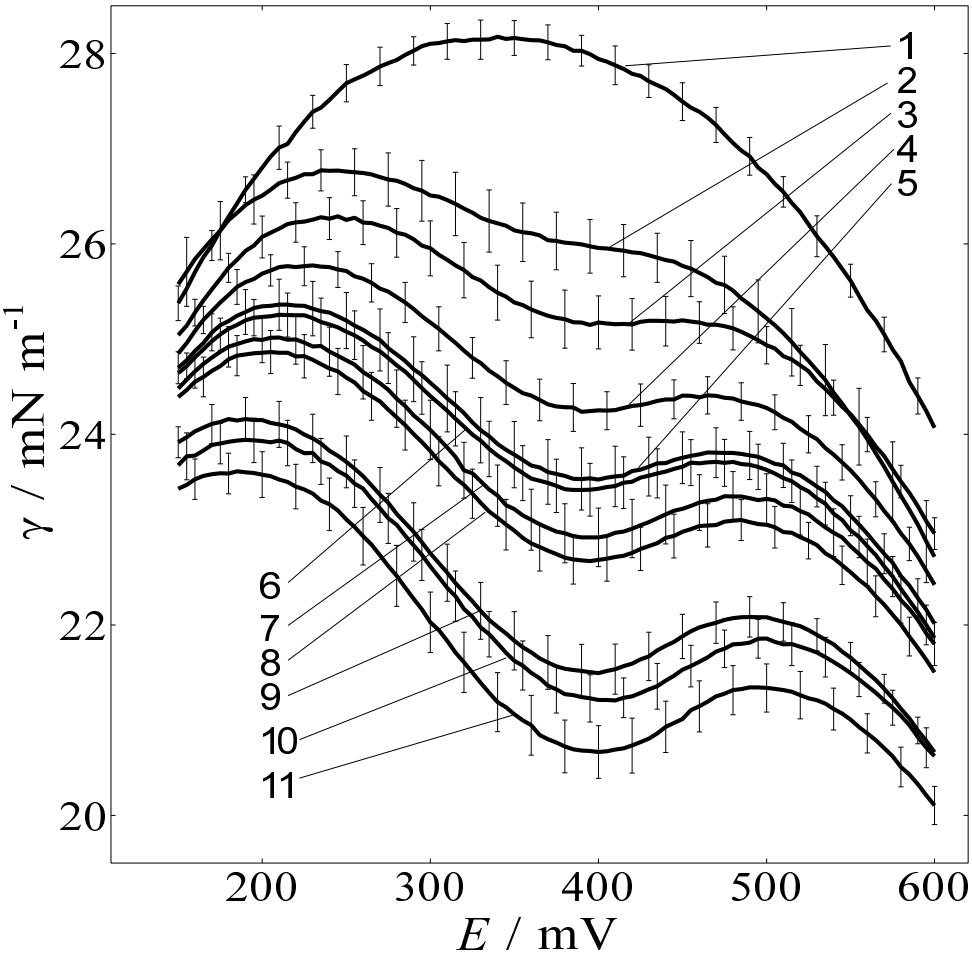

Figure 6.6: Electrocapillary curves at DCE|W interface recorded in the presence of G4PCl at v = 10 mV s^{-1}, $c^{\mathrm{b,W}}_{\mathrm{G4PCl}}$ = 0 (1), 10 (2), 20 (3), 40 (4), 50 (5), 60 (6), 80 (7), 100 (8), 150 (9), 200 (10), and 250 (11) μmol dm^{-3}. Vertical bars show the 90% confidence interval for 8 independent measurements.

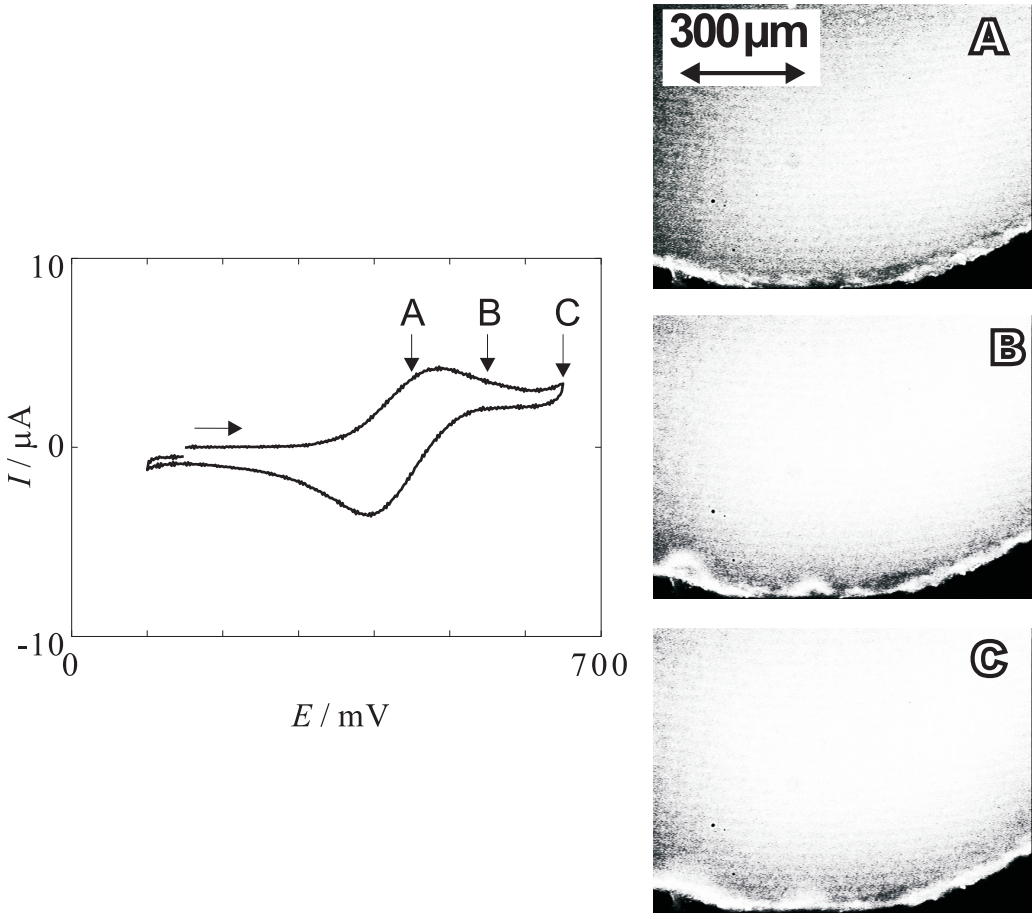

Figure 6.7: Voltammogram for the transfer of G3P across the DCE|W interface modified with 0.7 μmol dm^{-3} D3815 at $v = 50$ mV s^{-1}, $c^{\mathrm{b,W}}_{\mathrm{G3PCl}} = 1$ mmol dm^{-3} and simultaneously recorded fluorescent image of the interface. The alphabetic labels in the images correspond to that in the voltammogram.

that the difference in γ values in the unstable and stable regions is not large enough to induce a macroscopic movement of the interface.

Direct observation of the liquid|liquid interface by using confocal fluorescence microscopy (CFM) is useful to determine the potential region where the electrochemical instability emerges (instability window) [23]. Voltammograms for the transfers of G3P and G4P at $v = 50$ mV s^{-1} and $c^{\mathrm{b,W}} = 1$ mmol dm^{-3}. CFM images of the interface which is modified with fluorescent phospholipid (D3815, Molecular Probes) are shown in Figures 6.7 and 6.8, respectively. The CFM images are simultaneously recorded with voltammogram, and the alphabetic labels in

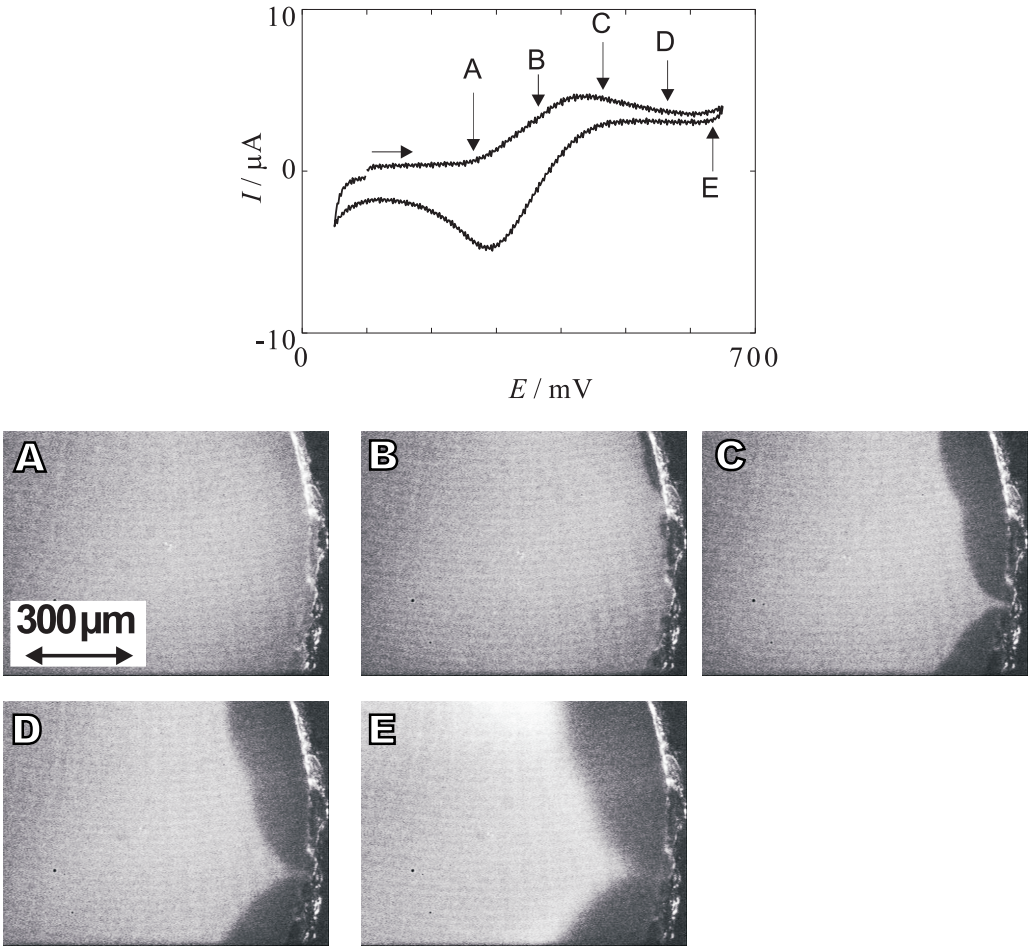

Figure 6.8: Voltammogram for the transfer of G4P across the DCE|W interface modified with 0.7 μmol dm^{-3} D3815 at $v = 50$ mV s^{-1}, $c^{\mathrm{b,W}}_{\mathrm{G4PCl}} = 1$ mmol dm^{-3} and simultaneously recorded fluorescent image of the interface. The alphabetic labels in the images correspond to that in the voltammogram.

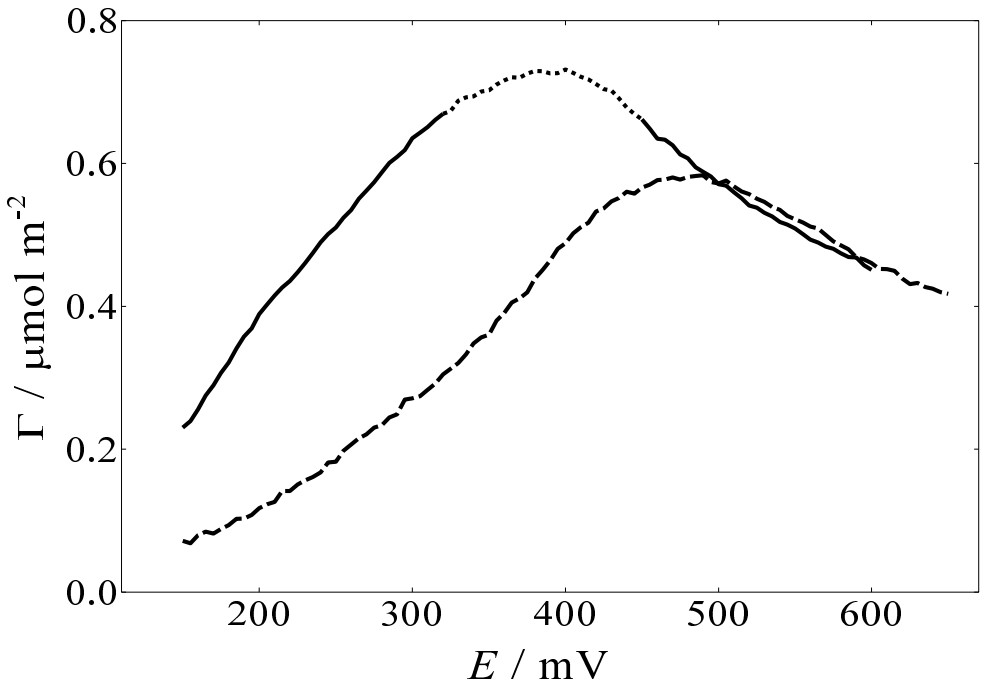

Figure 6.9: Potential dependence of surface excess of G3P (broken line) and G4P (solid line) at 60 μmol dm^{-3}. The dotted line represents the region where the interface is possibly under the electrochemical instability.

images correspond to the alphabetic labels in voltammograms. In the presence of G3P, the dark domains appeared in the region 500 mV $< E$ in the forward scan (images B and C in Figure 6.7). In the presence of G4P, the dark domains appeared in the region 350 mV $> E$ in the forward scan (images B to E in Figure 6.8). The positive ends of the instability windows were not observed. The CFM observation demonstrates that the transfers of G3P and G4P do induce the heterogeneity of the interface, a characteristic phenotype of the EI. The macroscopically convective motion at the interface was not observed even in this relatively higher concentration of the surfactants.

The surface excesses (Γ) of G3P and G4P at a given value of E were evaluated from the data in Figures 6.5 and 6.6. The values of Γ in Figure 6.9 were obtained using a weighted seven-point moving average method of γ vs. $\ln c_i^{\mathrm{b,W}}$. The potential dependence of Γ of G3P and G4P at the concentrations of 60 μmol dm^{-3} are shown as the broken and the solid lines in

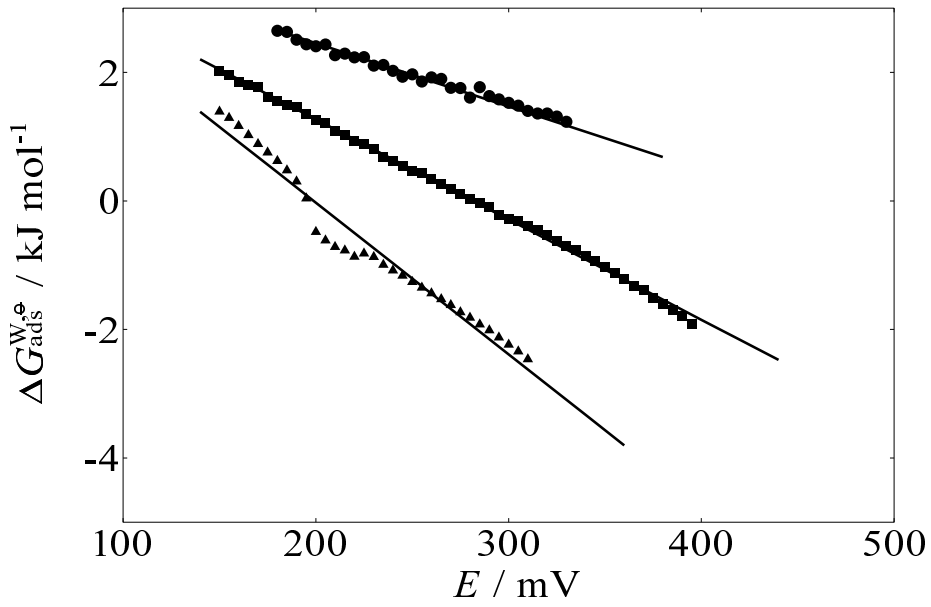

Figure 6.10: Potential dependence of $\Delta G_{\mathrm{ads}}^{\mathrm{W},\ominus}$ of decylammonium (circles), G3P (squares), and G4P (triangles) at DCE|W interface.

Figure 6.9, respectively. The dotted part in solid line indicates the data taken in the potential range where electrocapillary curves show a positive curvature and the interface is possibly under the electrochemical instability. The maxima of Γ for G3P and G4P exist at 490 mV and 400 mV, respectively.

The values of $\Delta G_{\mathrm{ads}}^{\mathrm{W},\ominus}$ were estimated from the fitting of the Langmuir isotherm to the dependence of γ on $c^{\mathrm{i,W}}$ [3]. The fitting was made in the potential region where G3P and G4P are mainly distributed in the W phase and the transfer of surface-active ions into the pendant drop does not accumulated within the drop to a saturated concentration.

Figure 6.10 shows the potential-dependence of $\Delta G_{\mathrm{ads}}^{\mathrm{W},\ominus}$ of decylammonium (circles), G3P (squares), and G4P (triangles), which were derived from fitting γ values at a given potential to the Langmuir isotherm, assuming that the maximum adsorption is 8.5×10^{-6} mol m^{-2} . Linear relationships between $\Delta G_{\mathrm{ads}}^{\mathrm{W},\ominus}$ of G3P and G4P and E are observed. The straight lines in Figure 6.10 show linear regression line for each data. The slopes of the regression lines are

-15 kJ mol^{-1} V^{-1} for G3P and -24 kJ mol^{-1} V^{-1} for G4P. The values are smaller than that for decylammonium of -10 kJ mol^{-1} V^{-1}. The corresponding β values for G3P and G4P are 0.85 and 0.75, respectively, smaller than β of 0.9 for decylammonium.

6.4 Conclusion

Novel surface-active ions, G3P and G4P, having a charged hydrophobic part and an uncharged hydrophilic part demonstrate unique features of adsorption. G3P and G4P are aerophobic surfactants, that is, they are adsorbed at the liquid-liquid interface but hardly adsorbed at the air|water interface. They are adsorbed at the liquid-liquid interface on the positive side of the mid-point potential of the respective ion. These features are distinctly different from conventional surface-active ions having a charged hydrophilic part and an uncharged hydrophobic part. G3P and G4P do not induce macroscopically appreciable interfacial turbulence under the electrochemically unstable condition, although the development of microscopic heterogeneity forming the domains of submillimeter size was confirmed with fluorescence microscopy. The β parameters of novel ions are smaller than β of the regular surface-active ions.

References

[1] Kakiuchi, T. *J. Electroanal. Chem.* **2001**, *496*, 137–142.

[2] Kakiuchi, T. *J. Electroanal. Chem.* **2002**, *536*, 63–69.

[3] Kitazumi, Y.; Kakiuchi, T. *Langmuir* **2009**, *25*, 8062–8068.

[4] Goto, T.; Maeda, K.; Yoshida, Y. *Langmuir* **2005**, *21*, 11788–11794.

[5] Hildreth, J. E. K. *Biochem. J.* **1982**, *207*, 363–366.

[6] Ohde, H.; Uehara, A.; Yoshida, Y.; Maeda, K.; Kihara, S. *J. Electroanal. Chem.* **2001**, *496*, 110–117.

[7] Jennings, J. W.; Pallas, N. R. *Langmuir* **1988**, *4*, 959–967.

[8] Touhami, Y.; Neale, G. H.; Hornof, V.; Khalfalah, H. *Colloid Surf. A-Physicochem. Eng. Asp.* **1996**, *112*, 31–41.

[9] Janńczuk, B.; Sierra, J. A. M.; González-Martín, M. L.; Bruque, J. M.; Wójcik, W. *J. Colloid Interface Sci.* **1997**, *192*, 408–414.

[10] Donahue, D. J.; Bartell, F. E. *J. Phys. Chem.* **1952**, *56*, 480–484.

[11] Rehfeld, S. J. *J. Phys. Chem.* **1967**, *71*, 738–745.

[12] Gillap, W. R.; Weiner, N. D.; Gibaldi, M. *J. Phys. Chem.* **1968**, *72*, 2222–2227.

[13] Mędrzycka, K.; Zwierzykowski, W. *J. Colloid Interface Sci.* **2000**, *230*, 67–72.

[14] Giribabu, K.; Ghosh, P. *Chem. Eng. Sci.* **2007**, *62*, 3057–3067.

[15] Tadmouri, R.; Zedde, C.; Routaboul, C.; Micheau, J. C.; Pimienta, V. *J. Phys. Chem. B* **2008**, *112*, 12318–12325.

[16] Vanýsek, P.; Behrendt, M. *J. Electroanal. Chem.* **1981**, *130*, 287–292.

[17] Katano, H.; Tatsumi, H.; Senda, M. *Talanta* **2004**, *63*, 185–193.

[18] Kakiuchi, T.; Chiba, M.; Sezaki, N.; Nakagawa, M. *Electrochem. Commun.* **2002**, *4*, 701–704.

[19] Kakiuchi, T.; Nishi, N.; Kasahara, T.; Chiba, M. *ChemPhysChem* **2003**, *4*, 179–185.

[20] Kasahara, T.; Nishi, N.; Yamamoto, M.; Kakiuchi, T. *Langmuir* **2004**, *20*, 875–881.

[21] Sakka, T.; Tanaka, K.; Shibata, Y.; Ogata, Y. H. *J. Electroanal. Chem.* **2006**, *591*, 168–174.

[22] Kitazumi, Y.; Kakiuchi, T. *J. Phys.: Condens. Matter* **2007**, *19*, 375104.

[23] Kitazumi, Y.; Kakiuchi, T. *Langmuir* **2009**, *25*, 10829–10833.

Chapter 7

Conclusions

Any interface is inevitably charged unless it is fortuitously or artificially made to zero. The electrical potential across the liquid-liquid interface, $\Delta_{\mathrm{O}}^{\mathrm{W}}\phi$, is a quantity of fundamental importance in studying as well as utilising two-phase systems of any kind. Electrochemistry is hence a useful tool to study interfacial phenomena at the liquid-liquid and solid-liquid interfaces. The present study clarified the relation between the unstable phenomena at the liquid-liquid interface and improved the model of electrochemical instability. However, many problems still remain unsolved. In this chapter, the current understanding about the unstable phenomena at the liquid-liquid interface based on this work is summarized and the remaining problems in the more than century-old research area are discussed.

7.1 Unstable phenomena at the liquid-liquid interface from viewpoint of the electrochemical instability

As already mentioned, spontaneous emulsification is a well-known phenomenon that is in useful industrial, agricultural, and medical applications [1–4]. In chapter 5, the author has shown the importance of $\Delta_{\mathrm{O}}^{\mathrm{W}}\phi$ in the spontaneous emulsification induced by ionic surfactants. When the spontaneous emulsification occurs, $\Delta_{\mathrm{O}}^{\mathrm{W}}\phi$ is kept in the potential region (instability window) where the interface is under the electrochemical instability. The instability window is deter-

mined by the standard ion-transfer potential ($\Delta_{\mathrm{O}}^{\mathrm{W}}\phi^{\ominus}$), the standard adsorption Gibbs energy ($\Delta G_{\mathrm{ads}}^{\ominus}$), the potential-dependency of the adsorption Gibbs energy (β), and the concentrations of coexisting electrolytes (Chapter 1). Spontaneous emulsification can be controlled by the adjustment of $\Delta_{\mathrm{O}}^{\mathrm{W}}\phi^{\ominus}$, $\Delta G_{\mathrm{ads}}^{\ominus}$, and β of the surface-active ion and by the selection of the counterion and the concentrations of the surfactant salt and of indifferent electrolyte in the system.

The oscillation of γ at DCE|W interface in the presence of tetraethylammonium dodecyl sulfate (Chapter 6) shows that the electrochemical instability is able to explain some oscillation phenomena at the liquid-liquid interface in the presence of ionic surfactants. However, many researchers have reported the oscillation not only γ but also $\Delta_{\mathrm{O}}^{\mathrm{W}}\phi$ [5–12]. The comparison of the current system with such studies is necessary to understand the oscillation phenomena based on the electrochemical instability.

The features of the polarographic maxima are very similar to those of the irregularly increased current on voltammograms of ion-transfer across the liquid-liquid interface when the electrochemical instability occurs. Many mechanisms, such as the adsorption of depolarizer [13, 14] and the streaming of the interface due to the heterogeneous surface potential or flow of mercury [15, 16], were proposed to explain the polarographic maxima. However, these mechanisms are not able to explain why the polarographic maxima appear in a certain potential region near the half-wave potential. The electrochemical instability clearly explains why the phenomena appear in certain potential region. At the moment, the interplay of potential-dependent adsorption and redox equilibrium of redox active species at the electrode surface has not been formulated. However, the phenomena should be described in the same way as the potential-dependent adsorption and partition of surface-active ions at the liquid-liquid interface. The quantitative understanding of polarographic maxima based on the electrochemical instability requires such a formulation and reliable data of the potential dependence of the adsorption Gibbs energy of the redox active species at the mercury surface.

7.2 Remaining problems and scope for future studies

Although many types of unstable phenomena at the liquid-liquid interface have been reported, the potential-dependence of the adsorption of surface-active ions has been quantitatively determined only for few species [17]. The determination of the potential-dependent adsorption for many more ions is necessary to get deeper understanding about the unstable phenomena; for example the potential dependent adsorption is important for the understanding of the surface active species employed in the digestive process such as bile salts [18] and the membrane active species such as melittin [19]. Moreover, the liquid-liquid interface seems to the most simple model of bilayer membrane. The stability of bilayer membranes like vesicles is highly affected by surfactant. The electrochemical instability should play an important role in this unstable phenomena at the bilayer membrane such as the fusion of membranes and the formation of pores.

We avoided discussing the interfacial tension at the interface which is under the electrochemically unstable condition. When the electrochemical instability emerges at the liquid-liquid interface, the interface does not disappear [17, 20–25] , and the interfacial tension is still measurable [17, 22, 23]. The meaning of the interfacial tension when the interface is under the electrochemically unstable condition is difficult to define but an interesting problem in technological viewpoints.

In this study, the author clarified the heterogeneity of the interface under the electrochemically unstable condition. However, the microscopic details of the emergence of the electrochemical instability remain unclear. In addition, the accurate detection of the instability window can allow the recognition of the surface-activity of ionic surfactants based on the electrochemical instability.

The model of the electrochemical instability has been improved in this study. However, many assumptions, whose validity has yet to be confirmed, are employed in the improved model. The clarification of the fine details of the potential-dependent adsorption of ions at the liquid-liquid interface and the determination of the structure of the interface are necessary to

analyze the electrochemical instability more quantitatively and realistically.

References

[1] Groves, M. J. *Chem. Ind.* **1978**, *17*, 417–423.

[2] Constantinides, P. P. *Pharm. Res.* **1995**, *12*, 1561–1572.

[3] Pouton, C. W. *Adv. Drug Deliv. Rev.* **1997**, *25*, 47–58.

[4] Frazer, A. C.; Schulman, J. H.; Stewart, H. C. *J. Physiol.-London* **1944**, *103*, 306–316.

[5] Dupeyrat, M.; Nakache, E. *Bioelectrochem. Bioenerg.* **1978**, *5*, 134–141.

[6] Yoshikawa, K.; Matsubara, Y. *J. Am. Chem. Soc.* **1984**, *106*, 4423–4427.

[7] Kihara, S.; Maeda, K. *Prog. Surf. Sci.* **1994**, *47*, 1–54.

[8] Sutou, S.; Yoshihisa, H.; Miyamura, K.; Gohshi, Y. *J. Colloid Interface Sci.* **1997**, *187*, 544–546.

[9] Pimienta, V.; Etchenique, R.; Buhse, T. *J. Phys. Chem. A* **2001**, *105*, 10037–10044.

[10] Kovalchuk, N. M.; Vollhardt, D. *Adv. Colloid Interface Sci.* **2006**, *120*, 1–31.

[11] Yui, H.; Ikezoe, Y.; Takahashi, T.; Sawada, T. *J. Phys. Chem. B* **2003**, *107*, 8433–8438.

[12] Pradines, V.; Tadmouri, R.; Lavabre, D.; Micheau, J. C.; Pimienta, V. *Langmuir* **2007**, *23*, 11664–11672.

[13] Ilkovič, D. *Collection Czechoslov. Chem. Communs* **1936**, *8*, 13–34.

[14] Bauer, H. H. *Streaming Maxima in Polarography*; Vol. 8 of *Electroanalytical Chemistry*; Marcel Dekker, Inc., 1975.

[15] Stackelberg, M. *Z. Elektrochem.* **1939**, *45*, 466–491.

[16] Kryukova, T. A. *J. Phys. Chem. USSR* **1947**, *21*, 365–375.

[17] Kitazumi, Y.; Kakiuchi, T. *Langmuir* **2009**, *25*, 8062–8068.

[18] Hofmann, A. F. *Biochem. J.* **1963**, *89*, 57–68.

[19] Habermann, E. *Science* **1972**, *177*, 314–322.

[20] Kakiuchi, T.; Chiba, M.; Sezaki, N.; Nakagawa, M. *Electrochem. Commun.* **2002**, *4*, 701–704.

[21] Kakiuchi, T.; Nishi, N.; Kasahara, T.; Chiba, M. *ChemPhysChem* **2003**, *4*, 179–185.

[22] Kasahara, T.; Nishi, N.; Yamamoto, M.; Kakiuchi, T. *Langmuir* **2004**, *20*, 875–881.

[23] Sakka, T.; Tanaka, K.; Shibata, Y.; Ogata, Y. H. *J. Electroanal. Chem.* **2006**, *591*, 168–174.

[24] Kitazumi, Y.; Kakiuchi, T. *J. Phys.: Condens. Matter* **2007**, *19*, 375104.

[25] Kitazumi, Y.; Kakiuchi, T. *Langmuir* **2009**, *25*, 10829–10833.

List of publications

Chapter 1: **A model of the electrochemical instability at the liquid-liquid interface based on the potential-dependent adsorption and Gouy's double layer theory**
Yuki Kitazumi and Takashi Kakiuchi
in preparation.

Chapter 2: **Potential-dependent adsorption of decylsulfate and decylammonium prior to the onset of electrochemical instability at the 1,2-dichloroethane|water interface**
Yuki Kitazumi and Takashi Kakiuchi
Langmuir **2009**, *25*, 8062-8068.

Chapter 3: **Imaging of the liquid-liquid interface under electrochemical instability using confocal fluorescence microscopy**
Yuki Kitazumi and Takashi Kakiuchi
Langmuir **2009**, *25*, 10829-10833.

Chapter 4: **Emergence of the electrochemical instability in transfer of decylammonium ion across the 1,2-dichloroethane|water interface formed at the tip of a micropipette**
Yuki Kitazumi and Takashi Kakiuchi
J. Phys.: Condens. Matter **2007**, *19*, 375104.

Chapter 5: **Spontaneous emulsification under the electrochemically enstable Condition**

Yuki Kitazumi and Takashi Kakiuchi

in preparation.

Chapter 6: **Adsorption characteristics of aerophobic surfactants having a charged hydrophobic part and an uncharged hydrophilic part**

Yuki Kitazumi and Takashi Kakiuchi

in preparation.

The following publications are not includied in this thesis.

Phase Transition of a Binary Room-Temperature Ionic Liquid Composed of Bis(pentafluoroethanesulfonyl)amide Salts of Tetraheptylammonium and *N*-Tetradecylisoquinolinium and Its Surface Properties at the Ionic Liquid|Water Interface

Ryoichi Ishimatsu, Yuki Kitazumi, Naoya Nishi, and Takashi Kakiuchi

J. Phys. Chem. B **2009**, *113*, 9321-9325.

Ultraslow Response of Interfacial Tension to the Change in the Phase-Boundary Potential at the Interface between Water and a Room-Temperature Ionic Liquid, Trioctylmethylammonium bis(nonafluorobutanesulfonyl)amide

Yukinori Yasui, Yuki Kitazumi, Ryoichi Ishimatsu, Naoya Nishi, and Takashi Kakiuchi

J. Phys. Chem. B **2009**, *113*, 3273-3276.

総説・解説

電気化学における有限要素法の実施例

北隅 優希

Rev. Polarogr. **2009**, *55*, 39-45.

Acknowledgements

The author would like to express his sincere gratitude to Professor Takashi Kakiuchi for his valuable advice and many helpful suggestions throughout the course of this work.

The author is deeply grateful to Professors Takeshi Abe, Koichi Eguchi, Masahiro Yamamoto, Koji Maeda, Sorin Kihara, and Kenji Kano for their kind advice and useful comment and discussion.

Sincere thanks are expressed to Drs. Naoya Nishi and Ryoichi Ishimatsu for their kind support and fruitful discussion.

The author is thankful to Drs. Tetsuo Sakka, Toshiyuki Osakai, and Yumi Yoshida for their valuable suggestions and advice.

The author wishes to thank to Messrs. Yosuke Matsuoka and Yukinori Yasui for their technical support.

Finally, the author is indebted to all members of Professor Kakiuchi's research group for their many contributions to this work.